Development of a Palladium Based Membrane Reactor System for Production of Ultra-Pure Hydrogen from Liquefied Petroleum Gas

By

Lungelwa Ethel Kula
BTech: Chemical Engineering

In fulfillment of the Requirement for the Degree of Masters of Engineering: Chemical Engineering, Faculty of Engineering, Cape Peninsula University of Technology.

Cape Town
April 2017

Development of a Palladium Based Membrane Reactor System for Production of Ultra-Pure Hydrogen from Liquefied Petroleum Gas

---

By

Lungelwa Ethel Kula

Supervisors:

Daniel Ikhu-Omoregbe

Ademola Rabiu

Abstract

Hydrogen is widely regarded as the clean energy carrier for future use in both transportation and electricity sectors. It has become an important new focus as an alternative fuel for cleaner energy technologies especially in the Polymer Exchange Membranes (PEM) fuel cells. However, specific technical and marketing demands must be met by a fuel processor for ultra-pure hydrogen production and at a very competitive cost. Liquid Petroleum gas (LPG) is seen as a potential source for low cost hydrogen production due to its relatively high energy density, easy storage and well-established infrastructure for fuel. There is a growing interest in the use of membrane in reaction engineering with the selective separation of the products from the reaction mixture provided opportunities to achieve higher conversion. Membrane separation technologies have potential to reduce operating costs, minimise unit operations and lower energy consumption. The overall goal of this project is to investigate the engineering feasibility associated performance of employing a palladium or palladium alloy membrane reactor for the production of ultra-pure hydrogen from the products of a liquefied petroleum gas (LPG) pre-reformer in determining the optimal process conditions for the production of high purity hydrogen from the LPG feedstock and evaluating of the performance of a Pd-based membrane in relation to maximizing the yield of hydrogen from the feedstock as well as minimizing the CO content of the reformate.

Simulation studies were carried out using AspenPlus v7.2 platform to optimize the pre-reformer product compositions as a function of process conditions including the temperature, steam-to-carbon ratio, reactor seize and modelling of the membrane reactor was performed to determine the pre-reformer conditions and syngas ratio's that will produce optimal ultra-pure hydrogen for PEM fuel cells.

The optimum S/C, temperature and pressure resulting in optimum yield is to have the SR operating at S/C = 3, T(^{o}C) = 550 at the pressure of 5atm.The ideal pre-reformer mixture to be fed into the palladium membrane reactor at optimal conditions are H_2 = 38.3 kmol/hr, H_2O = 13.7 kmol/hr, CO = 6.08 kmol/hr and C_3H_8 = 0.027 kmol/hr.

The evaluation of the performance of a Pd-based membrane in relation to maximizing the yield of hydrogen from the feedstock as well as minimizing the CO content of the reformate clearly indicate that it is feasible to employ a palladium-based membrane reactor for the production of ultra-pure hydrogen from the products of a liquefied petroleum gas (LPG) pre-reformer. Based on the results that have been obtained from the membrane permeate it can be concluded that the optimal reformer conditions results in the optimal hydrogen recovery and CO conversion in the membrane reactor at a pressure of 20 bar and temperature of 500^{o}C therefore, translating to a development of purification system.

After the steam reforming process for the production of ultra-pure hydrogen it is recommended that a palladium-based reactor be utilised for the production and separation of ultra-pure hydrogen therefore, removing WSG reactor and the Prox reactor after the steam reformer process. The cost analysis of the system can assist to improve the system.

Declaration

I, Lungelwa Ethel Kula, declare that the contents of this dissertation/thesis represent my own unaided work, and that the dissertation/thesis has not previously been submitted for academic examination towards any qualification. Furthermore, it represents my own opinions and not necessarily those of the Cape Peninsula University of Technology.

Signed **Date**

Acknowledgements

I would like to thank Jehovah God for the strength and grace towards me throughout my research.

I would like to thank my supervisor (Professor D. Ikhu-Omeregbe) and co-supervisor (Mr A. Rabiu) for the guidance and support and for providing me with the opportunity to work with them.

I would like to acknowledge SAIMMC and CPUT for their financial support and the Department of Chemical Engineering for providing me with opportunity to further my studies

Lastly, I would like to thank, my friends and family for supporting me throughout my life, I would particularly like to thank my mother Phumla Marilyn Kula for being my rock and greatest supporter, and I would also like to thank my little sister Inam Kula for always keeping the smile on face when things seem a bit gloomy. I would also like to thank Landy Marekwa for always helping me to see the positive in every situation.

Table of Contents

List of Figures

List of Tables

Nomenclature

Item	Description	Unit
r_1	Reaction rate	
k_j	Rate coefficient	
k_{equil}	Equilibrium constant	
F_{H_2}	Molar flux	mol/m^2.h
$P_{H_2}^F$	H_2 partial pressure	bar
$P_{H_2}^P$	H_2 partial pressure	bar
$n_{H_2}^F$	H_2 molar flow rate	mol/h
$n_{H_2}^P$	H_2 flow rate	mol/h?
V	Volumetric flow rate	m^3/h
r^F	WGS reaction rate	mol/g.h
n_j^F	Molar feed flow rate for j components	mol/h
n_j^P	Molar product flow rate for j components	mol/h
P^F	Pressure	bar
A^F	Cross-sectional area	m^2
d_p	Particle diameter	m
G^F	Superficial mass velocity	g/m^2.h
P_0^F	Inlet feed pressure	bar
P_0^P	Inlet permeate pressure	bar
n_{jo}	Inlet molar flow rate for component j	mol/h
X_{CO}	CO conversion	
n_{CO0}^F	CO molar flow rate in the inlet	mol/h
$n_{CO,exit}^F$	CO molar flow rate at the exit	mol/h
$n_{H_{2,exit}}^F$	Molar flow rate in the feed exit	mol/h
$n_{H_{2,exit}}^P$	Molar flow rate in the permeate exit	mol/h

Greek

ν_j	Stoichiometric coefficient	
α_m	Surface area of the membrane per unit reactor volume	m^2/m^3
ρ_c	Catalyst density	g/m^3
μ^F	Viscosity	$g/m^2.h$
ε_v	Bed porosity on the feed side	
β_c	Solid volume occupied by the catalyst	

Subscript

i	Reaction 1 and 2
equil	Equilibrium
F	Feed-side
P	Permeate-side
j	CO, CO_2 and C_3H_8
C	Catalyst
0	Inlet

Abbreviations

LPG	Liquid petroleum gas
HT	High temperature
LT	Low temperature
PEM	Proton exchange membrane/Polymer electrolyte membrane
PEMFC	Proton exchange membrane fuel cell
PROX	Preferential oxidation
PSA	Pressure swing adsorbed
SR	Steam reforming
WGS	Water gas shift

Chapter 1: Introduction

1.1 General Overview

South Africa has recognised the need for a more sustainable and diversified energy supply (Morell, 2001). In a 2010 report the Department of Minerals and Energy (DME) reported that the largest contributors to South Africa's economy are very energy intensive industries (Pegels, 2010). The country's economy is dominated by the mining, mineral, manufacturing, agricultural, oil and gas industries (Jörissen, 2012). These industries are heavy energy users and inherently energy inefficient. South Africa is highly dependent on coal, generating around 75% of its electricity from coal-fired plants (Bartels, Pate, & Olson, 2010). The majority of this coal comes from the Witbank Coalfield, but this source will be exhausted in the next century (Weyten, Luyten, Keizer, Willems, & Leysen, 2000). This is aside from the serious environmental impact of the fossil fuels consumption.

In the Copenhagen Climate Summit December 2009, South Africa pledged to reduce carbon emission by 34% in 2020 and 42% in 2025 (Holladay, Hu, King, & Wang, 2009). Research direction in South Africa is geared towards sustainable energy sources that will address the issue of over-reliance on coal and the associated air emissions at the same time. The clean energy policy is formulated to facilitate the move from the heavy polluting coal-based energy industry in South Africa to cleaner energy system particularly in the power industry. The hydrogen economy is geared towards this, to promote the increasing use of cleaner burning hydrogen especially for power generation.

The growing interest in distributed power system has led to investments in fuel cell system. South Africa being the largest producer of platinum is primly positioned to play an active role in fuel cell system development and its application. The country holds about 75% of the global reserve of platinum (Bartels *et al.*2010), the key and most costly component of a fuel cell system. Fuel cell systems have received increased attention in recent years for transportation application due to their potential for high fuel efficiency and low emissions and they also have the attractive feature of low maintenance cost (Sharaf & Orhan, 2014).

A fuel cell is an electrochemical device that converts hydrogen fuel into electric power (Rajasekar, Jacob, Balasubramanian, Sangeetha, & Sudhakar Babu, 2015). It produces electric power by directly converting hydrogen and oxygen into water while directly generating electrical energy from chemical energy without any limits from the Carnot cycle (Hahn, Gabler, Thoma, Glaw, & Lang, 2015). Fuel cells are characterised based on the electrolyte used, start-up time require, temperature and pressure. Proton Exchange Membrane (PEM) fuel cells are the preferred fuel cells compared to the Solid Oxide (SO) fuel cells due to their first start-up time compared to the SO fuel cell with a start-up time of 10 minutes under normal operating conditions (Rajasekar et al., 2015) (Rajasekar et al.). PEM fuel cell is also known for its distinctive feature such as zero or waste generation, high efficiency and low operating temperatures (Taner, 2015).

The bulk of hydrogen is produced from natural gas; a cleaner feedstock compares to coal. However, South Africa has insignificant natural gas resources. Reforming of Liquefied Petroleum Gas (LPG) provides a way out of this crisis. Liquefied petroleum gas (LPG) is a component of crude oil or the condensate of natural gas fields. LPG consists of propane (C_3H_8) and butane (C_4H_{10}) hydrocarbons respectively which have the property of being gases at normal ambient temperature but can be liquefied and kept in the liquid state by quite moderate pressure (Lai, 2013) and it is a clean, low carbon energy source.

South Africa produces 600 000 tons per annum of LPG of which 350 000 tons per annum is exported (Lloyd, 2014). LPG roughly delivers the same power, acceleration, and cruising speed characteristics as gasoline (Laosiripojana, Sutthisripok, Charojrochkul, & Assabumrungrat, 2011). It has the potential to provide electricity to small businesses households for cooking, lighting and refrigeration. Hydrogen can be efficiently produced from the reforming of several compounds e.g. methanol, methane, ethanol, Liquefied Petroleum Gas (LPG) and other oil derivatives (Winter, 2009). Among these feedstock, LPG is a good candidate for hydrogen production in remote areas where natural gas pipelines are not available (Laosiripojana et al., 2011). Hydrogen rich gases can be produced from LPG via various technologies(Kumara et al., 2014):

- Steam reforming
- Dry reforming

- Autothermal reforming

However, specific technical and marketing demands must be met by a fuel processor for ultra-pure hydrogen production and at a very competitive cost (Holladay et al., 2009). For high purity hydrogen production the objective is to maximize hydrogen yield and to minimize carbon monoxide (CO) content (Navarro, Guil, & Fierro, 2015). The system should also be able to process feeds of varying compositions, with minimal reactor volume, able to operate for many years with minimum service and maintenance and minimal shut downs and cold start-ups (Corbo, Migliardini, & Veneri, 2011). Steam reforming of liquefied petroleum gas is seen as the preferable technology for hydrogen production (Senanayake, Stacchiola, & Rodriguez, 2013).

The hydrogen produced from the steam and autothermal reforming process normally consists of carbon monoxide and sulphur compounds which are poisonous to the Proton Exchange Membrane (PEM) (Kolb et al., 2012). It therefore, becomes imperative to find an economic way of removing the contaminants from hydrogen (Bartels et al., 2010) and better still convert some of these compounds such as CO and H_2O to hydrogen and carbon dioxide (for instance via the water gas shift reaction). These challenges have led to growing interest in application of membrane reactors for hydrogen production as alternative to conventional reformers (Bredesen, Peters, Boeltken, & Dittmeyer, 2015). Chemical reactors making use of membranes are usually referred to as membrane reactors (Patrascu & Sheintuch, 2015). The membrane can be employed to add reactants or more commonly for selective extraction of reactants (typically the desired products) from the reaction zone (Noureldin, Elbashir, & El-Halwagi, 2013). Such systems are actually a combination of two unit operations in one step, membrane separation with the chemical reaction (Deutschmann, Beller, Renken, & van Santen, 2012).

One of the products of a given reaction is removed from the reactor through the membrane, forcing the equilibrium of the reaction "to the right" (according to *Le Chatelier's* Principle), so that more of that product is produced (Y. Chen et al., 2014). The result is a more compact reactor design and with associated higher conversion, yield and desired purity (Weyten et al., 2000). It has been argued that membrane reactors also allow for a wider range of temperatures and pressures for a reaction (Wetwatana, Kim-Lohsoontorn, Assabumrungrat, & Laosiripojana,

2010). Results have shown that the reactions are preferentially performed at high pressures rather than low pressures since higher pressures allow much smaller reactors and more efficient purification (Augustine, Ma, & Kazantzis, 2011). Membrane reactors can be advantageous also for sequential endothermic and exothermic reactions, by using the product extraction to promote heat transfer (Bhargav, Lyubovsky, & Dixit, 2014). All these result in significantly reduced reactor volume, lower capital costs, and often fewer side-reactions.

Palladium membranes are used for hydrogen selection and purification. When compared to porous membrane reactors, palladium membrane reactors give higher hydrogen selectivity (Schädel, Duisberg, & Deutschmann, 2009). These membranes are known to exhibit high permeability to hydrogen. Typically, Palladium membrane is produced by the electroless plating of Pd on the oxidised porous stainless steel (PSS) with a 0.5μm grade (Maximini, Engelhardt, Brenner, Beckmann, & Moritz, 2014) on porous alumina supports by sputtering by the metal-organic chemical vapour deposition. The electroplating technique has the advantages of easy operation and simple equipment (Laosiripojana et al., 2011).

1.2 Problem Statement

The government of South Africa in 2003 released a white paper on fostering the uptake of renewable energy in the economy. The policy has a number of objectives, that include: ensuring that equitable resources are invested in renewable technologies; directing public resources for implementation of renewable energy technologies; introducing suitable fiscal incentives for renewable energy and; creating an investment climate for the development of renewable energy sector (South Africa. Department of Minerals and Energy, 2003: page 1).

Liquefied petroleum gas (LPG) is a potential source of low-cost hydrogen production due to its higher energy density, easy storage and the well-established infrastructure for processing and distribution. The primary technology of steam reforming together with the purification stages required for high purity hydrogen production poses an economic challenge. A membrane reactor that permits selective separation of the reforming products will enable a cost-effective LPG reforming and increased hydrogen purity. Therefore, this study investigates the

feasibility of a palladium membrane reactor for the production of ultra-pure hydrogen from the products of an LPG pre-reformer.

1.3 Research Aims and Objectives

The overall goal of this project is to investigate the feasibility and the associated performance of employing a palladium-based membrane reactor for the production of ultra-pure hydrogen from the products of a liquefied petroleum gas (LPG) pre-reformer. It reported the optimal process conditions for the production of high purity hydrogen from the LPG feedstock. In realising this aim, the specific objectives include,

a) The optimisation of the pre-reformer system process variables (including temperature, steam-to-carbon ratio and pressure) versus the reformate composition.
b) Determining the ideal pre-reformer mixture to be fed into the Palladium membrane reactor at the optimal conditions.
c) Evaluation of the performance of a Pd-based membrane in relation to maximizing the yield of hydrogen from the feedstock as well as minimizing the CO content of the reformate.

1.4 Motivation for the study

Hydrogen as an alternate fuel has been the new focus for cleaner energy technologies especially for use in Polymer Exchange Membranes (PEM) fuel cells. Currently, most of the hydrogen in South Africa is produced from fossil fuels particularly natural gas, oil and coal. Hydrogen produced from these sources contains residual compounds such as carbon monoxide and sulphur compounds, which are poisonous and could therefore; poison the PEM catalyst even at concentrations as low as 10ppm (Bereketidou & Goula, 2012).

An economic way of removing the contaminants from hydrogen is therefore required. There are three major approaches to separating hydrogen from the reformate gases: a) pressure-swing adsorption (PSA) b) fractional distillation, and c) membrane separation (Zornoza, Casado, & Navajas, 2013). Currently, membrane separation is considered to be the most promising for portable power applications because of low energy consumption, possibility for continuous

operation, lower volume, ease of operation and cost effectiveness (Gutierrez, Karinen, Airaksinen, Kaila, & Krause, 2011).

Dense membranes made of palladium, nickel, platinum, and the metallic elements in group III-V of the periodic table are able to transport hydrogen in dissociated form and are thus capable of theoretically infinite selectivity (Velasco, Lopez, Cabrera, Boutonnet, & Järås, 2014). Palladium membranes are of particular note for their high permeability and tolerance to hydrocarbon containing streams, and their ability to self-catalyse the H_2 dissociation reaction. Hence, the relevance of this study lies in the development of optimal process conditions for a palladium membranes reacting system for the production of ultra-pure hydrogen from LPG feed stocks.

1.5 Scope of Study

The study will be limited to the reforming of the propane component of the LPG and at steady state operation. The simulation study will be performed at temperature ranging from 50 – 850^{o}C to locate the optimal temperature range that will maximize the yield of hydrogen. The reformate will be fed to the palladium membrane reactor and the permeate results reported.

1.6 Outline of Thesis

The content of this work is composed of five chapters which are as follows: **Chapter 1** which gives the background on hydrogen economy, different reforming technologies, membrane reactors and palladium-based membrane reactors. **Chapter 2** gives comprehensive literature review of LPG reforming and modelling of the palladium membrane reactor for the production of ultra-pure hydrogen. **Chapter 3** focuses on the methods development and optimisation of LPG for optimum hydrogen production in the palladium membrane reactor. **(3.1)** which focuses of the LPG reforming simulation model and section **(3.2)** which focuses on the palladium membrane determined using Engineering Equation Solver (EES) **Chapter 4** consists of two sections, **(4.1)** which focuses on the LPG reforming simulation and section **(4.2)** which focuses on the palladium membrane results

using EES. **Chapter 5;** summarizes and concludes on the work performed and provides recommendations for future work.

Chapter 2: Literature Review

2.1 Hydrogen Economy

Due to the depletion of non-renewable fossil fuels and increasing global warming caused by the combustion of fossil fuels has triggered an interest in research finding for better energy source that will produce low emission (Pudukudy, Yaakob, Mohammad, Narayanan, & Sopian, 2014). Hydrogen is widely regarded as a clean energy carrier for future use in both transportation and electricity sectors. Hydrogen as an alternate fuel has been the new focus of cleaner energy technologies especially as feedstock into Proton Exchange Membranes (PEM) fuel cells for power generation.

Hydrogen is considered as alternative energy source because it can be converted to thermal and electrical energy (Al-Mufachi, Rees, & Steinberger-Wilkens, 2015). Due to the weakness of the gravitational field pure hydrogen gas is currently not available for use therefore hydrogen fuel must be produced from a variety of sources (Almansoori, Liu, Elkamel, & Fowler, 2015). The industrial production of hydrogen is dominated by fossil fuels as feedstock (Rajasekar et al.). Hydrogen can be produced from both renewable and non-renewable sources (Sharma & Ghoshal, 2015).

Currently, and in the immediate future, the bulk of hydrogen world-wide will still be produced from fossil fuels including natural gas, oil and coal with only 4% originating from water electrolysis (Gade, Thoen, & Way, 2008). Amongst the fossil fuels, coal is the most widely distributed and abundant (Battersby, Duke, Liu, Rudolph, & Costa, 2008) particularly in South Africa. The country though has a modest local natural gas reserve but is strategically placed to economically access and exploit large gas reserves in Mozambique, Angola, and increasingly the rich basin off the coast of West Africa. Aside from the fossil fuels, there is growing interest in converting hydrocarbon fuels such as petroleum gas, gasoline and diesel into hydrogen rich gases.

South Africa experienced energy crisis in the year 2008, resulting in domestic and industrial users having to suffer power outage all over the country (Inglesi, 2010).

This has prompted South Africa to investigate alternative sources for energy production due to the substantial economic loss suffered (Hernantes, Rich, Laugé, Labaka, & Sarriegi, 2013).
Fuel cells are seen as having potential in playing a major role in the substantial transformation to a more flexible, less vulnerable energy system which meets the need for a cleaner, more effective and cost effective energy supply (Watkins & McKendry, 2015).

The choice still remains to be made as to which method of hydrogen production will be appropriate for the fuel cell process (Niaz, Manzoor, & Pandith, 2015). Apart from the concerns of being non-renewable, there is an increasing concern on the problem of air pollution which is providing more incentives for less polluting and sustainable sources (Hou et al., 2015).

2.2 Hydrogen Production Technologies

Hydrogen is produced from hydrocarbons such as natural gas, liquid petroleum gas gasoline, and methanol via several processes (Jörissen, 2012). The processes for hydrogen production from LPG include:

- Steam reforming of Liquid Petroleum Gas (LPG)
- Dry reforming of LPG
- Autothermal reforming of LPG

The major difference between these reforming technologies is that steam reformers use steam, dry reformers use carbon dioxide and autothermal reformers use both steam and oxygen (Abbasi, Farniaei, Rahimpour, & Shariati, 2014). Fuel processors use air and steam as practical oxidants (Kolb et al., 2012). When air is used an oxidant it is known as partial oxidation and when steam is used as oxidants it is known as steam reforming (Mortola, Damyanova, Zanchet, & Bueno, 2011). However, the selection of a reformer type highly depends on the number of factors relating to the characteristics of each technology. Steam reforming was chosen as a method of hydrogen production for this due to the size of production plant considered and available feedstock (Noureldin et al., 2013).

The water-gas shift (WGS) and preferential oxidation (PROX) reactions are added for further conversion of CO to more hydrogen and/or for further purification of the hydrogen in the reformate to prevent contamination of the fuel cell (Senanayake et al., 2013).

2.2.1 Steam Reforming of LPG (SR)

Steam reforming of hydrocarbon is an important chemical processes providing (H_2 and CO_2) which can subsequently be converted to numerous valuable basic chemical (Deutschmann et al., 2012). Nickel and Rhodium are the most catalysts used for the reforming of natural gas and nickel is the conventional catalysts in the industry (C. j. Liu, Ye, Jiang, & Pan, 2011). Rhodium has been extensively studied as a catalyst for steam reforming (SR) of methane and propane according to literature(Abatzoglou & Fauteux-Lefebvre, 2015).

LPG typically consists of C_4H_{10} and C_3H_{10} (with various ratios depending on its source) that exists as liquid under modest pressure and ambient temperature. Currently, LPG has been converted to hydrogen using the steam reforming process catalysed by previous metal catalysts (for example. rhodium, ruthenium and platinum). The main products from this reaction are H_2, CO and CO_2. Nevertheless, the formations of C_2H_6, C_2H_4 and CH_4 are also observed in the product gas due to the decomposition of LPG and methanation reaction (Wetwatana et al., 2010). The by- products formation and (or decomposition of LPG to carbon can contribute to decline in the catalytic activity. The catalyst stability can be improved and the carbon formation can be reduced by the addition of O_2 and H_2O in the oxidative steam reforming (Wetwatana et al., 2010). LPG reforming reactions can be described as follows (Bhargav et al., 2014):

Main reaction:

$$C_3H_8 + 3H_2O \rightarrow 3CO + 7H_2 \qquad \Delta H = 497.9 \quad kJ/mol \qquad (1)$$

$$C_4H_8 + 4H_2O \rightarrow 4CO + 8H_2 \qquad \Delta H = 649.9 \quad kJ/mol \qquad (2)$$

Minor reactions:

$$CO + H_2O \leftrightarrow CO_2 + H_2 \qquad \Delta H = -40.6 \quad kJ/mol \qquad (3)$$

$$C_3H_4 + CO_2 \rightarrow 2CO + 2H_2 \qquad \Delta H = 247 \quad kJ/mol \qquad (4)$$

$$CO_2 + 2H_2 \rightarrow C + 2H_2O \qquad \Delta H = -131 \quad kJ/mol \qquad (5)$$

$$C_3H_4 \rightarrow 3C + 2H_2 \qquad \Delta H = 75 \quad kJ/mol \qquad (6)$$

$$2CO \rightarrow 2C + CO_2 \qquad \Delta H = -172 \quad kJ/mol \qquad (7)$$

In the SR process, the required superheated process steam, propane and butane is mixed and passed over a catalyst bed to produce mainly synthesis gas. The main propane and butane feed is pre-treated to ensure that the feed sent to the catalyst bed is sulphur-free.

The overall process consists of reforming steps, water gas shift, WGS, and other minor reactions (equations 4 and 5) and propane disproportionation (equation 6) (Rostrup-Nielsen, 2008). Synthesis gas (mixture of hydrogen and CO) is produced by the irreversible reaction reforming steps involving reaction of propane (or LPG) with superheated steam at 750-800^{o}C (Seo et al., 2009). The water gas shift (WGS) occurs in two steps, the low temperature which occurs at 190-230^{o}C and high temperature shift that occurs at 350-420^{o}C producing hydrogen and carbon dioxide by consuming the carbon monoxide in the reforming step.

The extent of the reactions 3 through 6 and the reversible (Yoshida et al., 2009) depends on the following process conditions: steam to carbon ration, S/C, temperature, pressure, and the type of catalyst and support used (Steynberg, 2004). A heat jacket is installed in the reactor to heat the tubes filled with catalyst. This is due to the fact that the reactions are highly endothermic, and the SR reactor temperature is maintained by the heat released in the burner fitted (Maximini et al., 2014).

In Figure 2.1 Laosiripojana et al. (2011) reported his findings on a study which was based on determining the pre-eminent catalyst for LPG (C_3H_8 and C_4H_{10}) reforming the focus of this work was based on comparing Ni/Rh supported on Gd-CeO_2 (CGO) or Al_2O_3 at the temperatures 750-900 ^{o}C (with LPG/H2O ratio of 1.0/4.0). The authors reported that adding O_2 and H_2 over Ni/CGO and Ni/Al_2O_3 reduced the amount of decomposition and promoted the conversion of LPG to CO and CO_2. He also observed that Rh catalyst supported on CGO favoured the production of hydrogen yield in LPG reforming. This catalyst will be used on this work to increase the reaction rate in LPG reforming for the production of ultra-pure hydrogen.

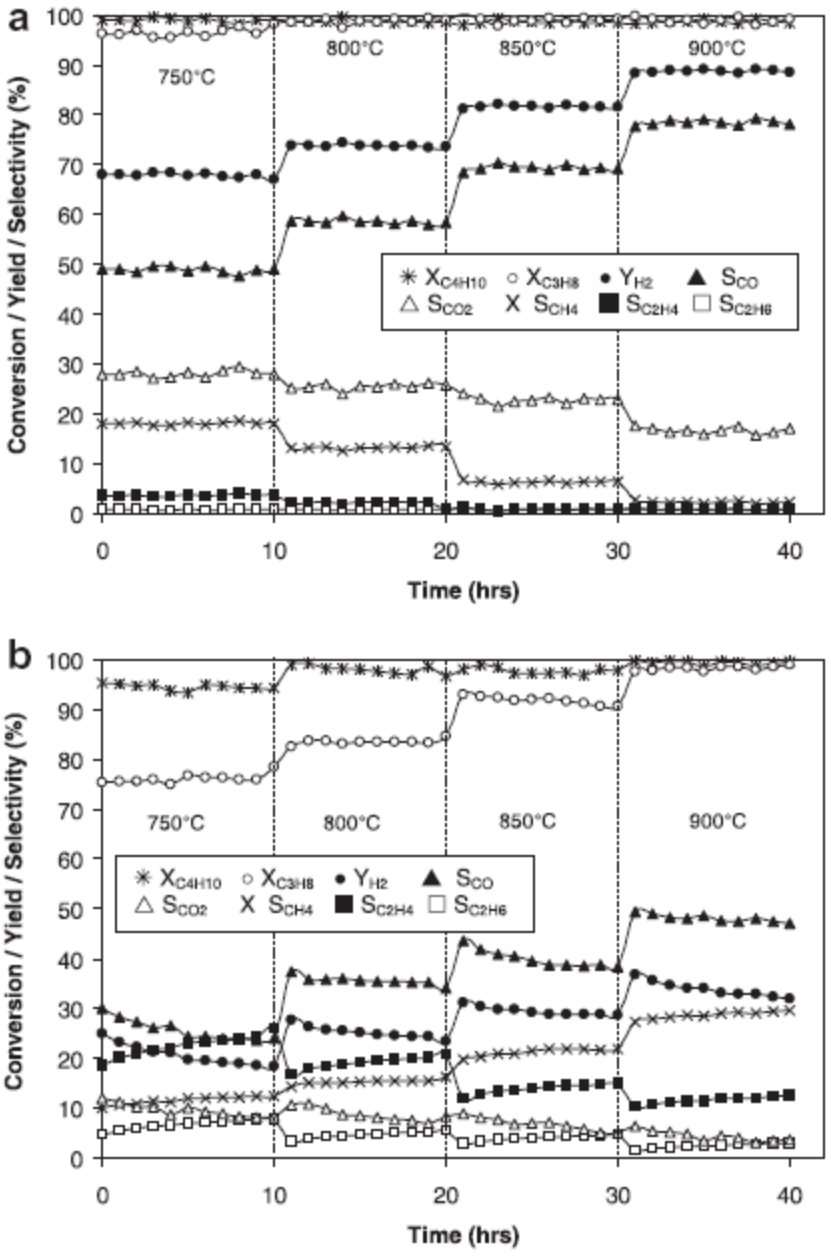

Figure 2. 1 Conversions and product distributions from steam reforming of LPG over (a) Rh/CGO and (b) Ni/Al_2O_3 (with LPG/H_2O ratio of 1.0/4.0) at several temperatures (Laosiripojana et al., 2011).

The simulation behaviour of propane in SR reactor with increasing temperature and steam carbon ratio was reported by Schädel *et al.* (2009) as presented in Figure

2.2. It can be observed that that the propane conversion is directly proportional to temperature and steam carbon ratio.

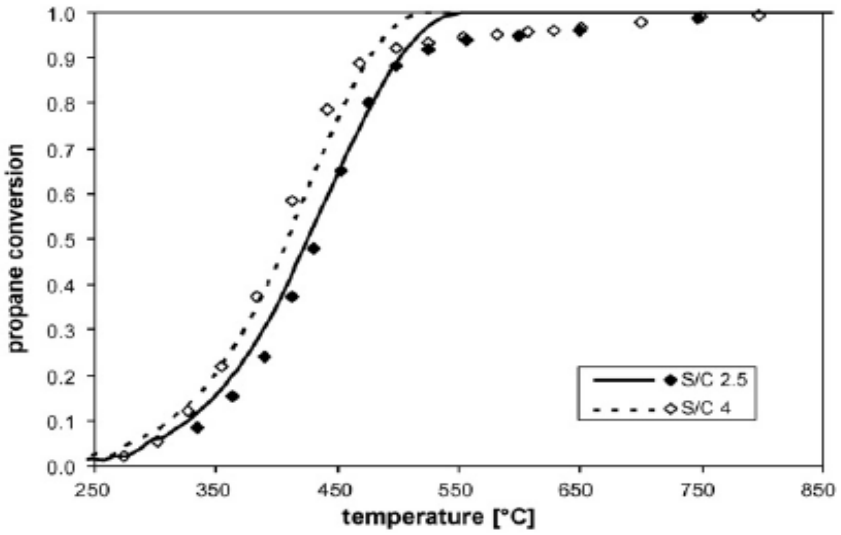

Figure 2. 2: Propane conversion as function of temperature for varying S/C in SR of propane (catalyst with 900 cpsi); symbols; experiment; lines; model predictions (Schädel et al., 2009).

Schädel *et al.* (2009) performed a study on the reforming of methane, ethane, propane and butane at the temperature range and steam carbon ratio of 250 - 900 ^{o}C and 2.2 - 4) respectively. He observed that an increase in temperature and steam carbon ratio results in a large hydrogen yield for all hydrocarbons (Figure 2.3). This will be used to compare the results that were obtained from this work focusing mainly on the propane.

Feyza *et al.* (2007) also performed a study and shown that over a Pt–Ni bimetallic system, low temperature favours high hydrogen purity that is low CO concentration in the LPG reformer product (Figure 2.4), which is desirable. However, low temperature will result in reduce reaction rate and hence lower yield of hydrogen.

The same author in Figure 2.5, shows the effect of residence time on CO concentration in a conventional LPG reformer. Residence time is determined by reactor volume. At low residence times the composition of CO in the reformer product becomes intolerable. Figure 2.6 shows that a decrease in residence time

(i.e. an increase in the total flow rate) enhances hydrogen production, whereas H_2/CO selectivity does not follow the same trend. To get over these problems, a membrane reactor becomes attractive as explained earlier.

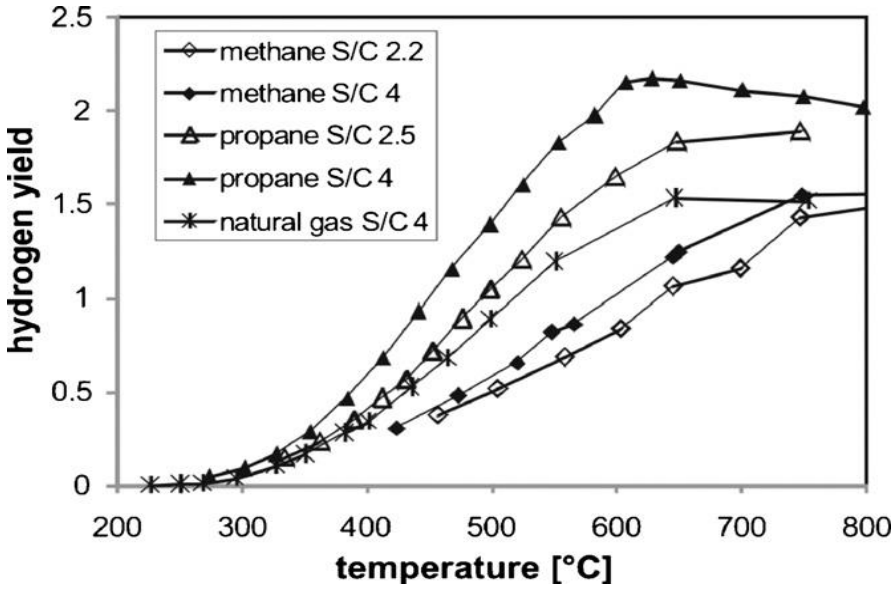

Figure 2. 3: Comparison of experimentally determined hydrogen yields in SR of methane with S/C 2.5 (◊) and S/C 4 (♦), steam reforming of natural gas with S/C 4(*), steam reforming of propane with S/C 2.5 (Δ) and S/C 4 (▲) (Schädel et al., 2009).

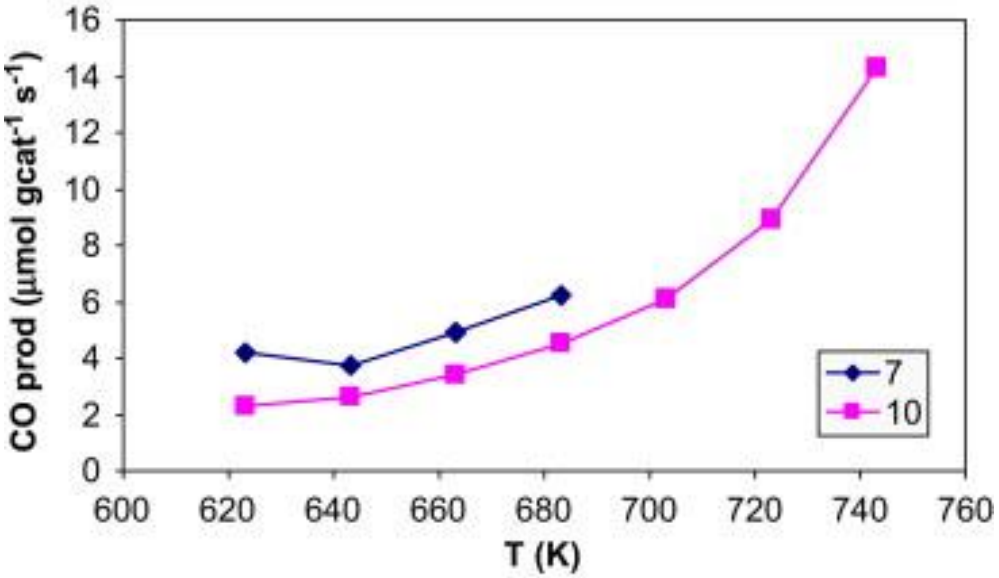

Figure 2. 4: Low CO content of the product stream at high H_2 production activity can be explained only by secondary WGS. [7: S/C=5, Set 10: S/C=7; C/O_2=2.70, W/F=0.51] (Gökaliler, Göçmen, & Aksoylu, 2008).

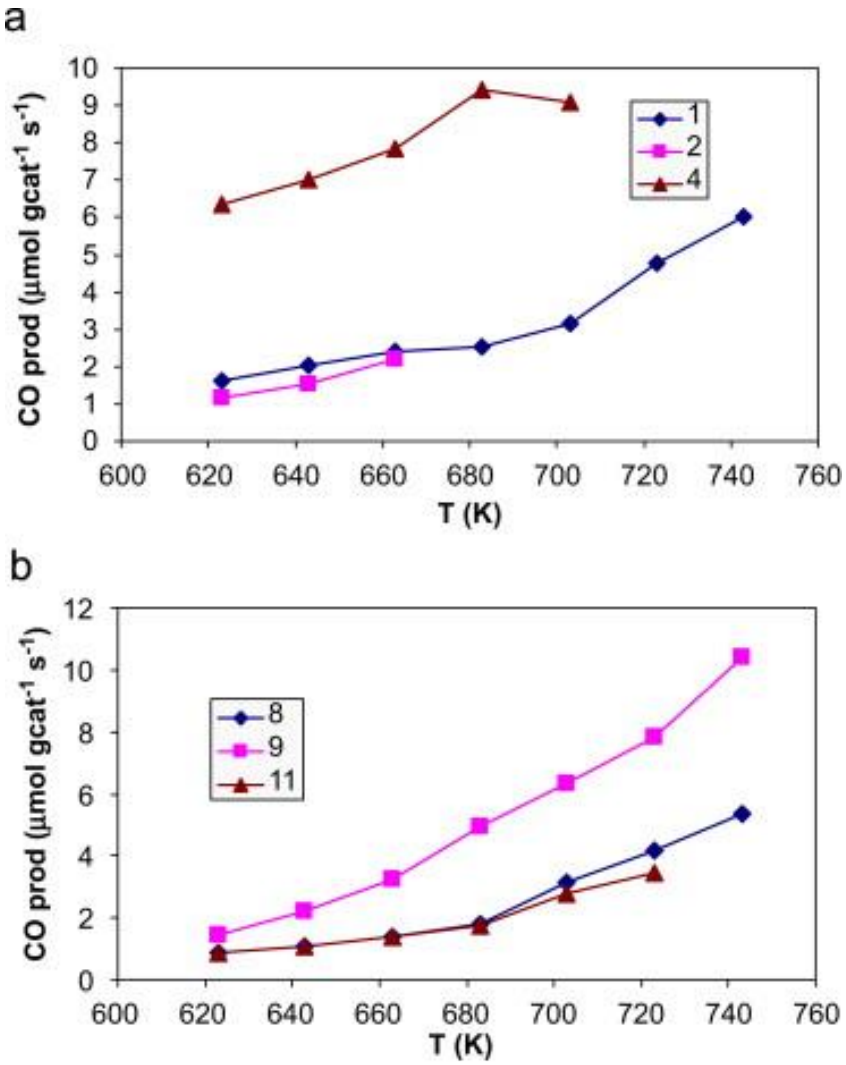

Figure 2. 5: Low residence times lead to an increase in CO production [(a) Set 1: W/F=1.12, Set 2: W/F=1.37, Set 4: W/F=0.51; C/O_2=2.12, S/C=5; (b) Set 8: W/F=1.37, Set 9: W/F=0.51, Set 11: W/F=1.12; C/O_2=2.12, S/C=7] (Gökaliler et al., 2008).

From other data, the author concluded that over the tested Pt–Ni bimetallic system, the hydrogen production rate increases with increasing temperature; the selectivity for hydrogen is highest at low temperatures and tends to decrease with increasing temperature. The optimum conditions were found to be a steam/carbon ratio of 7, a carbon/oxygen ratio of 2.70 and a residence time (W/F) ratio of 0.51. The highest hydrogen/carbon monoxide production ratio 5:6, was obtained for the 1:1 propane/*n*-butane mixture under these conditions.

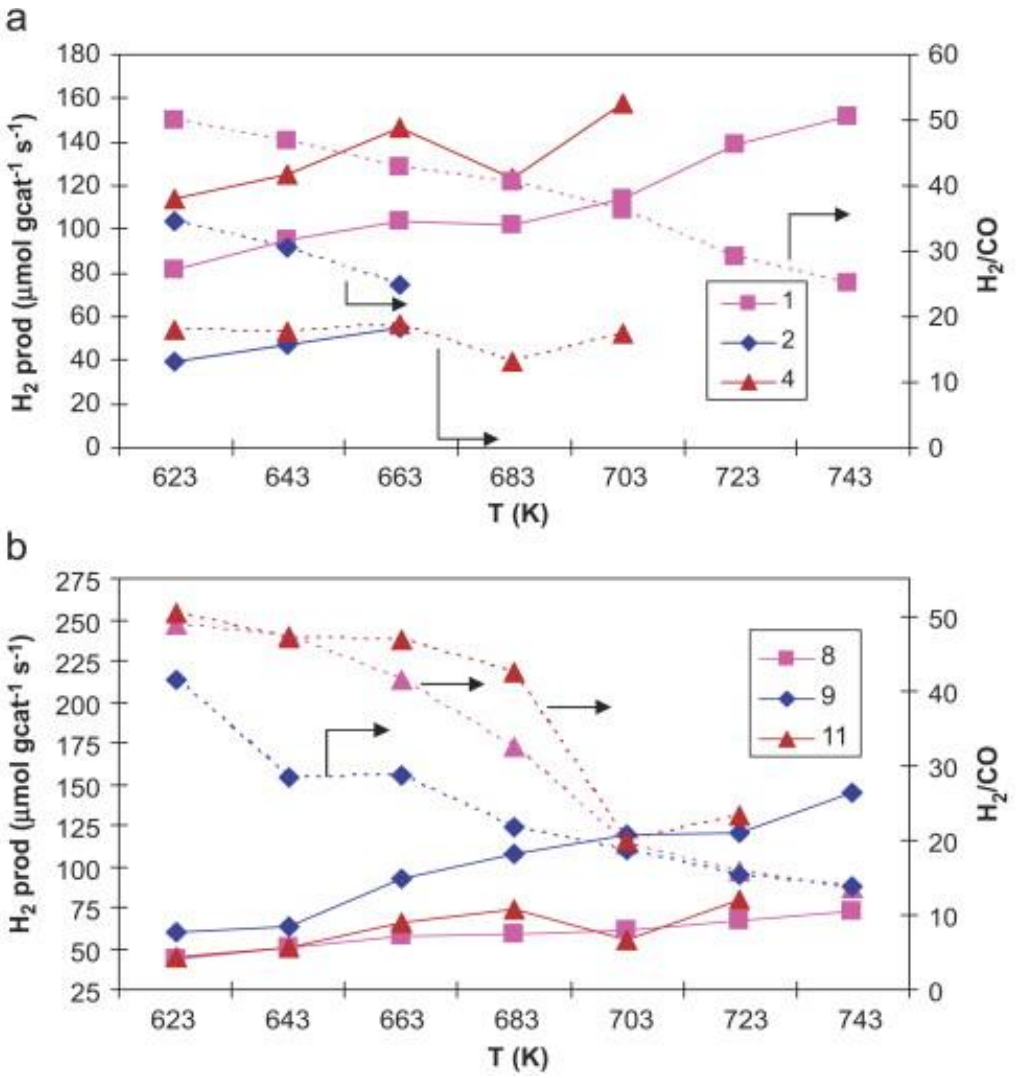

Figure 2. 6: Hydrogen production as a function of residence time [(a) Set 1: W/F=1.12, Set 2: W/F=1.37, Set 4: W/F=0.51; C/O_2=2.12, S/C=5; (b)Set 8: W/F=1.37, Set 9: W/F=0.51, Set 11: W/F=1.12; C/O_2=2.12, S/C=7] (Gökaliler et al., 2008).

2.2.2 Dry Reforming of LPG

Dry reforming is a method of producing synthesis gas (mixture of hydrogen and carbon monoxide) from the reaction of carbon dioxide with propane etc (Hou et al., 2015) . Synthesis gas is conventionally produced via steam reforming reaction. However, there has been growing interest in dry reforming. The propane carbon dioxide reaction is illustrated by the following equation:

$$C_3H_8 + 3CO_2 \rightarrow 6CO + 4H_2 \quad \textbf{(8)}$$

Dry (CO_2) reforming over Ni-based catalysts has received increased attention due to the utilisation of greenhouse gas in one hand and lower syngas ratio compatible

with Fischer-Tropsch synthesis process (Bereketidou & Goula, 2012). Several studies on dry reforming of propane have been published (Siahvashi, Chesterfield, & Adesina, 2013).

Solymosi *et al.* (2005) in Figure 2.7 indicates the findings of dry reforming of propane over rhenium catalyst utilizing a Fourier-transformed infrared spectroscopy and it was discovered that there's was no interaction between propane and the rhenium catalyst supported on aluminium oxide catalyst at 250-300K therefore resulting in the production of di-*σ*-bonded propylene or propylidyne.

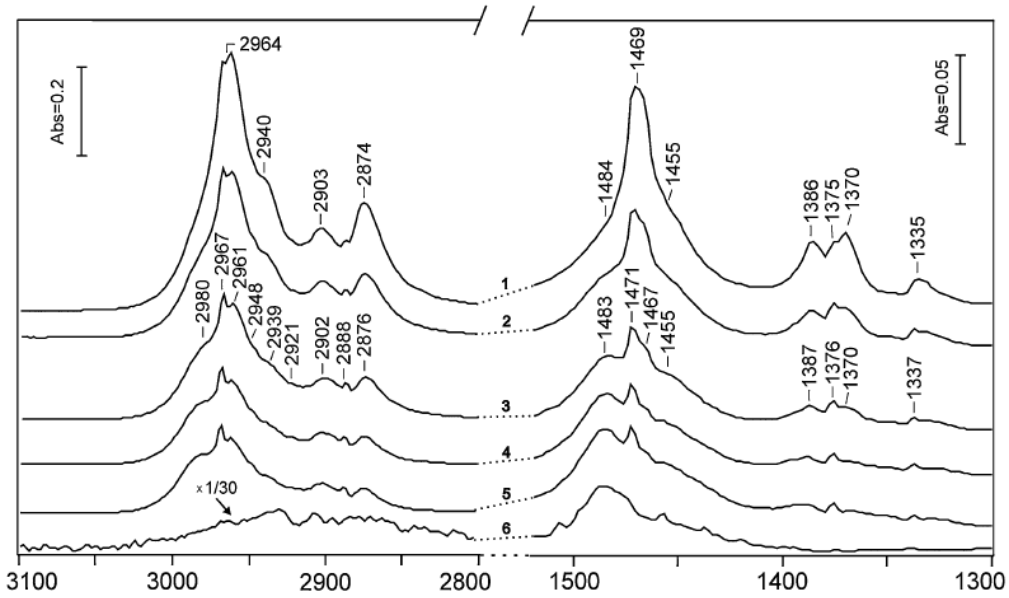

Figure 2. 7: FTIR spectra of 5% Re/Al2O3 (*T* R = 673 K) following the adsorption of propane (1 Torr): (1) 193; (2) 213; (3) 233; (4) 253; (5) 273; (6) 300 K after evacuation (Solymosi, Tolmacsov, & Zakar, 2005).

In Figure 2.8 CO_2 was molecularly absorbed on supported Re and reduced at 673K. The presence of propane induces its dissociation even at 300 K resulting in the formation of adsorbed CO absorbing at ~2041 cm^{-1}.

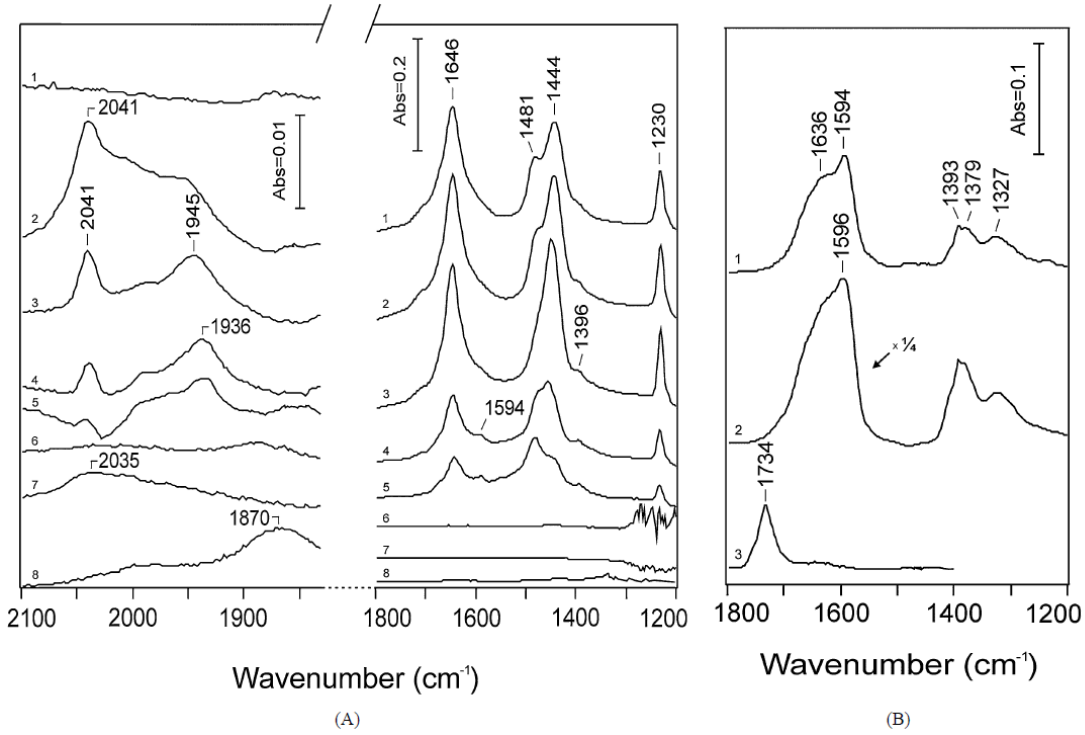

Figure 2. 8: FTIR spectra of 5% Re/Al_2O_3 and 5% Re/SiO_2 (T R = 673 K) following the adsorption of CO_2 (25 Torr) and C_3H_8 + CO_2 (1:1) gas mixture (50 Torr) at different temperatures. Re/Al_2O_3; (1) CO_2, 300 K; (2) C_3H_8 + CO_2, 300 K; (3) 373 K; (4) 473 K; (5) 573 K, Re/SiO2; (6) CO2, 300 K; (7) C_3H_8 +CO_2, 300 K; (8) 573 K. (B) FTIR spectra of different samples following the adsorption of HCOOH (0.1 Torr) and subsequent evacuation at 300 K. (1) 5% Re/Al_2O_3; (2) Al_2O_3; (3) 5% Re/SiO_2 (Solymosi et al., 2005).

The steady state conversion of propane depended on the composition of the reacting gas mixture: it was approximately 50% at C_3H_8/CO_2 (1/3) and approximately 80% at C_3H_8/CO_2 (1/6). The deposition of carbon was observed, the extent of which can be lowered with increasing CO_2 content of the reacting mixture and in the kinetic studies it was inferred that the CO_2 is involved in the rate-determining step of the dry reforming of propane.

2.2.3 Autothermal Reforming

Steam reforming is an endothermic reaction and partial oxidation is exothermic reaction. Autothermal reforming (ATR) or Oxidative steam reforming (OSR) is combination of partial oxidation and reforming, where steam reforming is carried

out in the presence of oxygen (Gutierrez et al., 2011). Instead of external combustion and heat transfer to the steam reforming reactor, in an autothermal reformer, heat is generated internally by partial oxidation, and the heat is then carried by reacting gases and partial oxidation products to the steam reforming unit. ATR is an adiabatic reactor and produced H_2/CO in the ratio of 1:2, which is the ideal for Fischer Tropsch (FT) process (Velasco et al., 2014).

These processes operate by direct oxidation of methane. Recent studies have shown that ATR is also one of the most promising processes to produce hydrogen from natural gas (Getman, Bae, Wilmer, & Snurr, 2011) . The overall equation of an ATR process is:

$$C_3H_8 + \frac{1}{2}O_2 + 5H_2O \rightarrow 3CO_2 + 9H_2 \qquad \Delta H = 85 \quad kJ/mol \qquad (9)$$

Zeng et al. (2010) performed a thermodynamic analysis of hydrogen production from propane by oxidative steam reforming (OSR) utilizing the Gibbs free energy minimization method. The relationship between H_2O/C_3H_8 and O_2/C_3H_8 at four temperatures (300, 500, 700 and 900 ^oC) on the amount of hydrogen produced (moles/mole propane) was observed in Fig 2.9 and it was founded that the hydrogen production is reduced at high O_2/C_3H_8 ratio, especially at high temperatures and H_2O/C_3H_8 ratios. At 700 ^oC, high H_2O/C_3H_8 ratio and low O2/C3H8 ratio are potential for hydrogen generation from propane OSR.

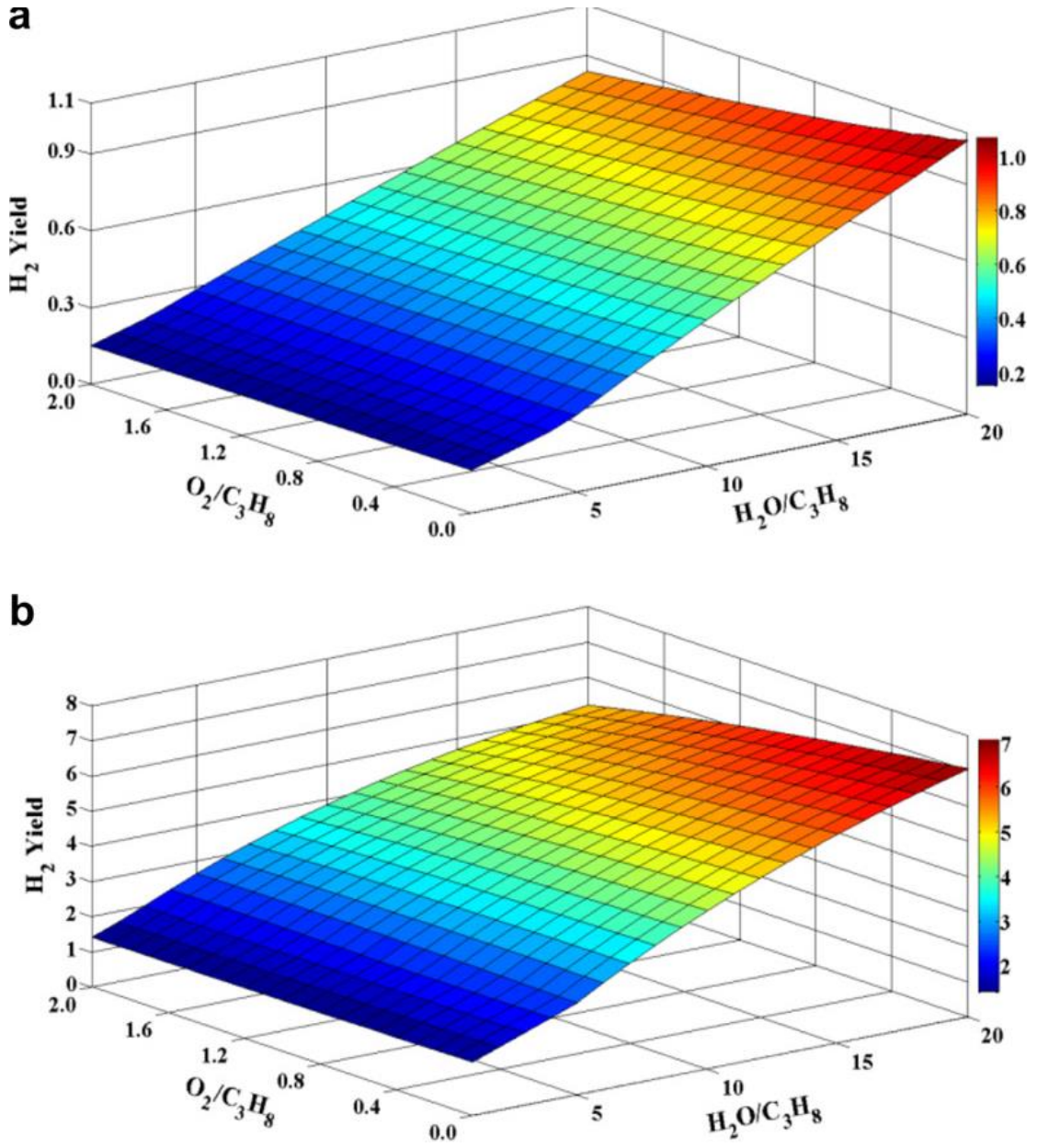
a
H2 Yield
1.1
0.9
0.6
0.3
0.0
2.0
1.6
1.2
0.8
0.4
0.0
O2/C3H8
5
10
15
20
H2O/C3H8
1.0
0.8
0.6
0.4
0.2
b
H2 Yield
8
7
6
5
4
3
2
1
0
2.0
1.6
1.2
0.8
0.4
0.0
O2/C3H8
5
10
15
20
H2O/C3H8
7
6
5
4
3
2

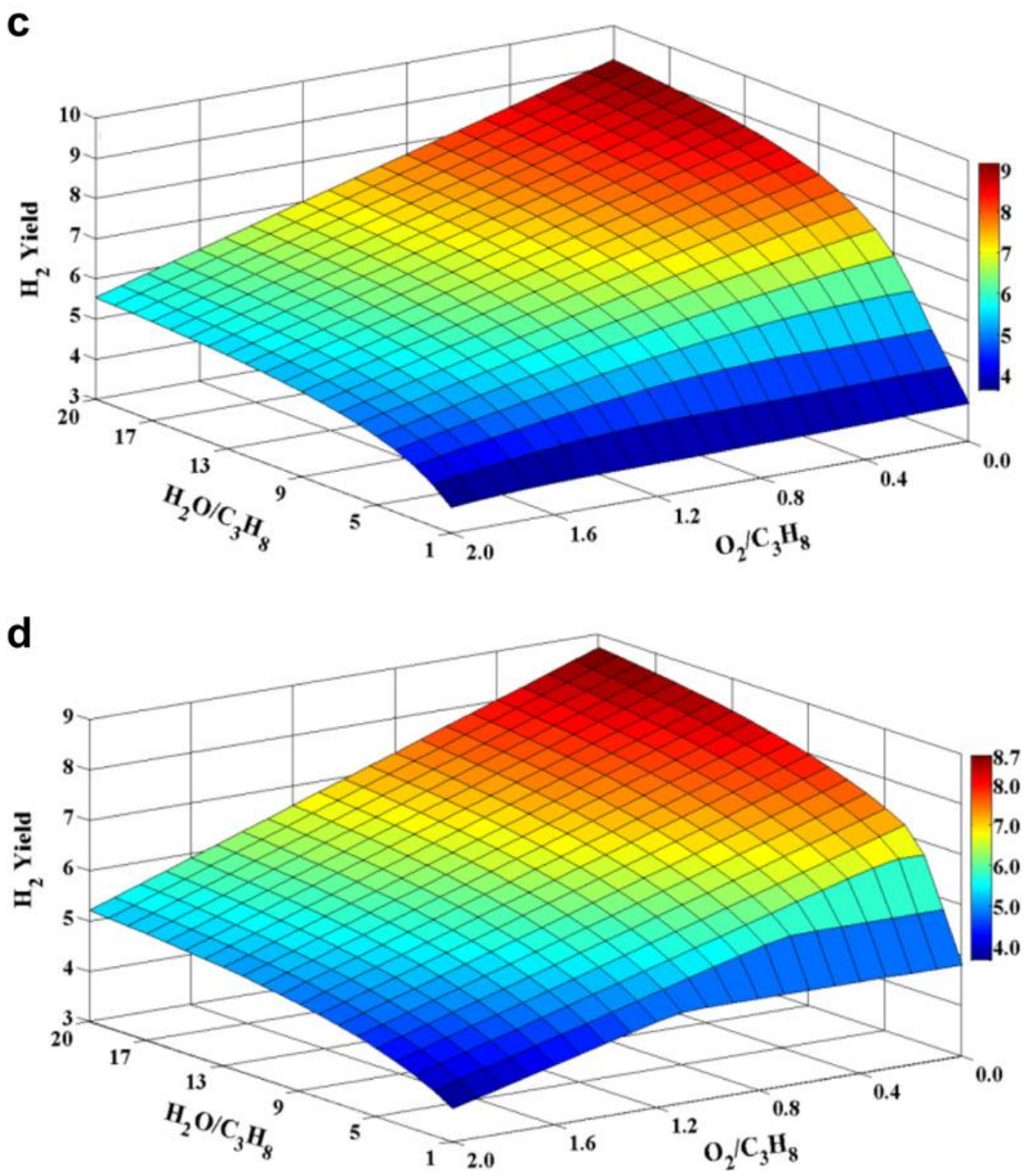

Figure 2. 9: Plots of the thermodynamic equilibrium H_2 yield (mol/mol propane) as a function of H_2O/C_3H_8 and O_2/C_3H_8 ratios at different temperatures: (a) 300 °C, (b) 500 °C, (c) 700 °C, and (d) 900 °C (Zeng, Tian, & Li, 2010).

Zeng *et al.* (2010) in Figure 2.10 also founded that the amount of carbon monoxide yield as known as a poisonous species increases with temperature and exhibit a complex profile with the increase of H_2O/C_3H_8 and O_2/C_3H_8 ratios. At 300 °C, the carbon monoxide yield was at maximum for H_2O/C_3H_8 ratio 4.0 or 5.0 which depended on O_2/C_3H_8 ratio. After reaching the maximum the response surface decreased slightly with increasing of H_2O/C_3H_8 ratio. The curves of 500 °C

indicated a similar trend and approach their highest carbon monoxide yield at H_2O/C_3H_8 = 3.0 for O_2/C_3H_8 ratios between 1.7 and 2.0. For the data of 700 and 900 ^oC, the carbon monoxide yields exhibited maxima at H_2O/C_3H_8 ratio below 4.0 and 3.0 respectively for all O_2/C_3H_8 ratios examined.

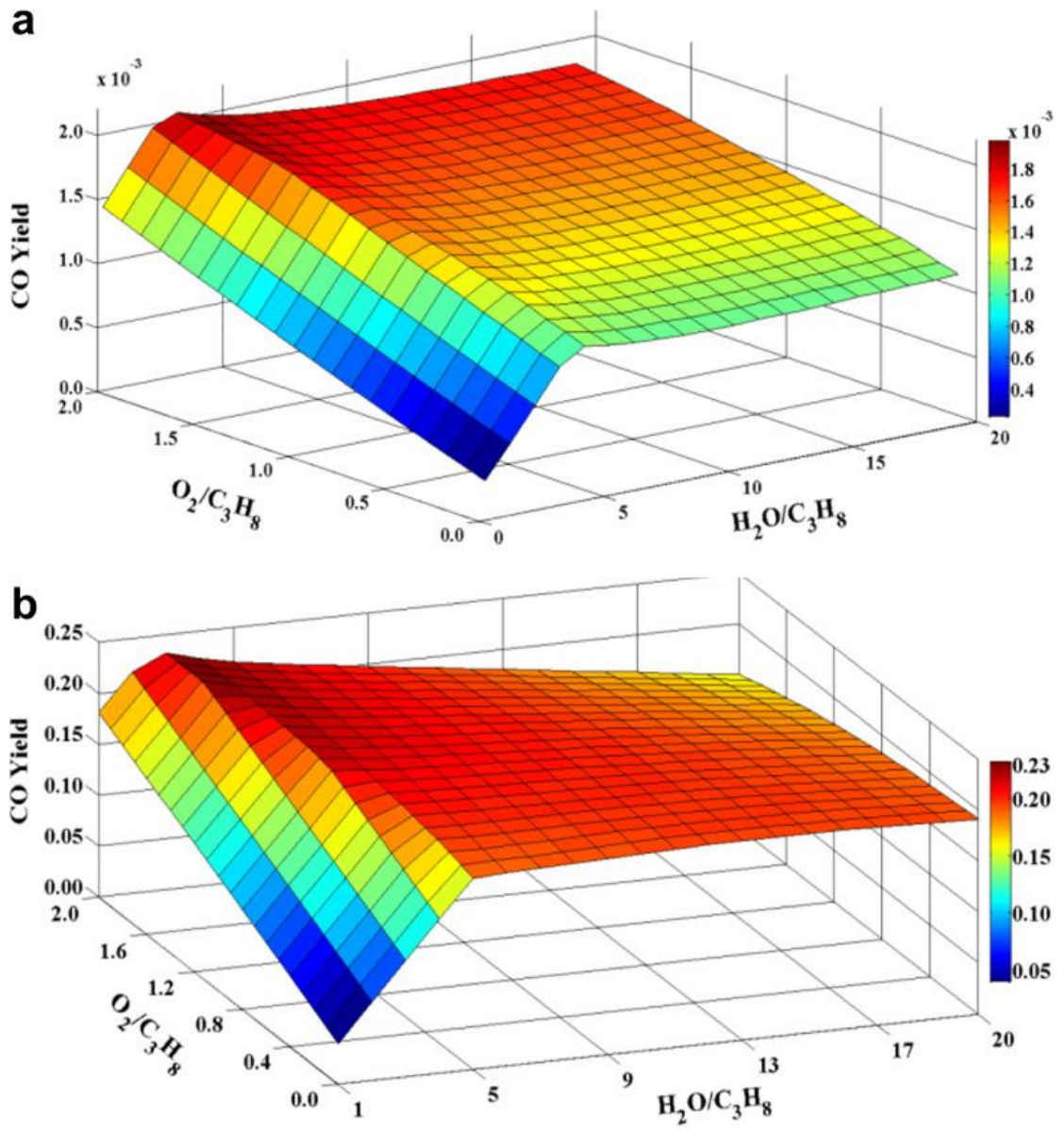

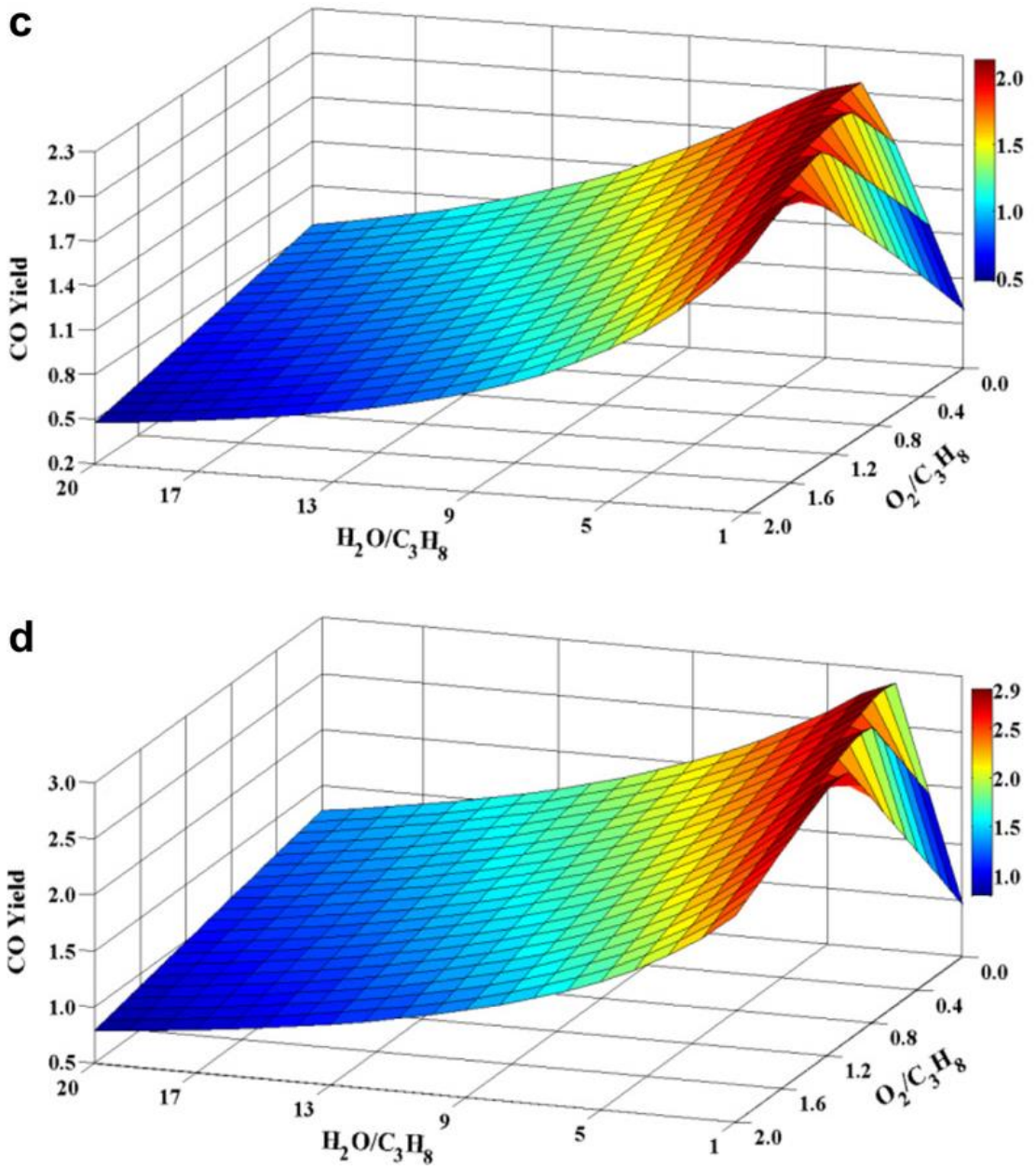

Figure 2. 10: Plots of the thermodynamic equilibrium CO yield (mol/mol propane) as a function of H_2O/C_3H_8 and O_2/C_3H_8 ratios at different temperatures: (a) 300 °C, (b) 500 °C, (c) 700 °C, and (d) 900 °C (Zeng et al., 2010).

Gökaliler *et al.* (2012) performed a study observing the kinetics of autothermal reforming (ATR) of propane on bimetallic platinum-nickel catalyst supported over sigma aluminium oxide at 673K with the aim of obtaining an easy to utilise power-law type equation. Figure 2.11 indicated the initial rate calculation for propane at a partial pressure of 5.57 kPa (runs 2a and 2b). Table 2.1 displayed C_3H_8 partial pressure (kPa) and reaction rate (µmol propane reacted/mg cat x s) data along with the R_2 values obtained in reaction rate calculations. The results in Table 2 showed that as propane partial pressure exceeds ca. 6.5 - 7.0 kPa, sites for propane

activation may become saturated, due to the high C/O_2 ratio in the feed and the constant E_A for the whole partial pressure range.

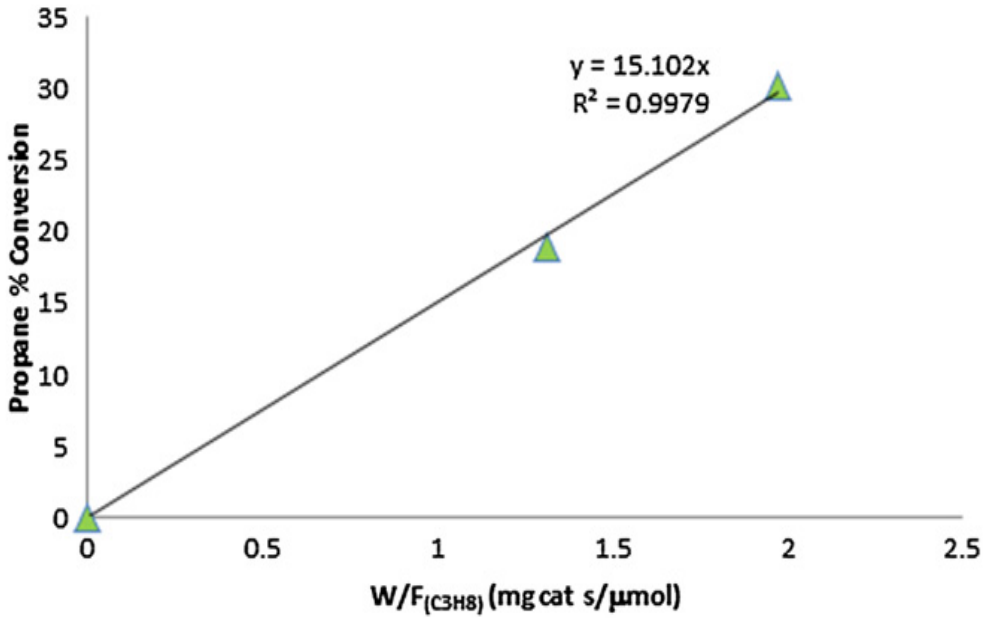

Figure 2. 11: Propane conversion levels for different residence time for a propane partial pressure of 5.57 kPa (Runs 2a and 2b)(Gökaliler, Önsan, & Aksoylu, 2012).

Table 2. 1: Reaction rates at different propane partial pressure levels (Gökaliler et al., 2012).

Run	**C_3H_8 Part, Pres. (kPa)**	**Rate (µmol C3H8) Reacted/mgcat x s)**	**R^2**
1a-1b	5.07	10.95	0.98
2a-2b	5.57	15.10	1.00
3a-3b	6.12	17.12	0.99
4a-4b	6.59	21.39	1.00
5a-5b	7.09	22.01	0.99
6a-6b	7.60	21.56	0.98

Table 2.2 and Figure 2.12 indicate the results obtained for the effect of oxygen partial pressure at constant propane and steam partial pressures at 6.59 and 46.28 kPa, respectively. A feed stream having a fixed oxygen and propane partial pressures of 5.57kPa and 6.59kPa respectively was utilised in which steam partial pressure was changed between 45.28 and 60.80 kPa. In Figure 2.13 In(rate) was plotted against In(Psteam) in order to see the effect of steam partial pressure on

propane consumption rate the experimental data was scattered almost horizontally implying a slightly negative dependence on steam flow rate under the reaction conditions utilised.

Table 2. 2: Reaction rates at different steam partial pressure levels (Gökaliler et al., 2012)

Run	**C_3H_8 Part, Pres. (kPa)**	**Rate (µmol C3H8) Reacted/mgcat x s)**	**R^2**
10a-10b	45.28	24.44	0.99
13a-13b	47.64	17.82	1.00
14a-14b	50.66	18.88	0.95
15a-15b	53.70	23.73	0.99
16a-16b	56.74	19.92	0.99
17a-17b	60.80	18.11	0.97

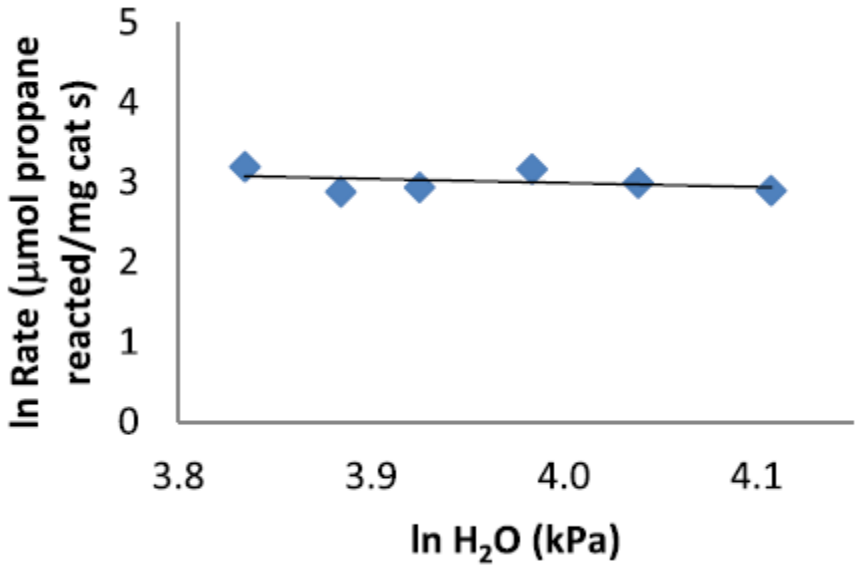

Figure 2. 12: Dependence of reaction rate on steam partial pressure (Gökaliler et al., 2012).

Faria *et al.* (2008) performed a study of autothermal reforming of propane for hydrogen production studied in supported cerium oxide/ aluminium oxide based Pd catalysts, prepared with different palladium precursors. The reaction was carried out under different feedstock conditions and the catalytic activity was evaluated by temperature programmed surface reaction (TPSR). The effects of palladium precursors on the activity and selectivity were studied. The products

distribution and reactant (mol%) as function of temperature for the palladium acetylacetonate catalyst and for R = 5 (O_2/C_3H_8 molar ratio) are displayed in Fig. 2.13. In this case, R = 5 correspond to the stoichiometric amount for total oxidation of propane. In this condition (R = 5), all propane was practically consumed. The conversion of propane was initiated at 523 K and reached about 85% conversion at 923 K.

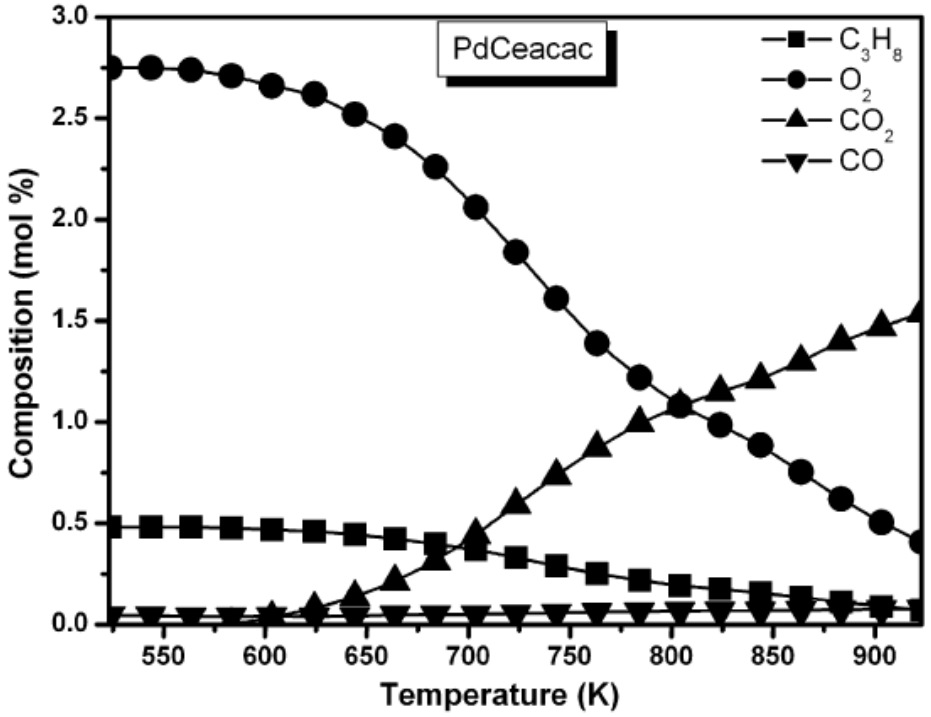

Figure 2. 13: Composition profile of PdCeacac catalyst in R = 5 condition (Faria, Dieguez, & Schmal, 2008).

Figure 2.14 indicates the profiles of thermodynamic equilibrium composition for 1 bar and temperatures varying between 323 and 923 K. The simulated inlet gas was the same as the experiment for R = 2.5, with a feed composition of 0.5% C_3H_8, 1.25% O_2 and 98.25% H_2. The profile indicated that the production of hydrogen initiated at low temperature, reaching a maximum around 600 K and, finally, decreases with increasing temperature.

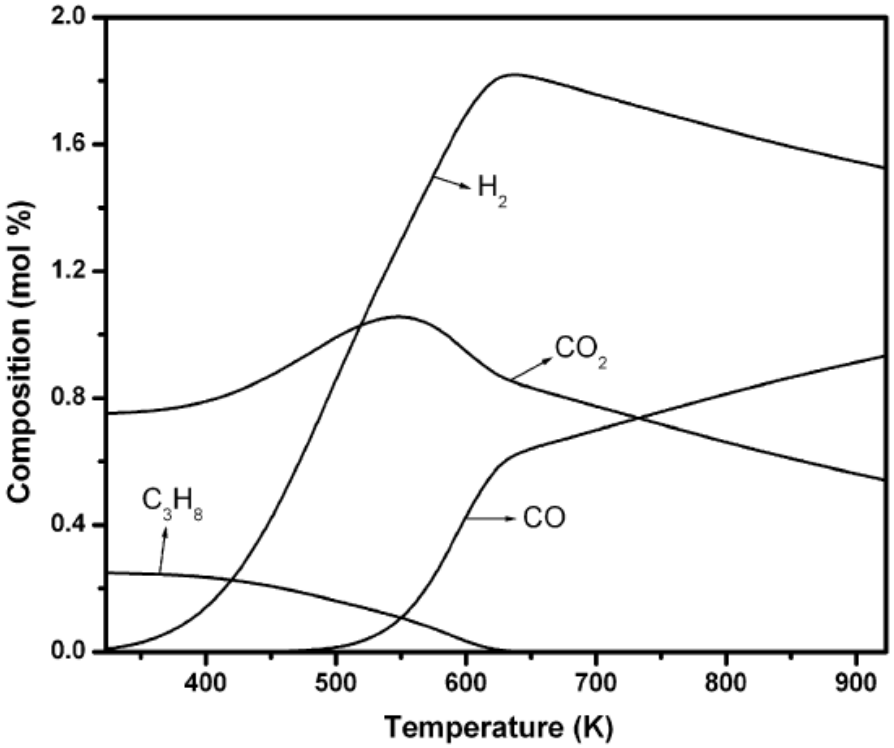

Figure 2. 14: Thermodynamic composition simulation on propane autothermal reforming (R = 2.5) (Faria et al., 2008).

2.3 Water Gas Shift Reaction (WGS)

The water gas shift (WGS) reaction is an exothermic reaction with equilibrium constant increasing in reverse order with temperature (Basile *et al.,* 1996). There has been a growing interest in the water-gas shift reaction for hydrogen production(Basile et al., 2005). When the water gas shift reaction is combined with steam reforming it becomes an endothermic reaction (LeValley, Richard, & Fan, 2014). The water gas shift reaction reduces the CO content in the fuel cell by 1% below the requirement(Guerra, Lanzini, Leone, Santarelli, & Brandon, 2014).

Typically, the WGS occurs in two stages, low temperature (200°C-250°C) in series with high temperature (400°C-500°C) reactors (Ratnasamy & Wagner, 2009). These types of reactions use different types of noble catalysts (Jeong, Potdar, Shim, Jang, & Roh, 2013). Iron-based catalysts are used in high-temperature water-gas shift (HTWGS) reactions and copper-based catalysts for the low-temperature water gas shift (LTWGS) reactions (Pastor-Pérez, Buitrago-Sierra, & Sepúlveda-Escribano, 2014).

The WGS reaction occurs in the water gas shift reactor:

$$CO + H_2O \leftrightarrow CO_2 + H_2 \qquad \Delta H = -41.2\,kJ/mol \tag{10}$$

Bi *et al.*(2009) investigated the water–gas shift reaction in a palladium (Pd) membrane reactor over $Pt/Ce_{0.6}Zr_{0.4}O_2$ catalyst which exhibits much faster kinetics than conventional high-temperature ferrochrome catalysts in the temperature range most suitable for operation of water gas shift palladium membrane reactors for temperatures above 623 K. Figure 2.15 compared carbon monoxide conversion and selectivity to methane over $Pt/Ce_{0.6}Zr_{0.4}O_2$ with the commercial ferrochrome catalyst in the fixed bed reactor at a temperature between 523 and 698 K at atmospheric pressure and Gas Hourly Space Velocity (GHSV) 4000 $kg^{-1}\ h^{-1}$.

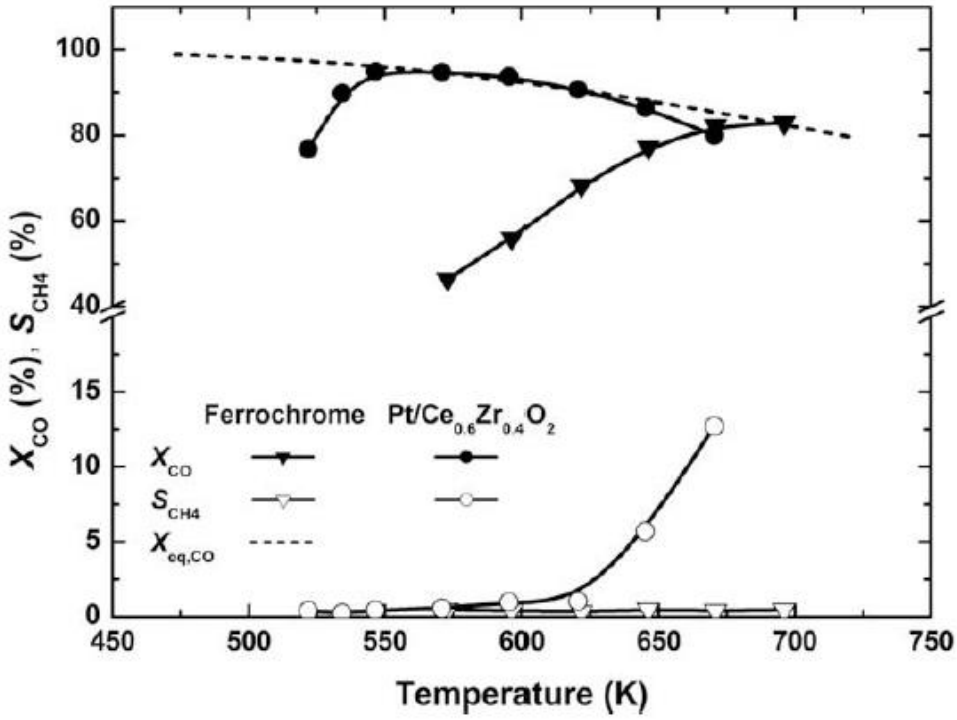

Figure 2. 15: Influence of temperature on CO conversion and CH_4 selectivity during WGS reaction over $Pt/Ce_{0.6}Zr_{0.4}O_2$ and a commercial ferrochrome catalyst in a fixed bed reactor at atmospheric pressure and GHSV 4000 $kg^{-1}\ h^{-1}$. The dashed line indicates thermodynamic equilibrium CO conversion according to Eq. (1) (Bi et al., 2009).

The Pt catalyst exhibited a higher activity than the ferrochrome catalyst over whole temperature range. The carbon monoxide conversion approached the thermodynamic water gas shift (WGS) limit already at 548 K and the carbon

monoxide (CO) equilibrium conversion was 96.1% over the Pt catalyst while the WGS equilibrium curve was only reached at 698 K and the carbon monoxide conversion at equilibrium was 82.4% over the ferrochrome catalyst. Meanwhile the methane (CH_4) formation became noticeable over the Pt catalyst as soon as water gas shift equilibrium carbon monoxide (CO) conversions were achieved and accelerated rapidly above 623 K.

Chen *et al.* (2008) modelled and simulated the behaviour of the high temperature and low temperature water gas shift for the production of hydrogen. Fig. 2.16a and b displayed the distributions of hydrogen and carbon monoxide concentration as well as carbon monoxide conversion of the hot temperature shift reactor (HTSR) and the low temperature shift reactor (LTSR), respectively, along the centreline of the reactor.

Due to the effect of the catalysts the concentrations of hydrogen grew rapidly downstream, the concentrations of carbon monoxide decay substantially. At the exit of the catalyst bed, the values of carbon monoxide conversion of the HTSR and the LTSR are 89.80% and 93.39%, respectively. After that, because of the diffusion of H_2 and CO_2 toward the centreline from the surrounding, the curves of H_2 concentration and CO conversion behind the catalyst bed rise a bit.

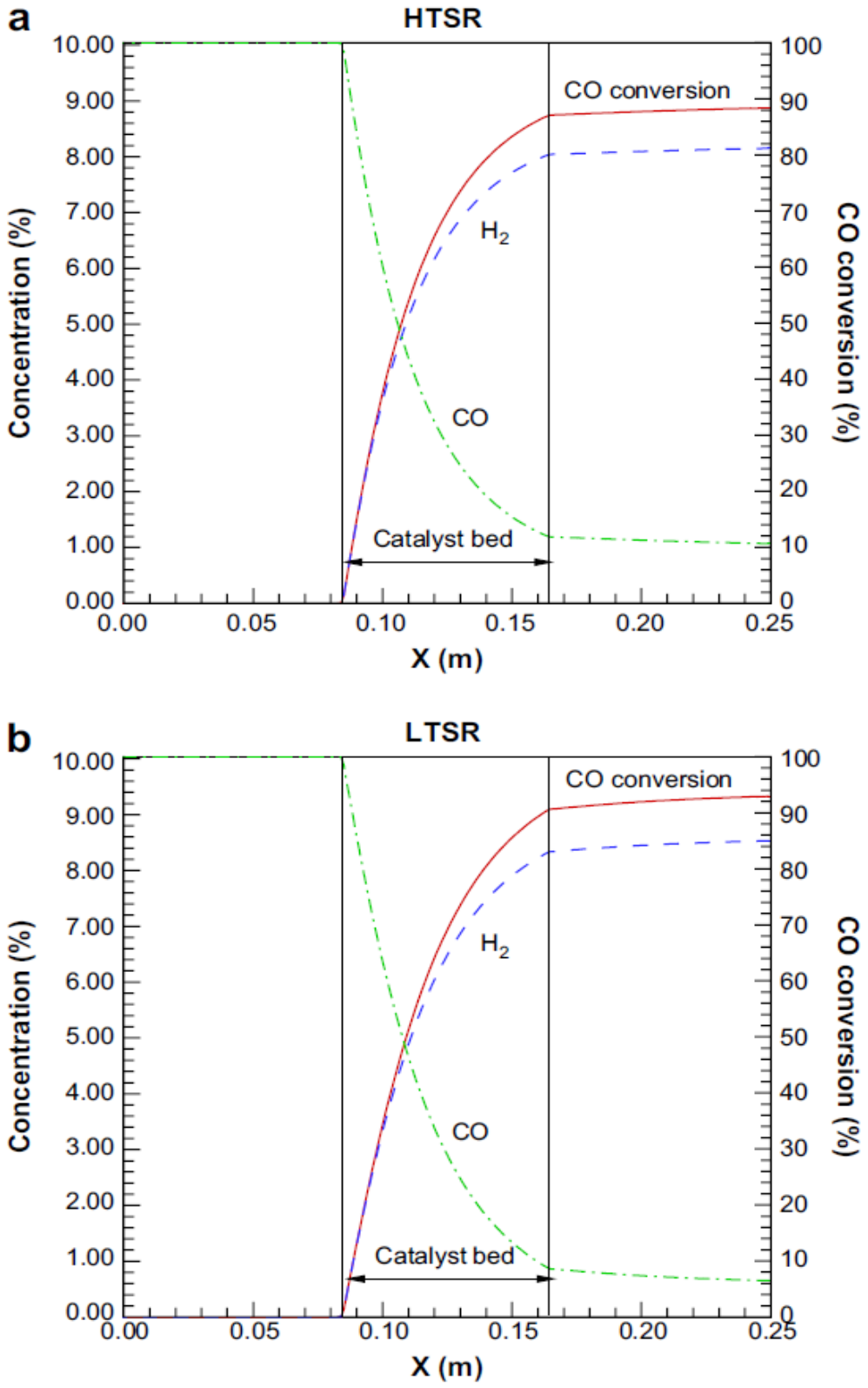

Figure 2. 16: Distributions of H_2 and CO concentrations as well as CO conversion along the centerline of the reactor under the effects of the (a) HTC (steam/CO = 4 and T = 500 ^{o}C) and (b) the LTC (steam/CO = 4 and T = 200 ^{o}C) (W.-H. Chen, Hsieh, & Jiang, 2008).

Figure 2.17 demonstrates the carbon monoxide conversion along the centreline of the reactor. Figure 2.18a indicated that 65.6% of carbon monoxide is transformed into carbon dioxide. Due to this the concentration of the carbon monoxide fast as shown in Figure 2.18b. The efficiency of carbon monoxide conversion from the high temperature shift reactor is not sufficiently high. In the second reaction stage, almost 100% of carbon monoxide conversion is achieved (Fig. 2.17 a), whereby the concentration of carbon monoxide approached zero (Fig. 2.17 b).

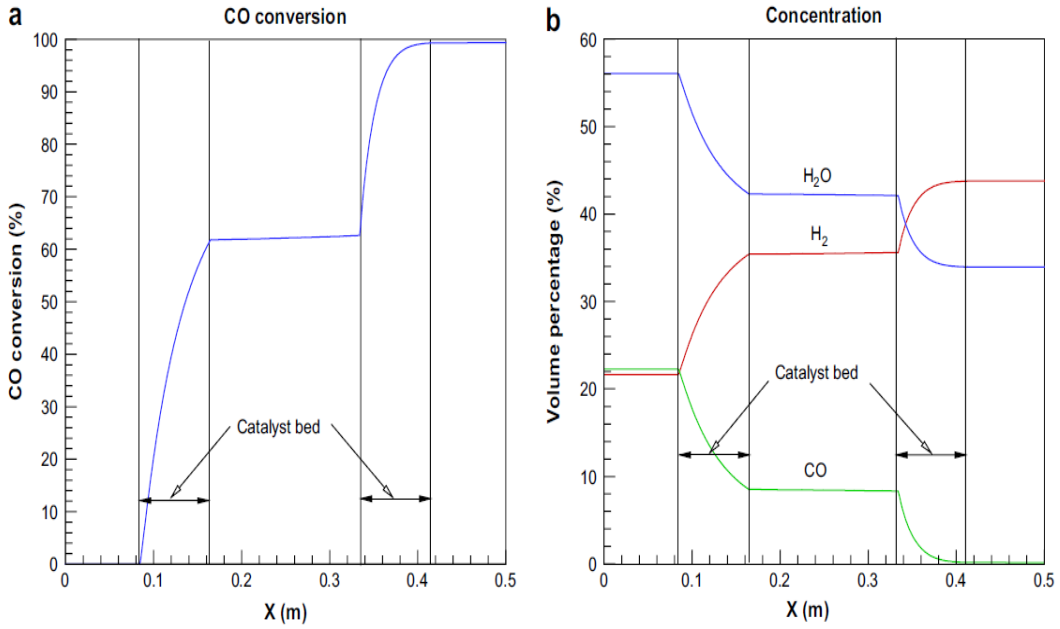

Figure 2. 17: Distributions of (a) CO conversion and (b) concentrations of CO and H_2 in the integrated reactor (W.-H. Chen et al., 2008).

Chen *et al.*(2008) performed an experimental study on the carbon monoxide conversion and hydrogen generation from the water gas shift reaction. The experiment was performed observing important parameters such as the catalyst type, residence time of reactants in a catalyst bed, reaction temperature and carbon monoxide /steam ratio. Two different catalysts, consist of a high-temperature catalyst (HTC) and a low-temperature catalyst (LTC), are taken into consideration.

Figure 2.18a demonstrated the concentrations profiles of carbon monoxide and carbon dioxide and the carbon monoxide conversion under the effect of the HTC. The concentrations were presented in terms of the volumetric percentage.

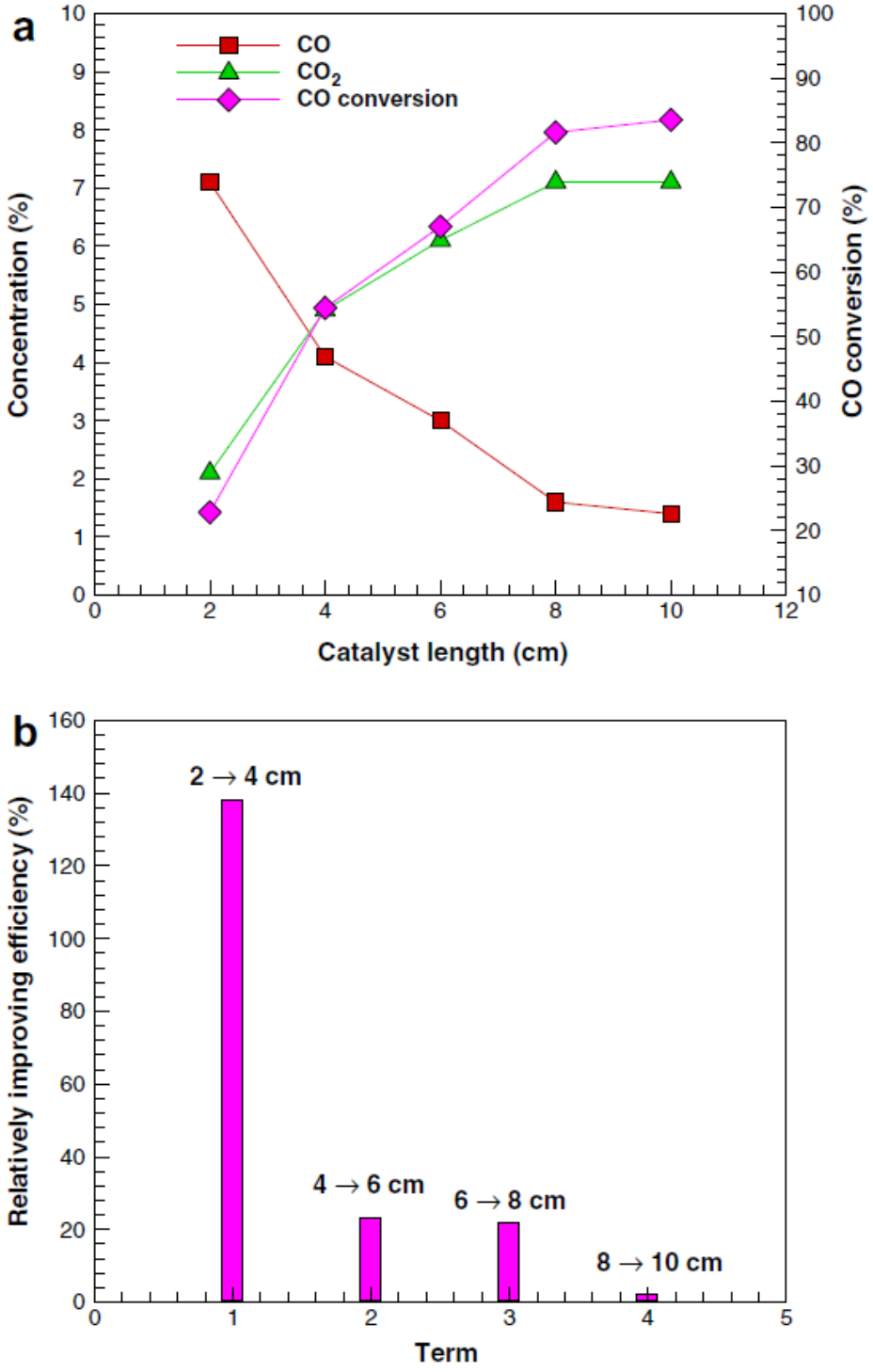

Figure 2. 18: Profiles of (a) the concentrations of CO and CO_2 as well as the CO conversion and (b) the relatively improving efficiency from the WGSR with the HTC (W.-H. Chen et al., 2008).

At 2 cm, due to the short residence time (0.0225 s), the concentration of carbon dioxide was very low and the carbon monoxide conversion was 22.8%. When the bed length was doubled (4 cm), the concentration of carbon monoxide decayed

significantly, whereas the concentration of carbon dioxide increased markedly. For this reason, was can be found that the carbon monoxide conversion was increased to 54%. When the bed length was 8 cm (residence time = 0.09 s), the carbon monoxide conversion was promoted to 81.6%. The value further increased to 83.5% for the bed length of 10 cm.

Figure 2.18b demonstrated the influence of increasing bed length (or residence time) on the performance of the water gas shift reactor and the distribution of the relatively improving efficiency (RIE) due to increased bed length. It was observed that when the bed length was increased from 2 cm (original) to 4 cm (extended), the relatively improving efficiency (RIE) was 138% and resulted in a remarkable improvement on the performance of the water gas shift reactor. Afterward, increasing bed length decayed the relatively improving efficiency RIE greatly. Nevertheless, the value was always larger than 20% when the bed length was less than 8 cm. Once the bed length was pushed to 10 cm from 8 cm, the relatively improving efficiency (RIE) decreased to 2.3%, implying that the increased bed length almost played no part in improving the performance. This also showed that, based on 10 cm of bed length, 20% of catalyst cost can be saved if 8 cm of bed length was employed.

Figure 2.19 illustrates profiles of the physical scales from the water gas shift reactor with the effect of the LTC for the reaction temperature and carbon monoxide/steam ratio at 200 ^{o}C and 1/4, respectively. As a whole the tendency in the concentration distributions of carbon monoxide and carbon dioxide shown in Figure. 2.19a resembled that shown in Figure 2.18a. However, the carbon monoxide conversion with the effect of the low temperature catalyst (LTC) was higher than that with the high temperature catalyst (HTC), indicating that the performance of the former was better than that of the latter. Specifically, for the reactions with the high temperature catalyst (HTC) and the low temperature catalyst (LTC), the carbon monoxide conversions of the former and the latter range from 22.8% to 83.5% and from 46% and 96%, respectively.

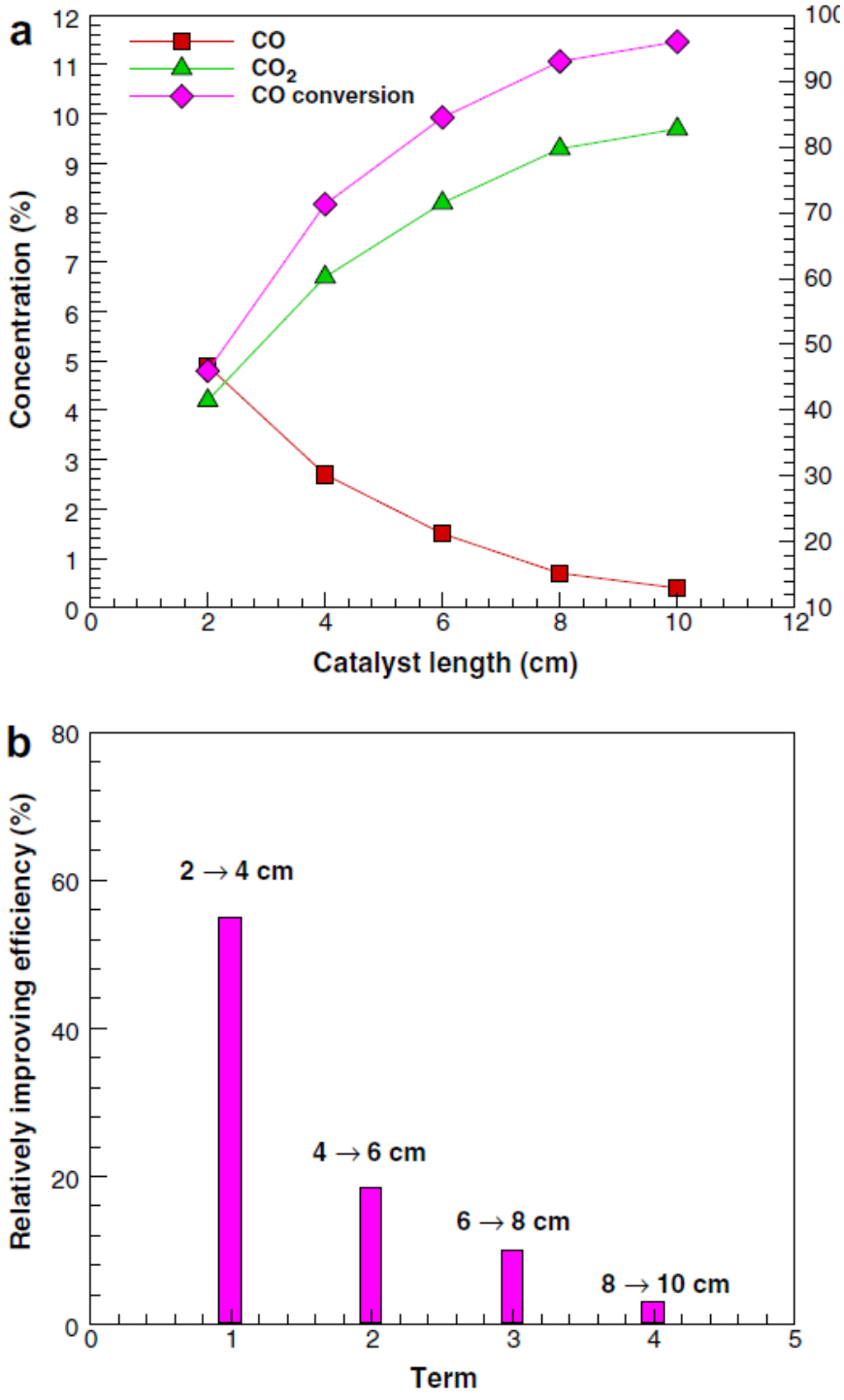

Figure 2. 19: Profiles of (a) the concentrations of CO and CO_2 as well as the CO conversion and (b) the relatively improving efficiency from the WGSR with the LTC(W.-H. Chen et al., 2008).

The performance of the water gas shift reactor with a low temperature catalyst for the relatively improving efficiency (RIE) in Figure 2.19b was not as significant as that shown in Fig. 18b for example when the bed length is increased from 2 cm to

4 cm, the relatively improving efficiency (RIE) shown in Figure 2.19b is 55% which is much smaller than 138% shown in Figure 2.18b.Similar to the characteristic of the high temperature catalyst (HTC), Figure 2.19b also suggested that, under the effect of the low temperature catalyst (LTC), the residence time of 0.09s was sufficiently long to develop the WGSR well. This was due to the fact that the relatively improving efficiency (RIE) was merely 3% when the bed length increased from 8 cm to 10 cm, but the catalyst cost could be reduced by 20% because the bed length of 8 cm was long enough for both the high temperature catalyst (HTC) and the low temperature catalyst (LTC) to carry out the WGSR well.

2.4 Preferential Oxidation (PROX)

Preferential Oxidation is used to decrease the amount of CO component to less than 10 ppm for instance in order to prevent PEMFC poisoning (Dai et al., 2014). According to Erickson and Vernon (2014), the PROX catalyst must meet the requirement of high CO oxidation activity, good resistance to H_2O and CO_2 and it must have high selectivity (so that no valuable hydrogen fuel is consumed). The PROX reaction can be represented as:

$$CO + \frac{1}{2}O_2 \rightarrow CO_2 \qquad \Delta H = 283 kJ/kmol \qquad (11)$$

The PROX operates at relatively low temperatures and atmospheric pressure, resulting in a compact reforming system that can quickly response to load changes and frequent starting and stopping of the operation (Ioanooa, Laguna, & Centeno, 2013).

Lomello-Tafin *et al.* (2005) performed a study on the preferential oxidation of carbon monoxide in hydrogen over highly loaded Au/ZrO_2 catalysts obtained by direct oxidation of bulk alloy. Figure 2.21 from the stability tests It was seen that the catalyst was stable under carbon monoxide oxidation conditions for 20 hours at 383 K (temperature of half-conversion). The testing conditions: 10 mg catalyst, total flow rate 50 sccm (standard cubic centimeter per minute), 2% CO (or 48% H2), 2% O_2 in He for the H_2-free (or CO-free) mixture (dark symbols) or 2% CO, 48% H_2, 2% O_2 in He for the PROX mixture (open symbols). In the H_2-free and CO-free mixtures, maximum conversions are reached (100% for CO and 8.3% for H_2)

when the oxidation rates become constant above 150 °C (Lomello-Tafin, Chaou, Morfin, Caps, & Rousset, 2005).

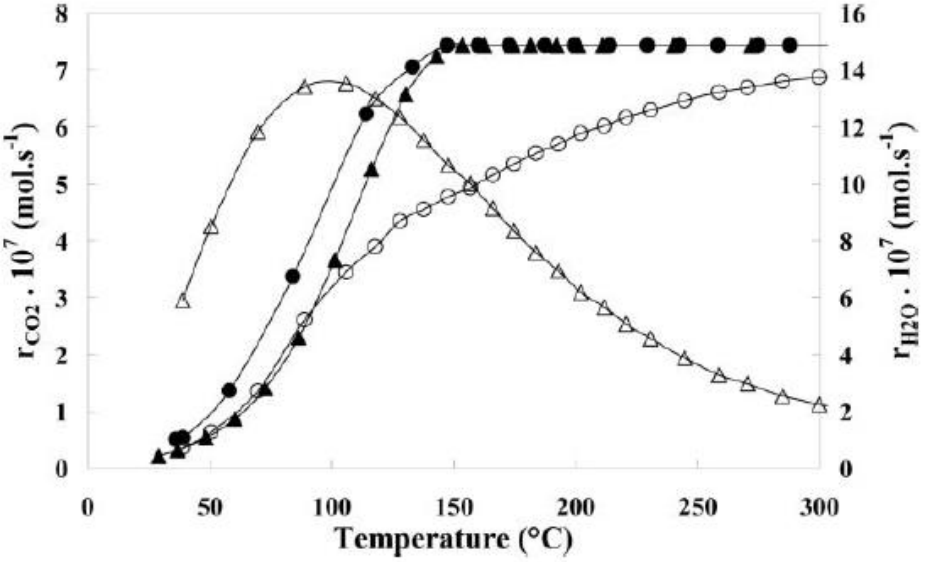

Figure 2. 20: CO oxidation rate (triangle) and H_2 oxidation rate (circle) over Au/ZrO_2 catalyst as a function of the reaction temperature.

The study performed by Lomello-Tafin *et al.* (2005) activity of the Au/ZrO_2 material was found to be 0.025 mmol g_{Au}^{-1} s^{-1} at 350 K (25% CO conversion), which compared well with the activity of other Au/ ZrO_2 catalysts described in Table 2.3.

Table 2. 3: Activity of various Au/ZrO_2 catalysts in the oxidation of CO (2% CO, 2% O_2 in He) (Lomello-Tafin et al., 2005).

Preparation	**Au (wt%)**	**d (nm)**	**P_{co} (mbar)**	**CO oxidation rate ($mmol_{co}g_{Au}^{-1}s^{-1}$)**	**Ref**
Laser vaporisation	0.05	2.9	20	0.078	7
Colloid deposition	1.7	2	2.5	0.008	10
Coprecipitation	1.0	4	2.5	0.027[a]	11
Oxidation of ZrAu alloy	61.5	> 7	20	0.025	This work
[a] Extrapolated from the temperature of 30% conversion to a temperature of 350K assuming an energy of activation of 30 $kJmol^{-1}$.					

Enger *et al.* (2008) reviewed the catalytic partial oxidation of methane to synthesis gas with emphasis on the reaction mechanisms over transition metal catalysts.

Table 2.4 indicated the essential reactions in the partial oxidation of methane and the product composition that were governed by or limited by the global thermodynamic equilibrium of all possible species.

Table 2. 4: Overall reactions in the methane partial oxidation system (Enger, Lødeng, & Holmen, 2008)

$CH_4 + 2O_2 \rightarrow CO_2 + 2H_2O$	(1)
$CH_4 + 0.5O_2 \rightarrow CO + 2H_2$	(2)
$CH_4 + O_2 \rightarrow CO_2 + 2H_2$	(3)
$CO + H_2O \rightleftharpoons CO_2 + H_2$	(4)
$CH_4 + H_2O \rightleftharpoons CO + 3H_2$	(5)
$CH_4 + CO_2 \rightleftharpoons 2CO + 2H_2$	(6)
$CO + H_2 \rightleftharpoons C + H_2O$	(7)
$CH_4 \rightleftharpoons C + 4H_2$	(8)
$2CO \rightleftharpoons CO_2 + C$	(9)
$CO + 0.5O_2 \rightarrow CO_2$	(10)
$H_2 + 0.5O_2 \rightarrow H_2O$	(11)

[a] All reactions involving O_2 are, for all practical purposes, thermodynamically irreversible.

Figure 2.21 illustrated the effect of temperature and pressure on a stoichiometric mixture of methane and oxygen (methane/oxygen = 2:0). At increasing pressures, higher temperatures were required to obtain high conversion and high selectivity to hydrogen and carbon monoxide.

Figure 2.22 indicated the equilibrium composition for different methane/oxygen ratios. Feeding methane/oxygen at a ratio of 0.5 yielded complete combustion products carbon dioxide and water (CO_2 + H_2O), but above this limited both hydrogen and carbon monoxide the major products in a wide range of methane/oxygen ratios.

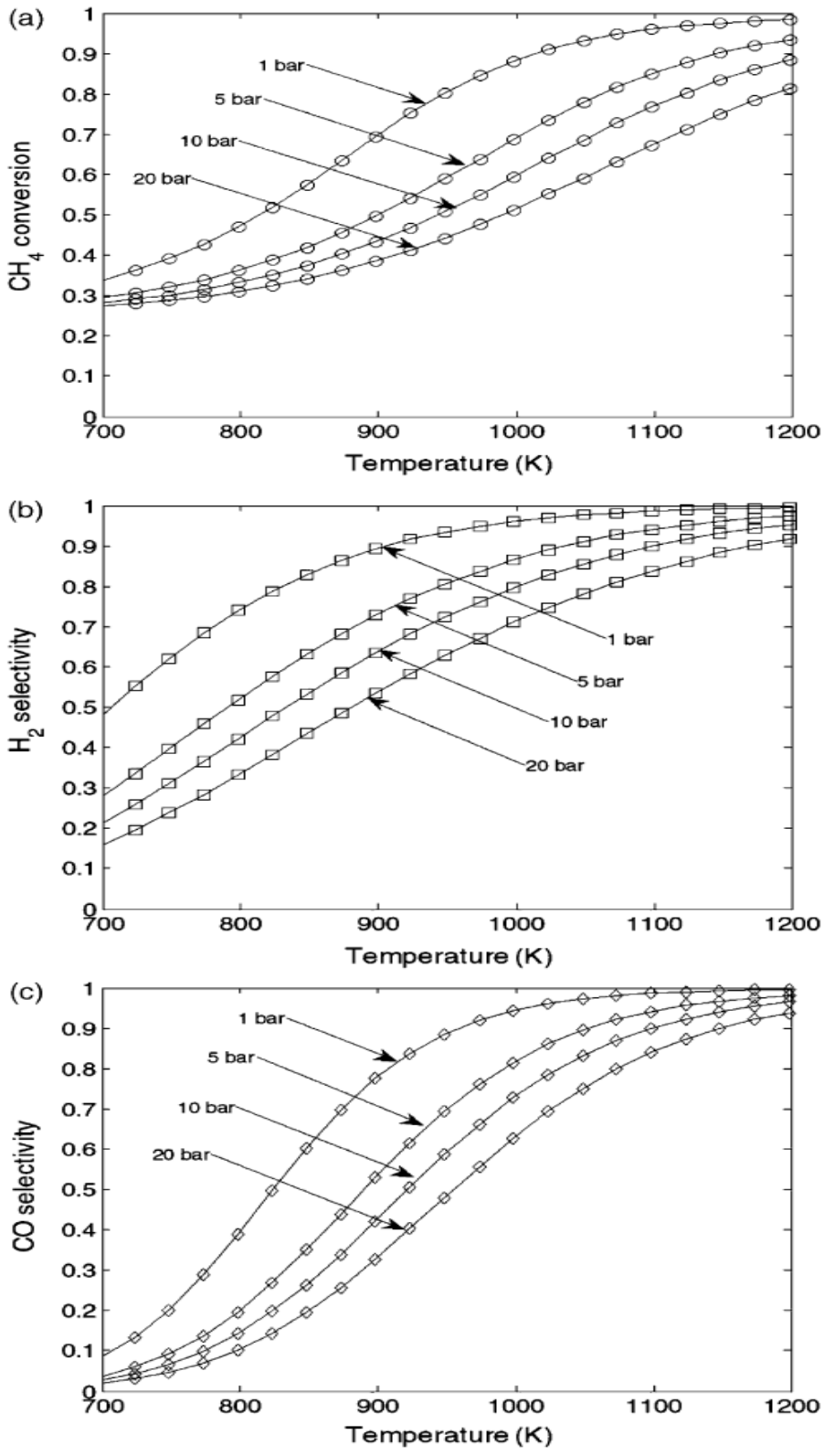

Figure 2. 21: Thermodynamic equilibrium as a function of the temperature at 1–20 bar from HYSYS 3.2 simulation using CH_4/O_2 = 2:0 and air as oxidant. (a) The CH_4 conversion, (b) the H_2 selectivity and (c) the CO selectivity (Enger et al., 2008)

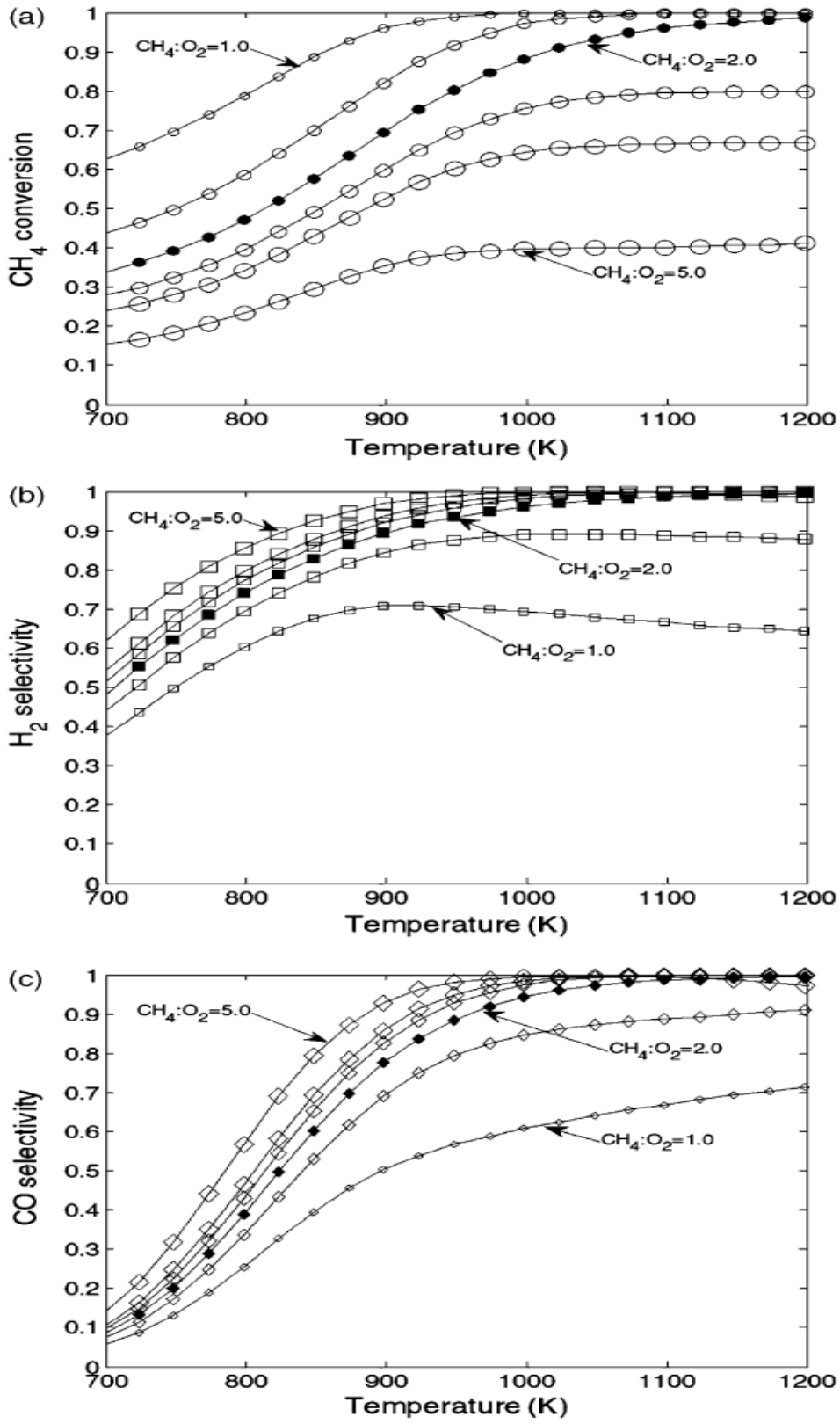

Figure 2. 22: Thermodynamic equilibrium as a function of the temperature at 1 bar from HYSYS 3.2 simulation using CH_4/O_2 = (1:0; 1:5; 2:0; 2:5; 3:0; 5:0) and air as oxidant. At CH_4/O_2 = 0:5 the equilibrium products are only CO_2 and H_2O. (a) The CH_4 conversion, (b) the H_2 selectivity and (c) the CO selectivity (Enger et al., 2008).

Figure 2.23 indicated that the methane activation was rate determined over cerium oxide/aluminium oxide and the oxidation of carbon appeared to be rate determined when adding platinum or rhodium to the system. Cerium oxide and platinum/cerium oxide had a beneficial effect of increasing the oxygen storage capacity and removing surface carbon.

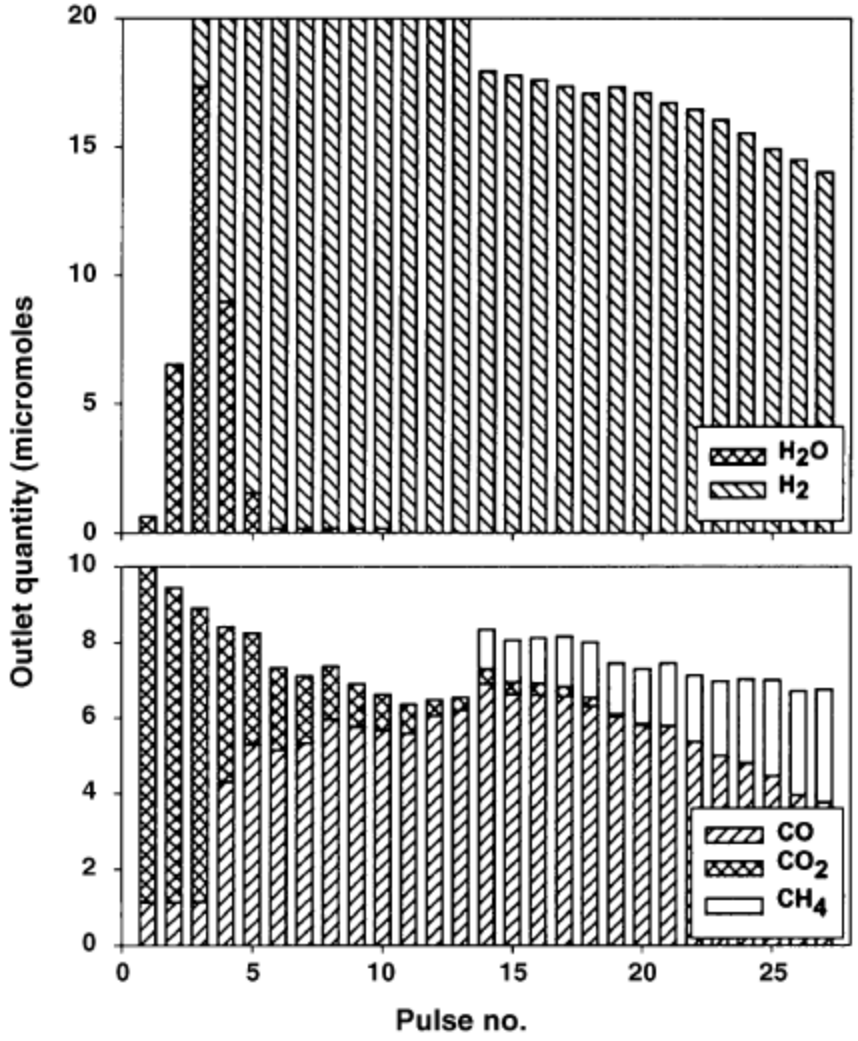

Figure 2. 23: Methane pulsing (10 mmol/pulse) over a fresh sample (0.5 g) of 0.5 wt% Pt/20 wt% CeO_2/Al_2O_3 (Enger et al., 2008).

Schneider performed an experimental and numerical investigation of the catalytic partial oxidation (CPO) of fuel rich mixtures which were heavily diluted in water and carbon dioxide (46.3% and 23.1% volumetric feed composition, respectively) at 5 bars. Table 2.5 indicated that increasing the inlet temperature to the ignition temperature (T_{ig}) caused an abrupt transition to vigorous steady combustion with measured outlet reactor temperatures in excess of 1000 K. The 1% rhodium/

zirconium oxide (Rh/ZrO_2) catalyst of the present study (No. 2 in Table 3 was promising for gas turbines *(T_{ig} = 670K)*. The other catalysts of Table 2.5 were only included to give a perspective on the ignition capabilities of the chosen catalyst.

Table 2. 5: Catalytic ignition experiments[a] (Schneider, Mantzaras, & Jansohn, 2006).

Catalyst	Rh (%wt)	Support	T_{ig} (K)
1	0.5	ZrO_2	700
2	1	ZrO_2	670
3	1	$Ce–ZrO_2$	655
4	1	$Ce_{0.9}La_{0.1}O_2$	710

[a]Ignition temperature for various investigated catalysts.

In the beginning the inlet temperature could be further reduced by as much as 200K while still maintaining high steady fuel conversion and reactor exothermicity. This was illustrated in Figure 2.25 which provided the measured continuous time history of the inlet and outlet temperature and the discontinuous GC-deduced outlet composition (on a dry basis). Reducing the inlet temperature by 200K led to a drop of the outlet temperature only 45K and to a moderate decline of methane conversion and synthesis gas yields (for instance decrease in hydrogen content from 36% to 30% volume).

Nonetheless, the outlet temperatures and hydrogen concentrations were still maintained to high levels for the subsequent gaseous combustion. It was noted that the observed large hysteresis in the catalytic ignition/extinction characteristics was beneficial for low part load and idle turbine operation (compressor discharge temperatures typically ~ 100K lower than the corresponding full-load values).

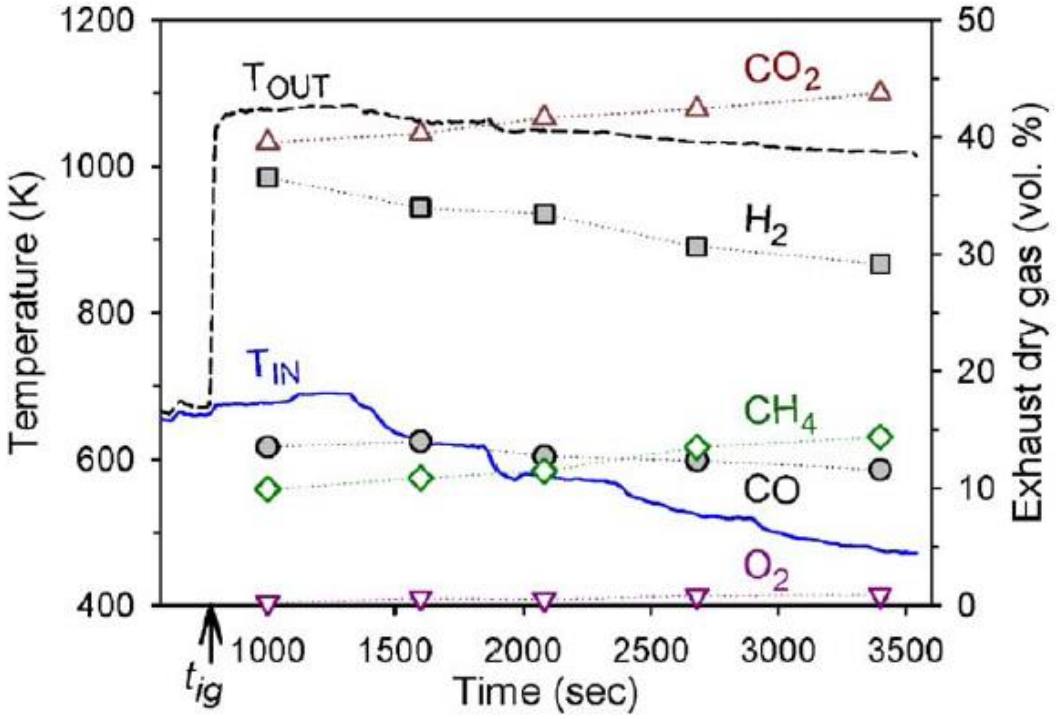

Figure 2. 24: Time histories of measured inlet (T_{IN}, solid lines) and outlet (T_{OUT}, dashed lines) temperatures and GC-measured dry-gas exhaust compositions. CO_2: open upper triangles, H_2: filled squares, CH_4 open diamonds; CO: filled circles; O_2: open lower triangles. The time $t = t_{ig}$ corresponds to catalytic ignition (Schneider et al., 2006).

2.5 Membrane Reactor

Membranes are widely investigated for pure hydrogen production (Adolfo Iulianelli, Liguori, Wilcox, & Basile, 2016). Membrane reactors are generally multiphase reactor incorporating reforming and water gas shift reactions as a single unit. This incorporation results in a high degree of process integration with the benefits of energy efficiencies and reduced reactor volume (Gallucci, Fernandez, Corengia, & van Sint Annaland, 2013).

Hydrogen as an alternate fuel has been the new focus of cleaner energy technologies especially as fuel for power production for instance in Polymer Exchange Membranes (PEM) fuel cells. There are three major approaches to separating H_2 from the reformate gases (1) pressure swing adsorption (PSA), (2) fractional Distillation and (3) membrane separation (H. Liu et al., 2016). Currently, membrane separation is considered to be the most promising for portable power applications due its low energy consumption, possibility for continuous operations, lower volume, ease of operation and cost effectiveness

(Ockwig & Nenoff, 2007). The concept of a membrane purifier is shown in Figure 2.25.

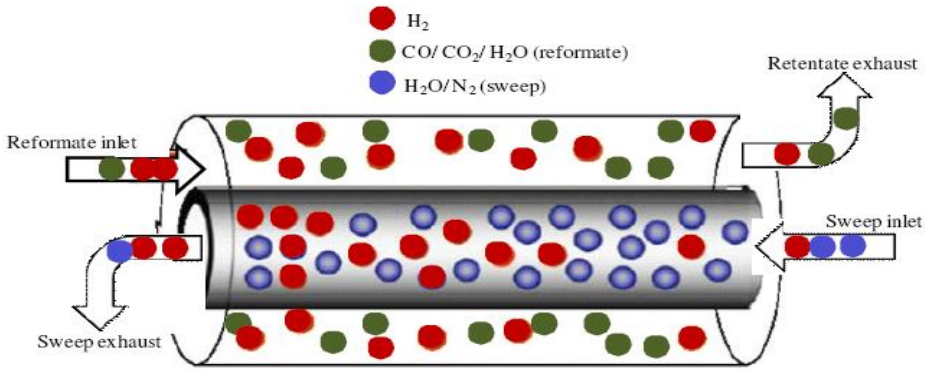

Figure 2. 25: Schematic illustration of a membrane purifier (Ockwig & Nenoff, 2007).

The H_2 perm-selective membranes separate reformate and sweep gases that are fed into the high-pressure side of the purifier, typically in a counterflow arrangement (Bhargav, 2010). The most geometrics are planar and cylindrical, just as in heat exchangers (Dadda, Abboudi, & Ghezal, 2013). The H_2 partial pressure difference between the two gas streams is the fundamental driving force for H_2 transfer, at any location along the length of the purifier (Cheng et al., 2007). Depending on the type of membrane employed the heat transfer may occur via various different processes. The reformate gases are usually maintained at an elevated pressure to increase this driving force and reduce the size of the purifier (Al-Mufachi et al., 2015). Similarly, the H_2 partial pressure on the sweep side must remain adequately low either by the use of a vacuum pump, or sweeping the H_2 using a "sweep" gas (Basile et al., 2005).

The H_2 flux is increased, while simultaneously reducing CO content by integrating a catalyst that promotes the water-gas shift reaction into the reformate side of the membrane purifier to take advantage of the shifting equilibrium as H_2 is selectivity withdrawn. Such a purifier with integrated WGS is often referred to as a WGS membrane reactor (Koc, Kazantzis, & Ma, 2011).

2.6 Palladium membrane supports

Although Pd and its alloys have advantages that make them attractive for portable PEMFC systems, their cost is a major concern in any commercial application. The H_2 flux through a Pd-alloy membrane is inversely related to its thickness (though not necessarily proportional) with other operating conditions being held constant (Anderson, Nasr, Yun, Kottke, & Fedorov, 2015). Hence, the total required membrane area reduces when thinner Pd-alloy membranes are employed. This in turn, results in a disproportionate decrease in the mass of precious metals (Pd or Pd + Au/Ag/Cu) required for the purifier. Rapid response to variation in H_2 demand is a result of a thinner membrane in a purifier. Due to the above reasons, very thin (approximately 1-10 µm) Pd-alloy films are preferred as opposed to thick Pd-alloy sheets or tubes (> 20µm) (Alimov, Busnyuk, Notkin, & Livshits, 2014).

The thin films do not have the mechanical strength to withstand the cross-membrane differential pressures that are required to be maintained in order to increase permeance and limit the purifier size. For this reason, the films are supported on a porous matrix. Material such as porous yttria stabilized zirconia YSZ (Zhang, Wang, Tan, & Ozkan, 2009) porous stainless steel (PSS) (Saadatinasab, Gharibi, & Zolfaghari, 2014) and porous $\alpha - Al_2O_3$ (Okazaki et al., 2011) are most commonly used for this purpose. A metallic film together with the porous support is a composite membrane. Reviews of the development of Pd membranes for H_2 separation have been presented by several authors(A Iulianelli, Ribeirinha, Mendes, & Basile, 2014) and (Ghasemzadeh, Morrone, Babalou, & Basile, 2014).

The minimum thickness of Pd film can make a reliable purifier depending inversely on the pore size that can be deposited on a porous substrate. However, the smaller pore sizes increase the resistance of the support gas transport. Hence, an intermediate nano-porous ceramic layer is usually applied on top of a meso-porous ceramic bulk substrate. In case of some PSS supports, the surface is oxidised before plating PD to avoid inter-metallic PD-Fe diffusion higher temperatures (Bosko, Miller, Lombardo, Gellman, & Cornaglia, 2011).

Abdollahi *et al.*(2012) performed a study which was based on the simulating the feed reformate composition of a steam reformer reaction through a palladium membrane for the production of ultra-pure hydrogen using realistic size, and ultra-permeable membrane. The membrane was characterised through single-gas permeation measurements before it was used in the reactor experiments. The effect of flow rate, feed pressure and sweep ratio on the membrane performance during the WGS experiments was also studied. The model was further used to study the design aspects of the process. It was shown that the Pd membrane reactor system under study is capable of attaining almost complete CO conversion and full hydrogen recovery at realistic experimental conditions similar to those utilised in industrial applications.

Figure 2.26 indicates a single-gas permeation of hydrogen at 300°C with the pressure exponent of n = 0.96. The transport of hydrogen through the Pd membrane was found to be pressure dependent.

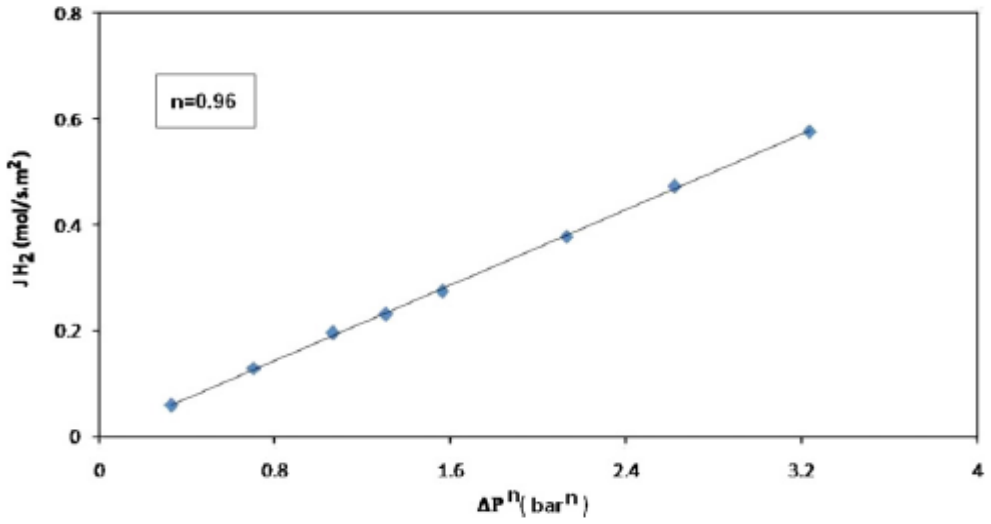

Figure 2. 26: Flux of hydrogen as function of $(P^F)^n$- $(PP)^n$ (Abdollahi et al., 2012).

Gielens *et al.*(2008) performed a study where he studied the permeability of H_2-selective palladium membranes fabricated with microsystem technology. The study was carried out the permeation experiments at H_2 feed partial pressures of 0.2-1.0bar and temperatures between 623 and 873K. The rate limiting step and the stability of the membranes was determined. At a temperature of 873K a permeance of 18 mol $H_2/m^2.s\ bar^{058}$ was obtained for Pd membrane with thickness

of 0.5μm. The formation of pinholes was noted at high temperatures because at 873K the H_2/He selectivity began to decrease rapidly.

2.7 Pd-H_2 and Pd-alloy-H_2 interactions

Thomas Graham first discovered the diffusion of hydrogen through a hot Pd tube and Pd-Hydrogen system has been one of the most studied since (Lukyanov et al., 2009). Yun *et al.*(2011) has summarized the hydrogen permeation mechanism through a Pd-alloy membrane as consisting of distinct steps as shown in Figure 2.27:

- Molecular diffusion of H_2 from the bulk of the feed gas to the vicinity of the metallic surface
- dissociative adsorption takes place on the metallic surface
- transition of surface adsorbed H-atoms into the bulk metal
- diffusion of H-atoms takes place across the membrane bulk
- transition to the permeate side surface
- associative desorption takes place from the metallic surface on the permeate side, and
- Molecular diffusion takes place away from the surface into the bulk of the permeate gas.

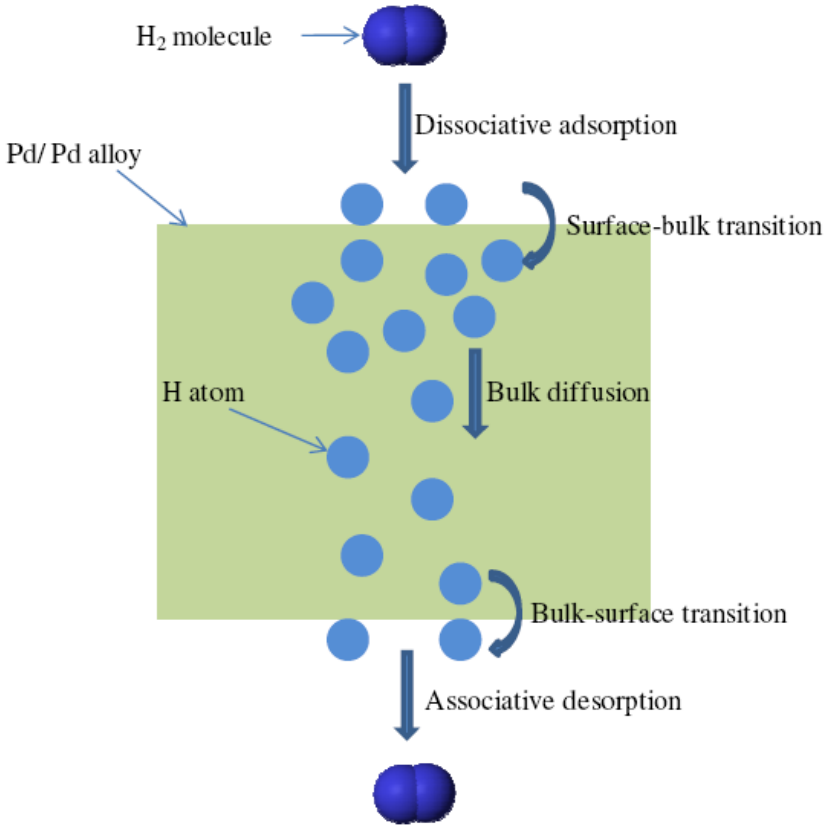

Figure 2. 27: Steps involved in H_2 transport across a Pd-alloy membrane (C. j. Liu et al., 2011).

Barbieri *et al.* (2011) investigated the performance of a palladium based membrane reactors for a one stage process of the water gas shift. The work proposed the use of one Pd-based membrane reactor (MR) operating at the same temperature range as the high temperature WGS reactor as a suitable alternative to the whole traditional reactor (TR) process.

Table 2.6 illustrated a typical composition of a syngas stream coming out from a reformer and was considered as reference for the feed stream. The mixture contained the reactants carbon monoxide (CO) and hydrogen (H_2O), products, specifically and quantitatively hydrogen, which was the permeable species, as well as the inert gas nitrogen (N_2). The table also reported the operating conditions considered in the simulations as a reference study, which are very close to the ones currently used at industrial level for the traditional process. In the membrane reactor (MR) the permeation driving force was generated only by feed pressure and no sweep gas was utilised. The feed pressure was kept lower at 15 bar, since this is the limit of the self-supported palladium–silver membrane considered in the

present work. MR was also simulated at 30 bar, a value closer to those typically used in industrial processes (20–30 bar).

Table 2. 6: Reference operating conditions considered in the simulations for the Pd-based MR and the Traditional process (Barbieri, Brunetti, Caravella, & Drioli, 2011).

	Pd–Ag MR	Traditional process (HT-WGS, 1st stage)
Inlet Temperature	300 °C	
Feed pressure	15 bar	
Feed mixture composition	$CO : CO_2 : H_2 : N_2 =$ 52 : 19 : 20.5 : 8.5 % molar (dry basis)	
H_2O/CO feed molar ratio	1	
GHSV	20 000 h^{-1}	

Figure 2.28 showed the adiabatic reaction paths (solid lines), highlighting the exit conversion by means of symbols, of the palladium based membrane reactor and traditional process (both stage) and the equilibrium conversion of a traditional process and of a palladium based membrane reactor, the latter was calculated at 15 bar, the same reaction pressure considered in the simulations. The carbon monoxide conversion achieved by the palladium based membrane reactor was around 10% higher than the overall one of the traditional process; it also exceeded significantly (approximately 25–30%) the traditional process.

The hydrogen removal from the reaction side due to the permeation shifted the reaction towards further conversion. The effect was well operated in the palladium based membrane reactor since a reaction pressure of 15 bar promoted the hydrogen permeation well. The temperature of the traditional process (first stage) reached approximately 370–380 °C and cannot go over the equilibrium limitation, that of the MR achieves a higher value (approximately 450 °C) to which corresponded to a higher conversion.

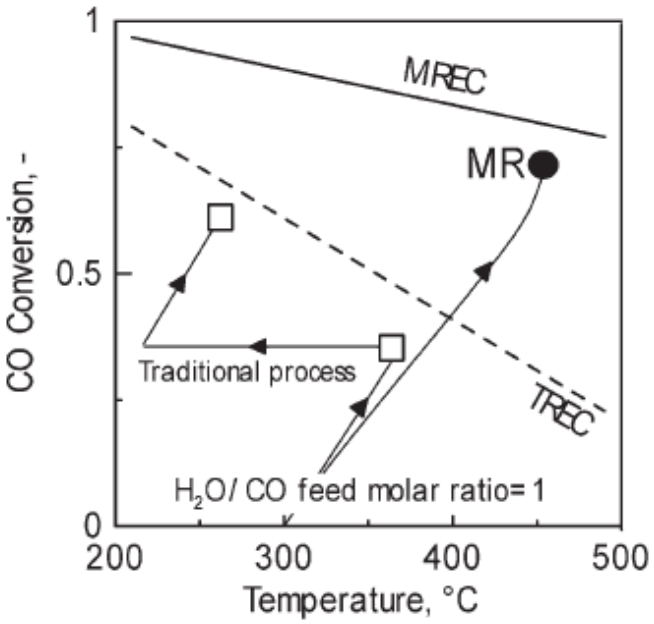

Figure 2. 28: CO conversion as a function of temperature for MR and Traditional process. Operating conditions as in Table 2.6 (Barbieri et al., 2011).

In figure 2.29 most of the hydrogen that was produced was recovered as pure gas in the permeate stream of the palladium–silver membrane reactor and the pure hydrogen could be directly fed to a polymer electrolyte membrane (PEM) fuel cells. In addition, the retentate was compressed and concentrated in 65 percent molar concentration of carbon dioxide therefore resulted in the carbon dioxide being easily captured and resulted in an important reduction in the successive separations.

The H_2 exiting from the traditional process at a 60 percent molar concentration was is still mixed with the other gases with approximately 5.5 percent molar concentration carbon monoxide that must be drastically reduced and, thus, required a further separation/purification stage before further use. The carbon dioxide concentration of the residual stream could be close to 70 percent only if all the hydrogen present in the stream was separated. Its concentration did not exceed 60 percent considering the actual separation efficiency of industrial pressure swing adsorption (PSA), where the H_2 recovery does not exceed 80–90 percent.

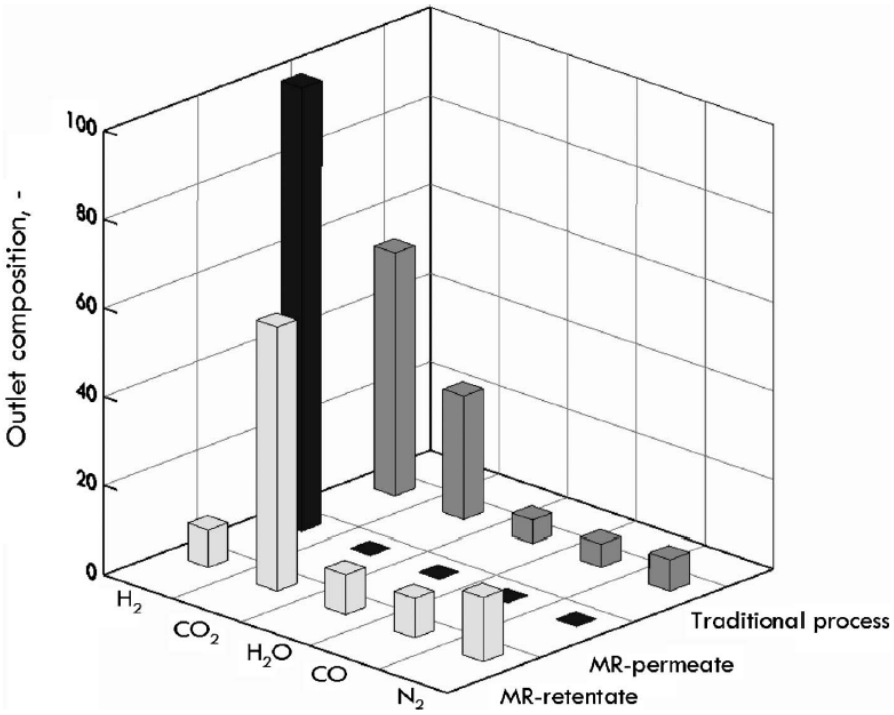

Figure 2. 29: Outlet stream composition of the MR and the traditional process. Operating conditions as in Table 2.26 (Barbieri et al., 2011).

Castillo *et al.*(2015) studied the effect of temperature and pressure on hydrogen production from steam reforming of biogas with palladium-silver membrane reactor. The study was conducted at low temperatures from 623 to 723 K and from 0.1 to 0.4 MPa of reaction side pressure. Figure 2.30 showed the hydrogen flow rate on the permeation side against the differential pressure between reaction side and permeation side at each temperature. It was observed that the flow rate of hydrogen was proportional to the difference of square root of the hydrogen partial pressure, which is the same as the case of Sievert's law. The hydrogen permeation rate increased with increasing temperature. The permeabilities were 9.0407×10^{-9}, 1.0412×10^{-8} and 1.2039×10^{-8} [mol/(m s $Pa^{0.5}$)] at 623, 673 and 723K, respectively.

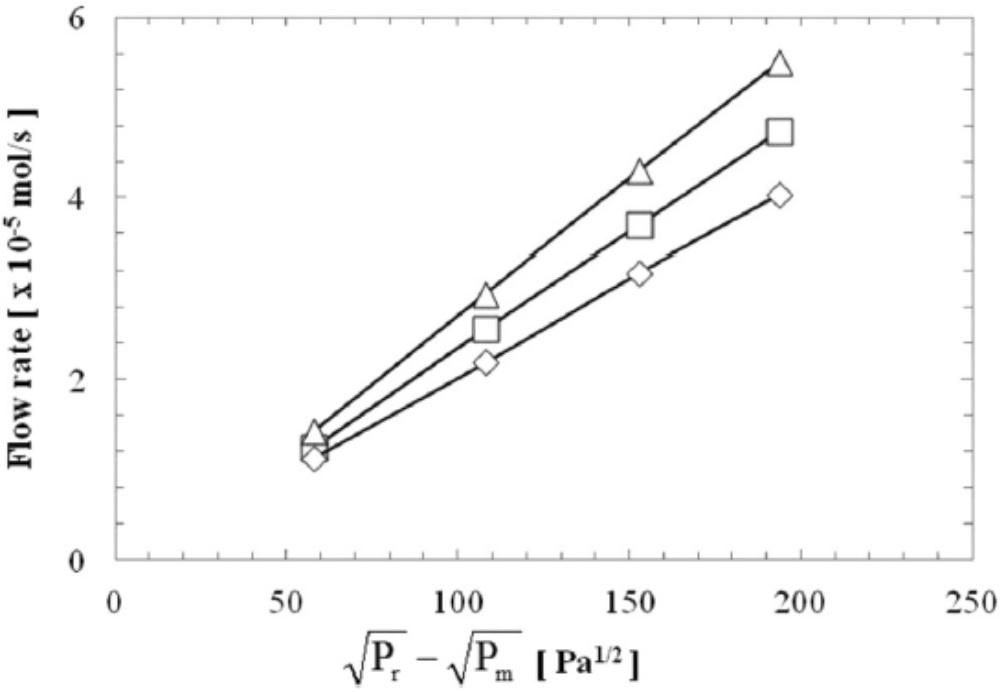

Figure 2. 30: Permeated hydrogen flow rate through the Pd-Ag membrane (⋄: 623 K, □: 673 K, △: 723 K) (Castillo, Sato, & Itoh, 2015)

Figure 2.31 indicated the flow rate of hydrogen for both reaction and permeation side at the steam/carbon = 3, 0.1 MPa on reaction side and 0.002 MPa on permeation side for the membrane reactor mode. The flow rate of hydrogen increased with increasing temperature for all the cases and the flow rate of hydrogen from permeation side was higher than that from reaction side for the membrane reactor. The hydrogen produced in excess against its equilibrium value was recovered mainly from the permeation side, which was probably due to the permeation effect.

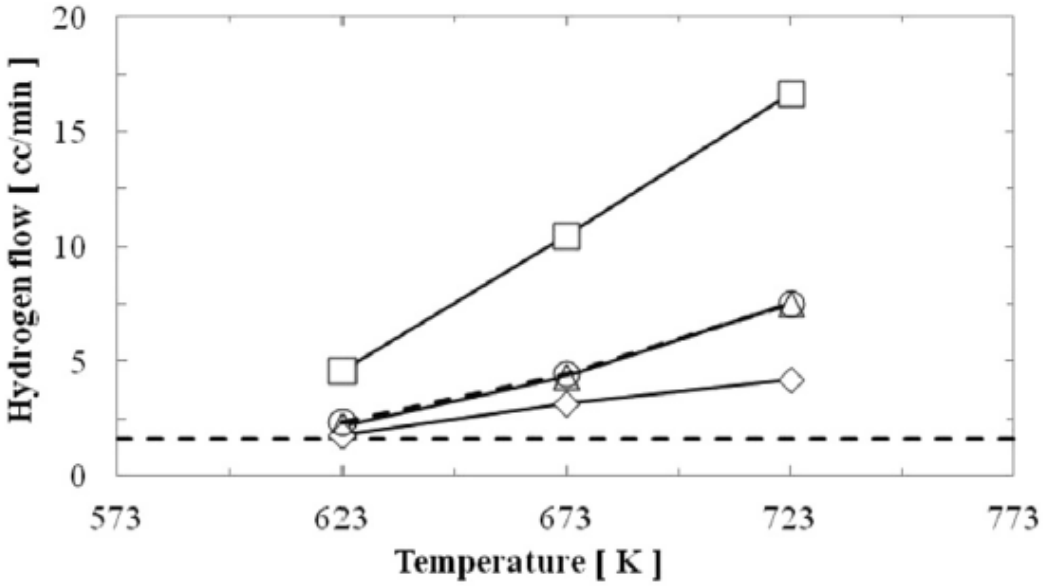

Figure 2. 31: Flow rate of hydrogen at S/C = 3, 0.1 MPa on reaction side and 0.002 MPa on permeation side (experimental results). - - -: hydrogen in biogas, Δ: conventional reactor mode, ◊: hydrogen from reaction side (membrane reactor mode),—○–: equilibrium,□ hydrogen from permeation side (membrane reactor mode) (Castillo et al., 2015).

Figure 2.32 illustrated the hydrogen recovery for all temperatures against reaction side pressure at S/C = 3 and 0.002 MPa on permeation side. The hydrogen recovery increased with increasing pressure on reaction side for all temperatures, attaining a maximum recovery of 80% at 723 K. The high temperature and high pressure regions are desirable for hydrogen recovery.

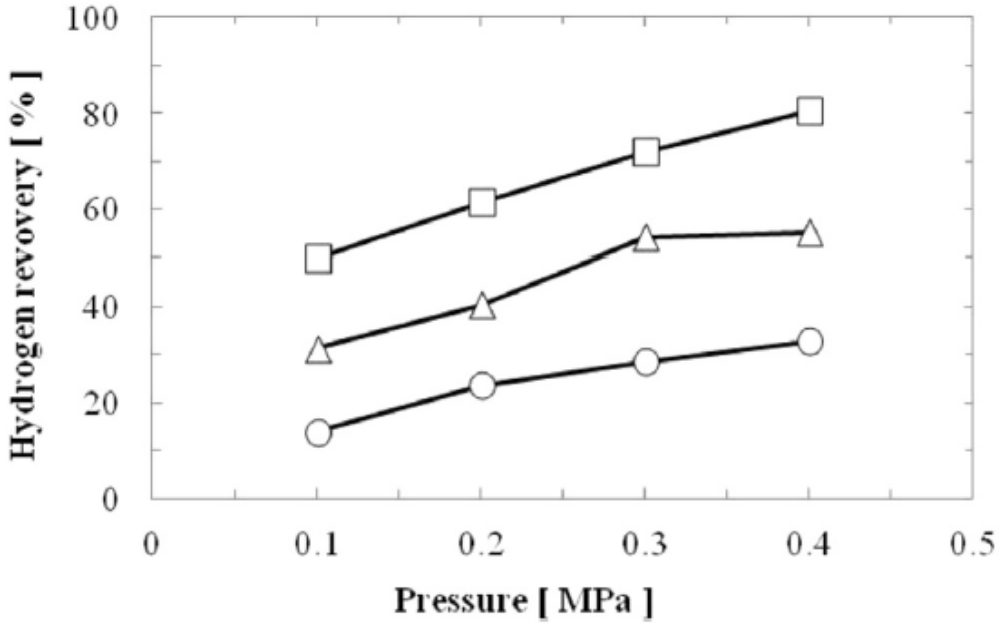

Figure 2. 32: Hydrogen recovery (experimental data) against reaction side pressure at S/C = 3 and 0.002 MPa on permeation side (○: 623 K, Δ: 673 K, □: 723 K) (Castillo et al., 2015)

In Figure 2.33 the molar methane composition at S/C = 3, 0.1 MPa on reaction side and 0.002 MPa on permeation side for both the conventional and membrane reactor mode were observed. In the conventional reactor the reforming of methane was enhanced with increasing temperature and thus the amount of produced hydrogen increased. A continuous decrease in methane composition was observed and the reaction was directed to the methane reforming except for the case of 623 K. In the case of the membrane reactor mode, the methane consumption was significantly enhanced than that for conventional reactor in each temperature. In particular, this trend was observed even in the case of lower temperature at 623 K.

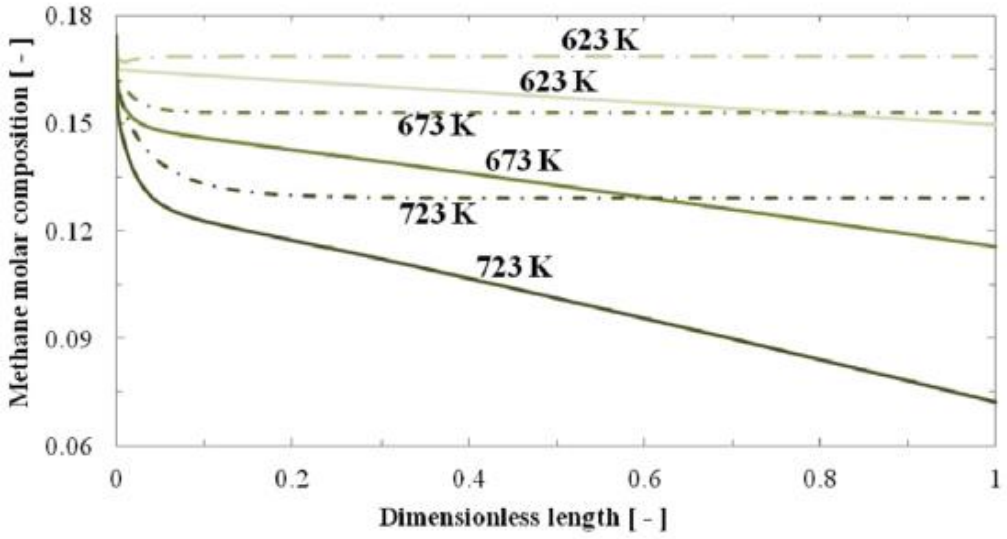

Figure 2. 33: Simulation results of the distribution of methane molar composition at S/C = 3, 0.1 MPa on reaction side and 0.002 MPa on permeation side. Dotted line represents the conventional reactor. Solid lines are the membrane reactor results (Castillo et al., 2015)

El Hawa *et al.*(2015) studied the application of a palladium–ruthenium composite membrane to hydrogen production in a high temperature membrane reactor. In the study approximately 5.0 μm thick palladium-ruthenium membrane with and estimated are of 13.3 cm^2, supported on a porous yttria-stabilized-zirconia/stainless steel substrate (ZrOD AccuSep, Pall Corp.) was used to carry out steam methane reforming (SMR) over a commercial Ni-based reforming catalyst at a temperature of 580°C and pressures up to 2.9 MPa.

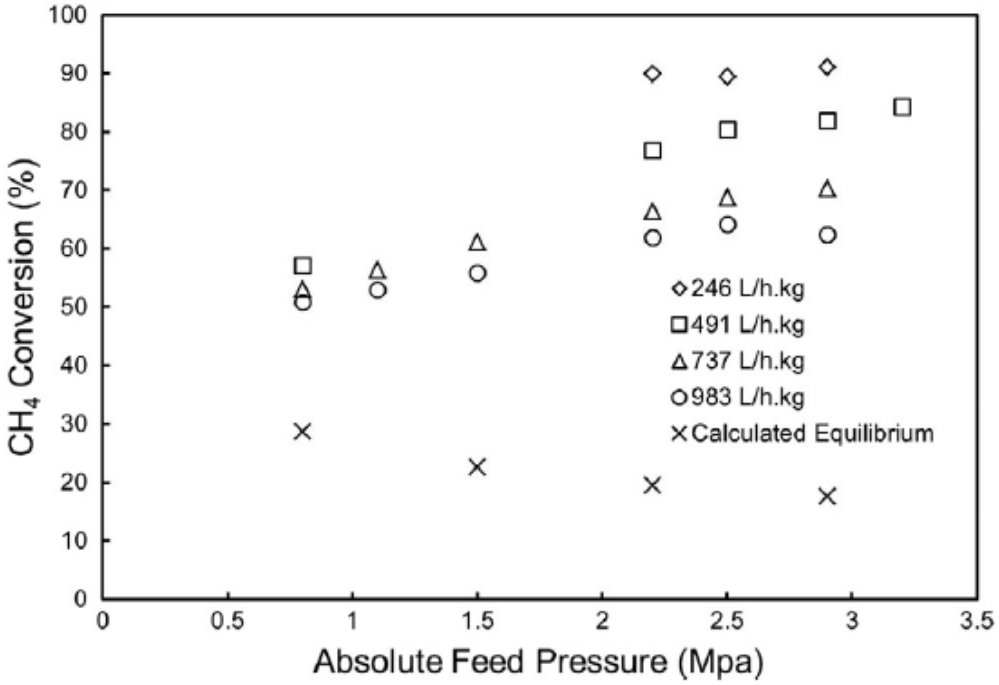

Figure 2. 34: Summary of SMR screening tests on the Pd–Ru membrane at SCR = 3 (100% CH_4 feed on a dry basis),~ 580°C, and variable space velocities, showing CH_4 conversions as function of reactor's absolute pressure. MR conversions exceeded the thermodynamic equilibrium indicated on the plot (El Hawa, Paglieri, Morris, Harale, & Way, 2015)

Chapter 3: Models Development

3.1 LPG Reforming

In this study Aspen Plus was utilised to simulate steam reforming process for the production of hydrogen, carbon monoxide and other species. In the simulation, the hydrogen concentration was increased at the reformer and carbon monoxide concentration was reduced using a water-gas shift reactor at low and high temperatures, and a palladium membrane reactor was used for the selective extraction of the hydrogen produced.

Simulations were performer in the reformer to obtain optimum hydrogen by changing the steam to carbon (S/C) ratio's, temperature and pressure. Propane and water were reacted in the steam reformer (SR) at a temperature of 550^{o}C resulting in the production of H_2 and CO and by products. The CO and H_2 and the by products from the reformer were reacted in a high temperature water gas shift (HT- WGS) reactor which was operated at temperatures between (400-500^{o}C) and it resulted in the conversion of carbon monoxide (CO) to carbon dioxide (CO_2) and it also resulted in an increased hydrogen concentration (H_2). The CO_2, H_2 and the by-products were further reacted in a low temperature water gas shift (LT-WGS) reactor which was operated at temperatures (200-250^{o}C). These reactors were modelled as adiabatic reactors since they involved exothermic reactions.

3.2 Aspen Simulation Platform

ASPEN (Advanced System for Process Engineering) is a process simulations software developed in the 1970's by researchers at MIT's Energy Laboratory (Øi *et al.,* 2007). It can be used in almost every aspect of process engineering from design stage to cost and profitability analysis. It has a built-in model library for reactors, heat exchangers, separators and distillation columns, etc. {Abu-Zahra *et al,* 2007).

The process flowsheet simulator is beneficial in all the three stages of a plant: research & development, design and production. In the research and development, it helps to cut down the laboratory experiments and pilot plant runs. In the design stage it enables a faster development with simpler comparisons of various alternatives. In the production stage it can be used for risk-free analyses of various what-if scenario's (Sarvar-Amini *et al.,* 2001).

The manual solution normally forces one to think deeper on the problem, to evaluate and re-evaluate the made assumptions (Sarvar-Amini *et al.,* 2007). It also might hide the complexity of the problem which makes it act as double edged sword, forcing one to concentrate on the real issues at hand. On the other hand, the hiding may also hide some important understanding of the problem as well.

3.3 Process Modeling and Simulation

A process flowsheet is used to describe the blue print of part of the plant (Pambudi *et al.,* 2016. It identifies all feed streams that inter-connect the unit operations and finally the product streams. The technical and operating conditions details are included depending on the level of the flowsheet. Figure 3.1 illustrates the process flowsheet for the reforming process. LPG which was assumed to be propane (C_3H_8) as it contains minimal butane percentage (Laosiripojana et al., 2011). The propane and water were both preheated from the room temperature of 25 ^oC to 180 ^oC both at the pressure of 1 atm in preparation for the reaction in the steam reformer.

Propane and water were reacted in the steam reformer at a temperature of 550 ^oC and at a pressure of 5 atm producing carbon monoxide and hydrogen and by products. The hydrogen, carbon monoxide and the by-products were cooled from a temperature of 550 ^oC at a pressure of 5 atm to a temperature of 450 ^oC at a pressure of 1atm in preparation for the reaction in the high temperature water gas shift reactor which was operated at a temperature of 400^oC and at a pressure of 1atm for the conversion of carbon monoxide to carbon dioxide. The hydrogen, carbon dioxide and by-products produced from the high temperature water gas shift reactor were further cooled from 400 ^oC to 250 ^oC in preparation for the reaction in the low temperature operated at a temperature of 200^oC and at a pressure of 1atm for further conversion of carbon monoxide to carbon dioxide.

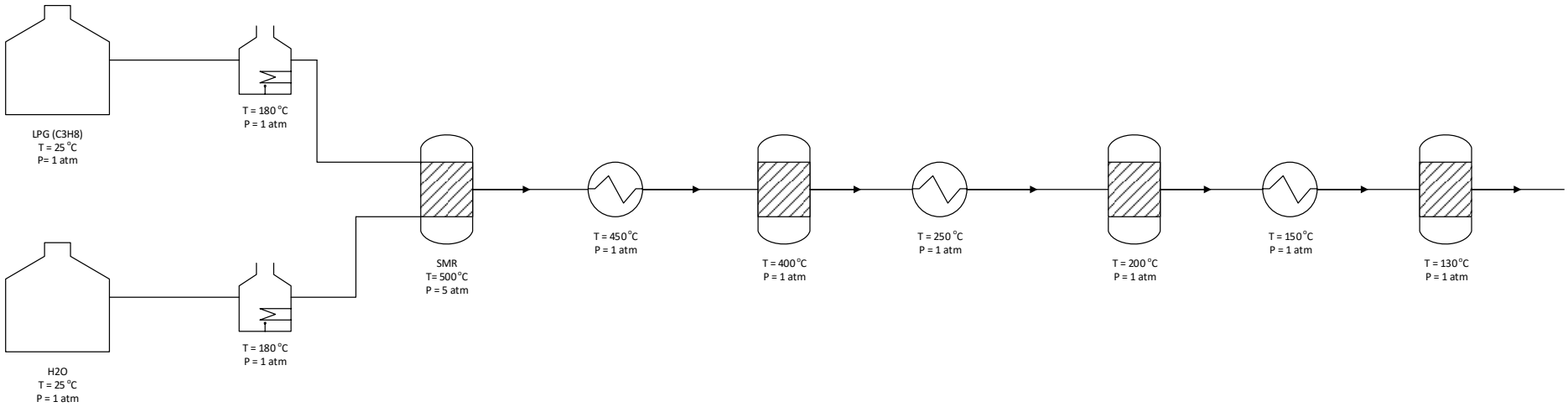

Figure3. 1: LPG reforming system

Optimisation on the reformer, WGS (HT and LT) were performed focusing on the varies parameters such as: reactor size, temperature, S/C, pressure, catalyst type and catalyst loading, these optimisations were necessary in order to maximise the hydrogen yield and a membrane reactor was latter utilised to separate the hydrogen gas from the other gases.

3.3.1 Reaction Kinetics of Reformer, High and Low Water-Gas Shift

The reaction kinetics developed by Shelepova *et al.,* (2011) and Xu *et al.* (1989) were utilised in this research project to describe the reaction rate expressions (see Table 3.1).

Table 3. 1: Rate expressions used in the reformer modelling (Shelepova, Vedyagin, & Noskov, 2011).

Reaction	**Expression for r_i**	**T(°C)**	**Catalyst**
$C_3H_8 + 3H_2O \rightarrow 3CO + 7H_2$	$r = \frac{k_2 P'^{0.93}_{c_3H_8} P^{-0.53}_{H_2O}}{1+\theta P'_{H_2} 0.86}$	250-900°C	Rh/CGO
$CO + H_2O \rightarrow CO_2 + H_2$	$r = k_4 \frac{(\frac{P_{CO}P_{H_2O}}{P_{H_2}} - \frac{P_{CO_2}}{k_4})}{DEN^2}$	200-500°C	$Ni/MgAl_2O_4$

where: $DEN = 1 + K_{CO}P_{CO} + K_{H_2}P_{H_2} + K_{CH_4}P_{CH_4} + \frac{K_{H_2O}P_{H_2O}}{P_{H_2}}$

r_i (I = 1, 2) are the reaction rates of reactions propane reforming and the water gas shift reaction in Table 3.1 respectively, reaction K_j is the rate coefficient of each reaction (I = C_3H_8, H_2O, CO, CO_2, H_2), the P_j is the partial pressure of each species j, K_{equi} is the equilibrium constants of each reaction I and K_j are the adsorption constants of each species j.

The Langmuir- Hinshelwood Kinetic model the most commonly used kinetic expression was used to describe heterogenous catalytic process (Seong *et al.,* 2014). This kinetic model was used on Aspen plus® and a plug flow reactor in order to simulate propane reforming, high temperature and low temperature water-gas shift reactors.

Table 3. 2: List of exponential factors (Shelepova et al., 2011).

Reaction number	Rate parameters	Units
1	K_2= 2.1428x10^{14} x $e^{-189.63x103/RT}$	mol/k$Pa^{0.4}m^2$
	θ = 1	$kPa^{-0.86}$
2	K_4 = 4.39 x 10^6 x $e^{-67.13x103/RT}$	kmol)/ (kgcat h bar)

Table 3. 3: Aspen simulation for specification and configuration of SMR, HT-WGS and LT-WGS.

Reactor	Type	Specification
SMR	Plug flow	Isothermal reactor, Reactor length =1 m, Reactor diameter = 0.5 m, Pressure = 5 atm, Catalyst loading = 2 kg, Bed voidage =0.01
HT-WGS	Plug flow	Adiabatic reactor, Reactor length = 1.6 m, Reactor diameter =0.5m, Pressure = 1 atm, Catalyst loading = 1.5 kg, Bed voidage = 0.01
LT-WGS	Plug flow	Adiabatic reactor, Reactor length = 0.5 m, Reactor diameter = 0.1 m, Pressure = 1 atm, Catalyst loading = 1.5 kg, Bed voidage 0.01

3.3.2 Preferential Oxidation (PROX) Model

As stated in chapter 2, the PROX reactor is used for the reduction of the CO component as it poisonous for the fuel cell in amounts at concentration above 10ppm (Chen *et al,* 2004). The Prox reactor reduces the CO content from LT-WGS reactor which normally contains 70% H_2 and 1% CO (Shelepova et al., 2011). The reactor is normally operated at the temperature of 120 – 150°C (Xie, Zhang, Li, & Zhang, 2014). The reactor excess oxygen is used for the oxidation of the carbon monoxide and the oxidation of the carbon monoxide is a quick reaction and the high concentration of H_2 in the reactor will also be combusted to form water. The Prox models are generally described by the conversion of (X_{co}) and the selectivity of carbon monoxide (S_{co}). The conversion and the selectivity of CO are described by the two reactions below (Pozdnyakova *et al.* 2006):

$$X_{CO} = \frac{(moles\ of\ CO\ in\ the\ inlet) - (moles\ of\ CO\ in\ the\ exit)}{(moles\ of\ CO\ in\ the\ exit)}\ X\ 100\% \quad (12)$$

$$S_{CO} = \frac{(moles\ of\ CO\ in\ the\ inlet) - (moles\ of\ CO\ in\ the\ exit)}{2\ X\ (moles\ of\ O_2\ in\ the\ inlet) - (moles\ of\ O_2\ in\ the\ exit)}\ X\ 100\% \quad (13)$$

An inlet composition of 1% CO and 70% H_2 results in an 95% CO conversion, and 85% selectivity of carbon monoxide and the total available hydrogen drops to 0.07%(Xie et al., 2014). If the hydrogen efficiency is defined in (moles of H_2 in)/ (moles of H_2 out), then the process has an efficiency of 99.9% (Boon *et al.,* 2016).

3.3.3 Plug Flow Reactor

In a conventional plug flow reactor with a cross-sectional area *A* (*x*) the reagents enters the section *at x = o.* The initial parameters such as temperature T_o, velocity U_o, mass density ρ_o and chemical composition X_{no}) are known. As the gas mixtures move through the working section the chemical reactions proceed. The products of the chemical reactions are removed from the exit of the section *(x = L)* (Jelezniak *et al.,* 2012) as indicated in the below figure:

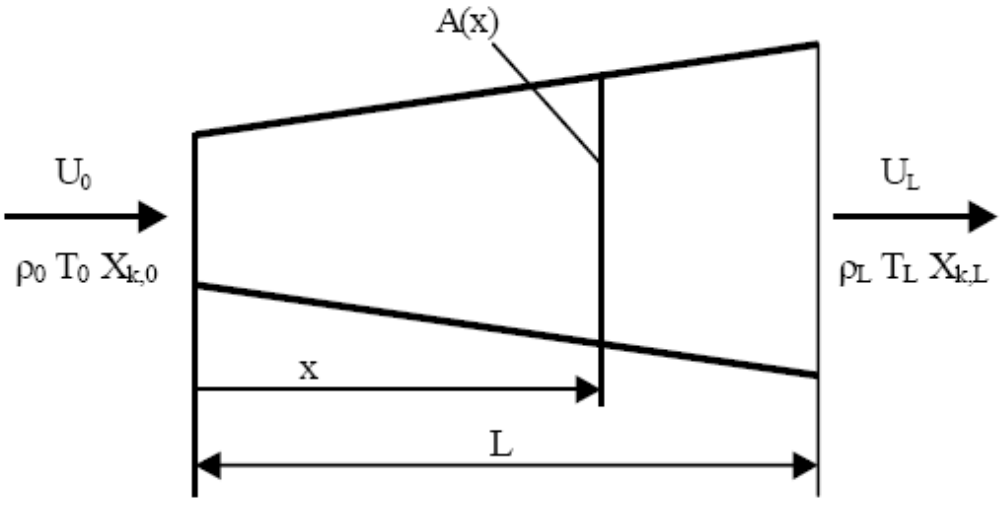

Figure 3. 2: Schematic diagram of plug-flow reactor (Jelezniak *et al.,* 2012).

The above Figure 3.3 plug flow reactor was assumed to operate at the below conditions:

- All the processes are steady state
- The reactor walls are well insulated
- There is no surface reaction with the gases
- Gas flow is subsonic (low Mach number)
- There is perfect mixing in the transversal direction
- There is no upstream or downstream mixing of gases

3.4 Conservation of Total Mass

The reactions in the plug flow reactor were assumed to be at steady-state which meant that the inlet mass must equal to the outlet mass and that there is no accumulation the system. The below equation describes the total mass conservation:

$$\frac{dQ}{dx} = 0 \quad ; \quad Q = A\rho\upsilon \tag{14}$$

where:

U = Axial flow velocity

Q = Mass flux across a surface A (the total mass of molecules which move across A per unit time, the Q units are g/sec). Equation (12) corresponds to a gas flow without mass accumulation in the reactor volume (Jelezniak *et al,* 2012).

3.5 Conservation of Energy

Conservation of energy was assumed for the plug flow reactor meaning the energy in equals to energy out and that there are no energy losses in the system. The below equations indicates the equation for a system with no energy losses

:

$$\frac{1}{A}\frac{d}{dx} \quad Q \quad (h + \frac{1}{2}u^2) \quad = 0 \tag{15}$$

where:

h = mean specific enthalpy

$$h = \sum_n Y_n h_n \qquad (16)$$

where,

h_n = specific enthalpy of the nth species in the units of (J/g) or (cal/g), the summation is over all species of the gas mixture.

Equation 14 represents the conservation of the total gas energy which is the sum of the kinetic energy and enthalpy. Again subsonic gas flow is considered where h >> $u^2/2$. The kinetic term can be omitted under these conditions. Differentiating out the products gives (Jelezniak *et al.,* 2012).

$$\frac{h}{A}\frac{dQ}{dx} + \frac{Q}{A}\frac{dh}{dx} = 0 \qquad (17)$$

The first term in equation (15) is equal to zero, then equation is written as:

$$\rho \frac{d}{dt} \sum_n Y_n h_n = 0 \qquad (18)$$

The ideal-gas specific enthalpy h_m is a function of the gas temperature only. Then the h_m derivative can be written as:

$$\frac{dh_n}{dt} = C p_n \frac{dT}{dt} \quad , \quad Cp_n = \frac{dh_n}{dT} \qquad (19)$$

where,

Cp_m is the specific heat capacity of the nth species at constant pressure, the units can be in (J/g.K) or (cal/g.K).

After differentiating the sum in equation (17) we obtain the final equation for the gas temperature:

$$\frac{dT}{dt} = \frac{1}{\rho \hat{C}_p} \sum_j u; \quad (20)$$

where,

the rates of heat of production in reaction U; are defined by the following equation:

$$U_j = -\Delta H_j \, q_{j,net} \quad (21)$$

The mean specific heat capacity at constant pressure $\hat{c}_p$ is:

$$\hat{c}_p = \sum_n Y_n \, Cp_n \quad (22)$$

Equations 19 and 20 coincide to together to use in Aspen plus.

3.6 Initial Conditions

$$\frac{dY_n}{dt} = \frac{m_n}{\rho} \sum_j w_{jn} \quad (23)$$

$$C_{tot} = \frac{P}{RT} \quad (24)$$

The equation of conservation of mass (12) and the conservation equations (13, 15, 17, 19, and 21) describes the temporal development of chemically reacting gas mixture in a plug flow reactor. However, these equations must be accompanied by the initial condition values U, P, T, ρ and Y_n must be known at t = 0 which is at x = 0 as shown in figure (3.2) (Jelezniak *et al.,* 2012).

The above equations were generic for the reformer, low temperature gas shift reactor and the low temperature water gas shift reactor.

3.7 Membrane Modelling

The performance of a Pd-based membrane in relation to maximizing the yield of hydrogen from the feedstock as well as minimizing the CO content of the reformate was evaluated using Engineering Equation Solver (EES).

In the membrane reactor the results that were obtained the SR out were used as a feedstock in the Pd-based membrane reactor. This was done to determine if it was necessary to have all the processes after the SR or is it plausible to use a membrane reactor instead of using HT and LT water gas shift reactors. The results from the SR at 500°C and at 5atm were fed into the membrane reactor to determine the flux, hydrogen purity, carbon monoxide conversion.

The palladium membrane was assumed to be isothermal co-current flow membrane reactor is used to describe the reactor performance. The hydrogen permeation through a membrane is described by the following equation (Roses *et al.,* 2011) at T = 500 °C, $P_{H2.\,feed}$ = 20 bar and $P_{H2.\,prem}$ = 1.013 bar, n = 0.5 and t = 50 x 10^{-6} m.

$$J_{H_2} = \frac{P_{H2}}{t}\left(P^n_{H2.\,feed} - P^n_{H2.\,prem}\right) \quad (25)$$

where:

J_{H_2} is the hydrogen molar flow per membrane surface measured in mol/ m^2.h

P_{H_2} is the permeability measured in bar

t is the membrane thickness measured in m

The term in the brackets is the driving force of hydrogen permeation

The hydrogen molar flow rate mass balance in the feed and permeate are determined by using the following equations respectively (Abdollahi et al., 2012) α_m = 1. 312 x 10^{-13} m^2/m^3, V = 1.211 x 10^{-8} m^3, ε_v = 600 μm, β_c = 0.05, ρ_c = 1.27 x10^7 m^3.

$$\frac{dn_{H_2}^F}{dV} = -\alpha_m U_{H_2}((P_{H_2}^F)^n - (P_{H_2}^P)^n) + (1-\varepsilon_v)\beta_C \rho_C r^F \quad (26)$$

$$\frac{dn_{H_2}^P}{dV} = \alpha_m U_{H_2}((P_{H_2}^P)^n - (P_{H_2}^P)^n) \quad (27)$$

where

$n_{H_2}^F$ and $n_{H_2}^P$ are the n_{H2} molar flow rate in the feed and permeate and are both measured in mol/h,

V is the volumetric flow rate (m^3),

α_m is the surface area of the membrane per unit reactor volume (m^2/m^3),

ε_v is the bed porosity on the feed side,

β_c is the of the solid volume occupied by the catalysts,

ρ_c is the catalyst density (g/m^3) and

r^F is the WGS reaction rate in (mol/g.h).

The mass balance for other components (CO, CO_2, C_3H_8) on the feed and permeate side were determined utilising the below equations (Abdollahi et al., 2012):

$$\frac{dn_j^F}{dV} = -\alpha_m U_{H_2}((P_j^F)^n - (P_j^P)^n) + \nu_j(1-\varepsilon_v)\beta_C \rho_C r^F \quad (28)$$

$$\frac{dn_j^P}{dV} = \alpha_m U_j((P_j^P)^n - (P_j^P)^n) \quad (29)$$

where,

n_j^F and n_j^P are the molar flow rate for the j components in the feed and permeate side respectively.

ν_j is the stoichiometric coefficient for the component j, and it is negative for reactants and positive for the products.

The pressure drop in the packed-bed reactor is determined using the Ergun Equation (Abdollahi et al., 2012):

$$-\frac{dP^F}{dV} = 10^{-6}\frac{f(G^F)^2}{A^F g_C d_p \rho^F} \quad (30)$$

$$f = \left[\frac{1-\varepsilon_v}{\varepsilon_v^3}\right]\left[1.75+\frac{150(1-\varepsilon_v)}{N_{\mathrm{Re}}^F}\right] \quad (31)$$

$$N_{\mathrm{Re}}^F = \frac{d_p G^F}{\mu^F} \quad (32)$$

Where P^F is the pressure on the feed side (bar), A^F is the cross-sectional area available to the flow for the reactor feed side (m^3), μ^F is the viscosity in (g/m.h), d_p is the particle diameter on the feed side (m), $G^F = \rho^F \mu^F$, is the superficial mass flow velocity on the feed side ($g/m^2.h$), μ^F is the average velocity of the fluid (m/h), ρ^F is the average fluid density (g/m^3) and g_c is the gravity conversion factor.

The following boundary conditions apply (Abdollahi et al., 2012):

$$V = 0 : n_j^F = n_{j0,}^F \quad n_J^P = n_{j0,}^P \quad P^F = P_{0,}^F \quad P^P = P_0^P \quad (33)$$

Where P_0^F and P_0^P are the inlet feed-side and permeate-side pressures in (bar) and n_{j0} is the inlet molar flow rate for the component j (mol/h).

The CO conversion and H_2 recovery are calculated using the following equations respectively (Anzelmo *et al.*, 2017).

$$X_{CO} = \frac{n_{CO,exit}^F + n_{CO,exit}^P}{n_{CO0}^F} \quad (34)$$

$$\mathrm{Re}_{H_2} = \frac{n_{H_{2,exit}}^P}{\left(n_{H_{2,exit}}^F + n_{H_{2,exit}}^P\right)} \quad (35)$$

where,

n_{CO0}^{F}, $n_{CO,exit}^{F}$ and $n_{CO,exit}^{P}$ are the CO molar flow rate in the inlet, CO molar flow rate at the exit of the reactor's feed side and the CO molar flow rate at the exit of the reactor's permeate side respectively and they are measured in (mol/h). $n_{H_{2,exit}}^{F}$ and $n_{H_{2,exit}}^{P}$ are the H_2 molar flow rates in the feed exit and permeate exit respectively.

Chapter 4: Results and Discussion

The focus of this work is the modelling and simulation study of the reforming process of LPG. The study will be limited to the reforming of the propane component of the LPG and at steady state operation. The simulation study will be performed at temperature ranging from 50 – 850 ^{o}C and the reformate will be fed to the palladium membrane reactor and the permeate results will be reported in this work.

4.1 Optimization of the Steam Reformer

The optimisation of the SR process was performed by manipulating the following parameters: temperature, steam-to-carbon (S/C) ratio, pressure, reactor length and diameter to obtain the optimal point of hydrogen production from propane conversion. The SR performance is evaluated using the conversion and hydrogen yield. Table 4.1 illustrates the SR at a temperature and pressure of 500 ^{o}C and 5atm respectively, HT-WGS at a temperature and pressure of 400 ^{o}C and 1 atm, LT-WGS at a temperature and pressure of 200^{o}C and 1 atm and PROX at a temperature and pressure of 130^{o}C and 1 atm performance in terms of molar concentration of the products produced.

Table 4. 1: Product composition from each reactor.

Component	**SR-out (kmol/hr)**	**HT-WGS-out (kmol/hr)**	**LT-WGS-out (kmol/hr)**	**PROX-out (kmol/hr)**
C_3H_8	0.915	0.915	0.915	0.915
H_2O	21.7	17.9	16.9	16.9
CO	10.2	6.36	5.32	1.35×10^{-9}
CO_2	0.157	4.50	5.54	10.86
H_2	26.0	29.8	30.9	30.9

In Table 4.1 it can observed that hydrogen has the highest mole fraction in the product stream in all reactors while propane has the lowest mole fraction in all the product streams and these results agree with the works of Schädel and Hardiman. In the results indicated in Table 4.1 it can also be observed that as the hydrogen mole fraction increase in the all the product streams the carbon monoxide mole fraction decreases in all the product streams.

4.2 Effect of Steam-to-Carbon Ratio

Table 4.2 and Figure 4.1 presents the effect of changing the reformer steam carbon ratio from 3-6 at a temperature and pressure of 500 ^{o}C and 5 atm on hydrogen, water and carbon monoxide. The hydrogen and water increase with increasing steam carbon ratio and the carbon monoxide produced decrease with increasing steam carbon ratio at the S/C below 3:1. When the S/C ratio increases, the hydrogen yield in the steam to carbon ratio of 4:1 is affected with the high yield of water. Hence a steam to carbon ratio of 3:1 is selected as optimal steam to carbon ratio.

Table 4. 2: Steam to carbon ratio optimization results for propane gas at a steam carbon ratio (1-5).

S/C	H_2 (kmol/hr)	H_2O (kmol/hr)	CO (kmol/hr)	C_3H_8 (kmol/hr)
1	18.5	2.0	8.00	2.18
2	32.4	5.70	7.30	0.57
3	38.3	13.7	6.08	0.027
4	29.5	21.0	9.67	0.0011
5	20.8	31.6	10.55	$9.15X10^{-05}$

In Figure 4.1 it is evident that steam to carbon ratio of 3:1 is the most applicable for reformats gases due to the high reduction of CO content based on the simulation and other authors such as Xu and Froment in 1989 and Patel and Sunol 2007. However, the excess steams in SMR is processed forward to the water gas shift reactor for further reduction of CO content and produces more hydrogen.

Figure 4.1 also show the results of water production in the system at the different steam to carbon ratio. Figure 4.1 also indicates that the water is increases with the increase of the steam to carbon ratio, which means more water content is expected as the s/c increasing which will affect the hydrogen production as steam to carbon ratio increasing.

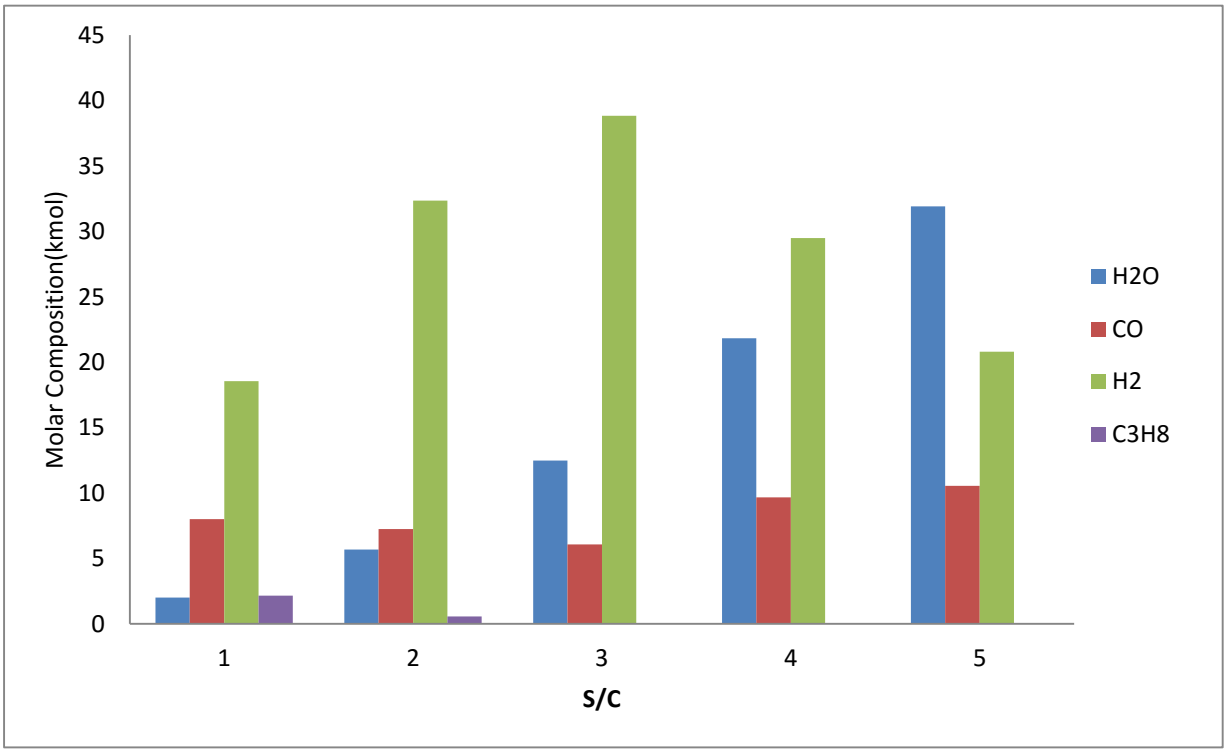

Figure 4. 1: Effect of steam-to-carbon ratio in the SR reactor at fixed conditions (T= 550°C and 5 atm).

4.3 Effect of temperature

Figure 4.2 illustrates the effect of changing the temperature in the reformer and it can be noted that hydrogen increases with increasing temperature, it increases from a molar fraction $7.38X10^{-5}$ at 50°C to 0.0485 at 550°C. After 550°C a slow decrease in the hydrogen production is noted until 900°C it decreases to a molar fraction of 0.0444 due to the high production of water. The water in the reformer decreases with increasing temperature it decreases from a molar fraction of 0.0447 at 50°C to a molar fraction of 0.0168 at temperature of 550°C and slowly starts increasing to a molar fraction of 0.0216 at 900°C. The C_3H_8 mole fraction in the reformer also decreases with increasing temperature it decreases from a molar

fraction of 0.0698 at 50°C to a molar fraction of 2.61×10^{-14} at 900°C. These fluctuations clearly indicate that the optimum temperature for propane reforming is 550°C. Similar trend was reported by Schädel et al., 2009 where optimum propane conversion was observed at around 500°C.

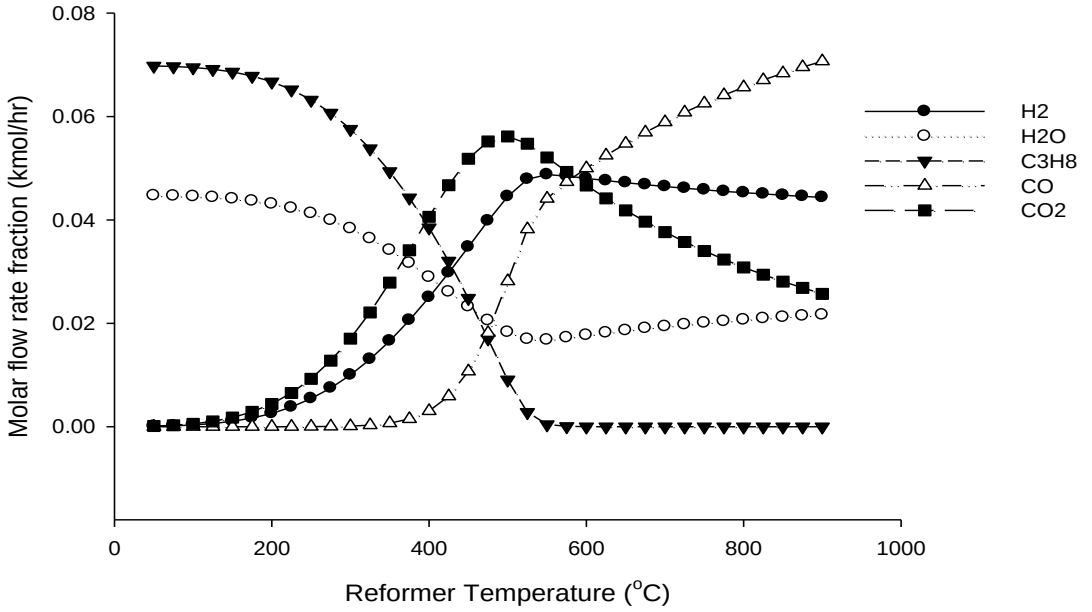

Figure 4. 2: Effect of changing the reactor temperature for hydrogen production in the SR at constant (P = 5 atm and S/C = 3).

In figure 4.3 it can be observed that at temperature above 500°C and the steam carbon ratio of 3 the yield of hydrogen is at its maximum. An increase in the SR reactor temperature increases the hydrogen yield but to a certain degree hence, it is operated at low temperature as reported by Hardiman *et al.,* (2004).

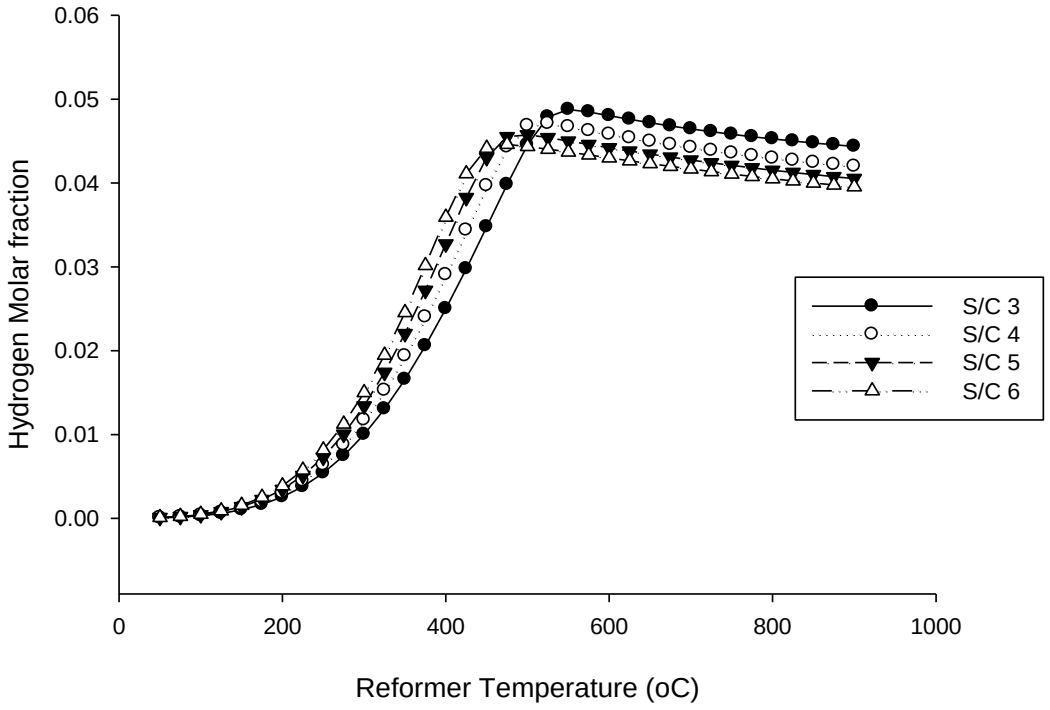

Figure 4. 3; Effect of temperature on the production of hydrogen at various steam-to carbon ratio's.

4.4 Effect of pressure

Figure 4.4 illustrates the effect of pressure at a steam carbon ratio of 3 and temperature of 500°C.

The effect of pressure in the SR indicates that there is a decrease in the amount of propane with increasing pressure (for example from 4.38 kmol/hr at 0.5 atm to 0.915 kmol/hr at 5 atm) as it is expected due to the fact most of the propane is being converted to hydrogen and carbon monoxide as an increase in both species is noted (for example hydrogen increases from 1.07 kmol/hr at 0.5 atm to 26.0 kmol/hr to 5 atm) and the (carbon monoxide increases from 0.458 kmol/hr at 0.5 atm to 1.02 kmol/hr at 5 atm). The amount of water in the SR decreases with increasing pressure (for example 32.9 kmol/hr at 0.5 atm to 27.7 kmol.hr at 5 atm) due to the water gas shift reaction which results in the increase of carbon dioxide and hydrogen amount (e.g. the carbon dioxide increases 0.000515 kmol/hr from 0.707 kmol/hr at 5 atm) as indicated by Castillo et al., 2015)

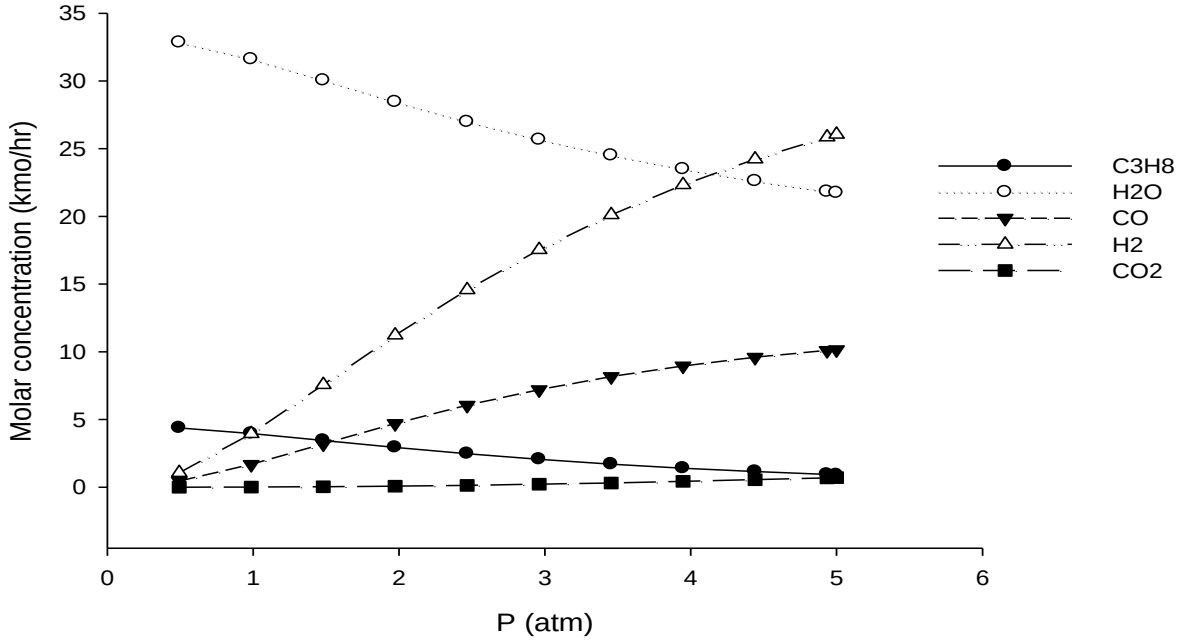

Figure 4. 4: Effect of pressure in the SR at constant temperature (T = 550°C).

4.5 Effect of reactor diameter

Figure 4.5 indicates the effect of changing the diameter on the conversation of propane and water and the hydrogen yield, carbon monoxide and carbon dioxide yield in the steam reforming reactor. Propane and water conversion increases with increasing diameter in the SR as the propane and water being converted to hydrogen and carbon monoxide and this is evident when analysing the hydrogen yield and carbon monoxide yield as indicated in figure 4.5 it is noted that both the hydrogen yield and increase with increasing SR diameter. In the results obtained in figure 4.5 it is evident that there is no change in the amount of carbon dioxide produced in the SR this is due to the fact that the propane and water are converted to hydrogen and carbon monoxide.

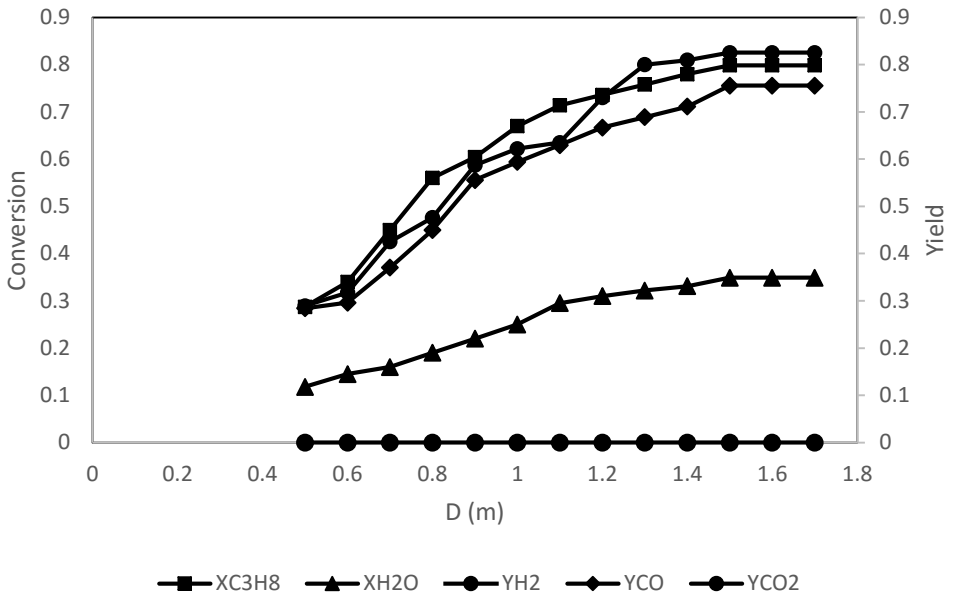

Figure 4. 5: Effect of the reactor diameter on the conversion of propane, water and its effects on the hydrogen yield, carbon monoxide yield and carbon dioxide yield in the SR at constant conditions (T = 550°C, P = 5 atm)

4.6 Effect of reactor length

Figure 4.6 represents the effect of changing the length of the reactor in the SR, the results obtained indicated a decrease in mole concentration for propane with increasing diameter (e.g. it decreases from 1.65 kmol/hr at the length of 0.5m to 0.915 kmol/hr at the length of 1m) as it is expected due to the fact most of the propane is being converted to hydrogen and carbon monoxide as an increase in both species is noted (e.g. hydrogen increases from 20.5 kmol/hr at the length of 0.5m to 26.0 kmol/hr at the length of 1m) and the (carbon monoxide increases from 8.32 kmol/hr at the length of 0.5m to 10.2 kmol/hr at the length of 1m). The amount of water in the SR decreases with increasing length (e.g. it decreases from 24.3 kmol/hr at the length of 0.5m to 21.7 kmol.hr at the length of 1m) due to the water gas shift reaction which results in the increase of carbon dioxide and hydrogen (e.g the carbon dioxide increases from 0.335 kmol/hr from the length of 0.5m to 0.707 kmol/hr at the length of 1m).

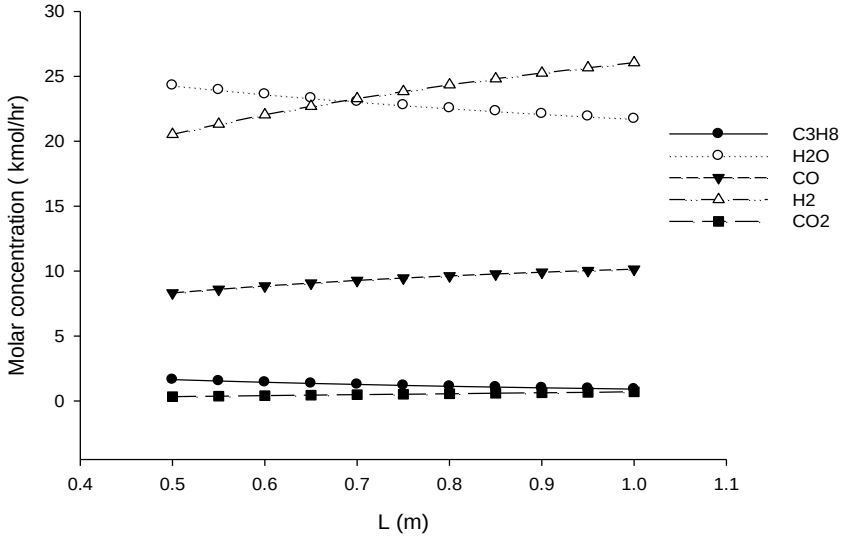

Figure 4. 6: Effect of the reactor length at conditions (T = 550°C, P = 5 atm).

Based on the simulation results it can be concluded the optimum steam-to-carbon ration in the SR is 3 at a temperature and pressure of 550°C and 5 atm for propane reforming with a reactor length of 1m and diameter of 1.5m respectively.

4.7 High and Low temperature WGS analysis

The water gas shift reactor was designed to further decrease the CO concentration in the reactor to form carbon dioxide and hydrogen. This was performed in two stages with a HT-WGS and LT-WSG reactors were operated at pressure of 1atm both changing temperatures in order to determine the CO to CO_2 conversion and the hydrogen yield in both HT-WGS and LT-WGS reactors. In figure 4.10 and it can be observed that increasing the temperature in the HT-WGS reactor increases the carbon monoxide and carbon dioxide conversion to 80% and 70% respectively while the rest is converted in the LT-WGS reactor which indicates that results obtained agrees with work done by Chen *et al* in 2008.

In figure 4.11 it observed that increasing the HT-WGS reactor temperature using Ni/$MgAl_2O_4$ catalyst increases the rate of the reaction in the HT-WGS reactor therefore, increasing the hydrogen yield to 80%.

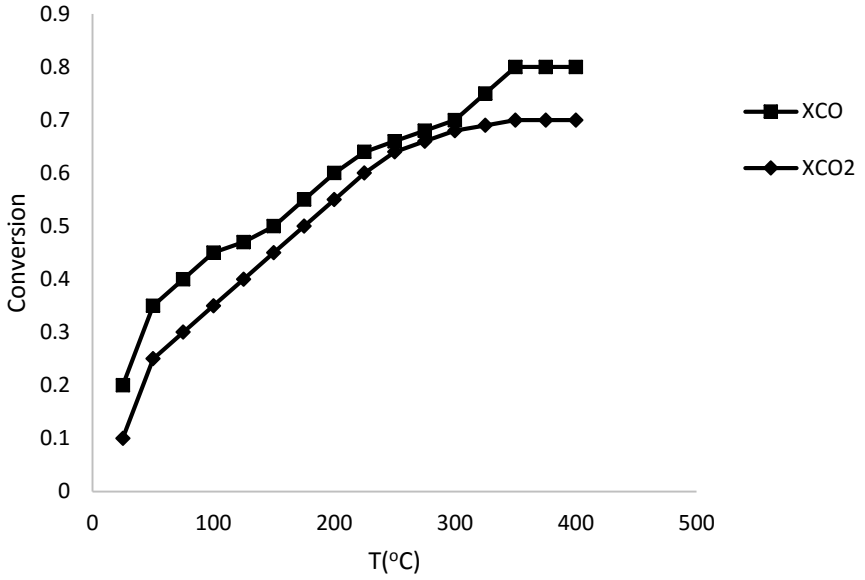

Figure 4. 7: Comparison of carbon and carbon dioxide conversions in an HT-WGS reactor with an increasing temperature using Ni/$MgAl_2O_4$ catalyst.

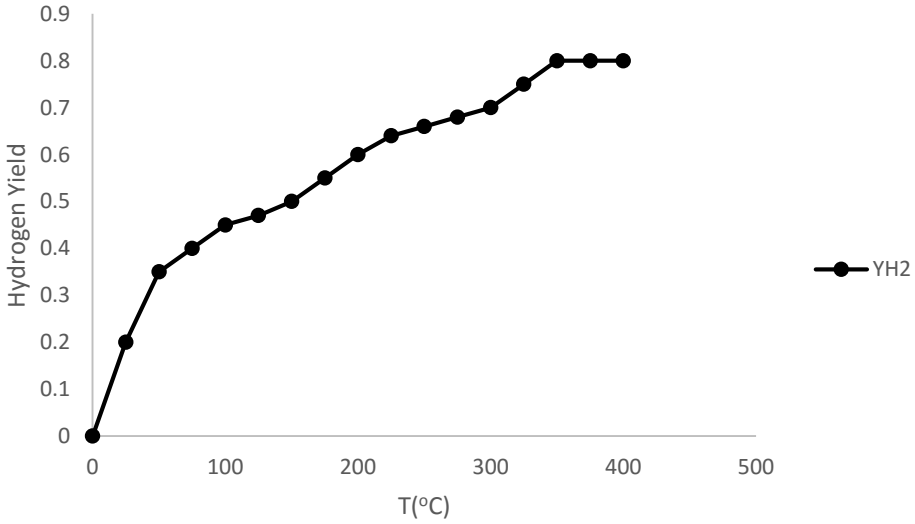

Figure 4. 8: Hydrogen yield in a HT-WGS reactor with an increasing temperature using Ni/$MgAl_2O_4$ catalyst.

In figure 4.9 and it can be observed that increasing the temperature in the LT-WGS reactor increases the carbon monoxide and carbon dioxide conversion to 90% and 80% respectively while the rest is converted in the PrOx reactor in the range of around 99.9%.

In figure 4.10 it observed that increasing the LT-WGS reactor temperature using Ni/$MgAl_2O_4$ catalyst increases the rate of the reaction in the LT-WGS reactor therefore, increasing the hydrogen yield to 90%.

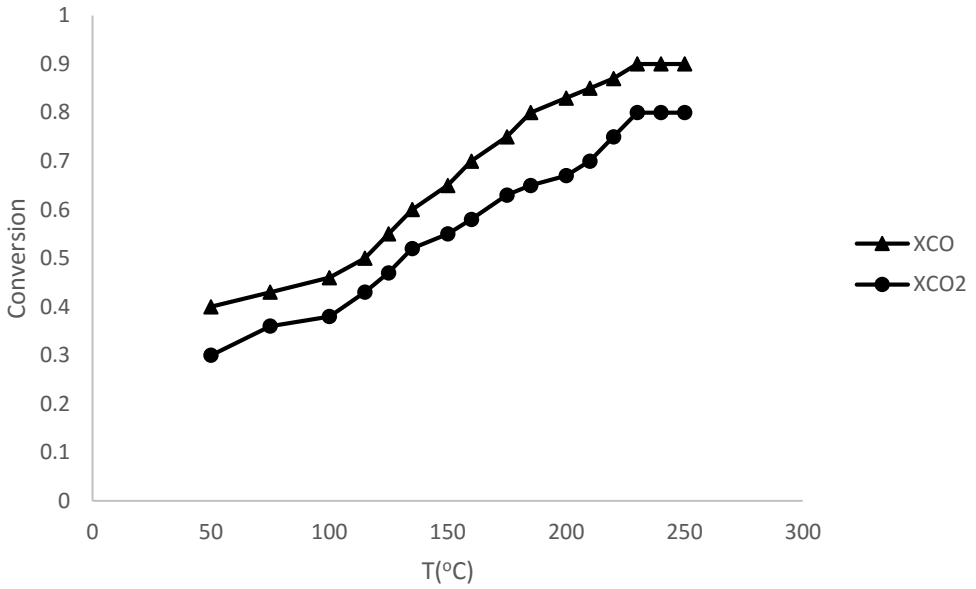

Figure 4. 9: Comparison of carbon and carbon dioxide conversions in an LT-WGS reactor with an increasing temperature using Ni/$MgAl_2O_4$ catalyst.

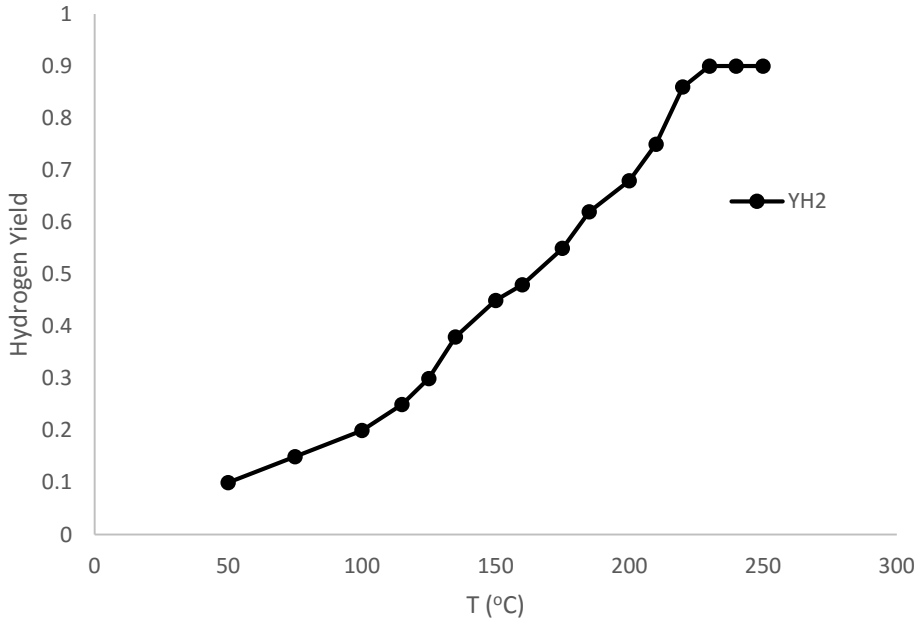

Figure 4. 10: Comparison of carbon and carbon dioxide conversions in an LT-WGS reactor with an increasing temperature using $Ni/MgAl_2O_4$ catalyst.

4.8 Prox Analysis

The purpose of the Prox reactor is to reduce the CO content for the PEM fuel cell system. The CO content need to be lower than 10ppm which is what is required in the PEM fuel cell to prevent cell contamination. The Prox reactor is operated at a temperature and pressure of 130°C and 1 atm respectively. The Prox models are generally described by the conversion of (X_{co}) and the selectivity of carbon monoxide (S_{co}).

The results obtained indicated that the amount of carbon monoxide entering the Prox reactor was 5.32 kmol/hr and the amount leaving the reactor was $1.35x10^{-9}$ kmol/hr, which is less than 10ppm of CO required for PEM fuel system. However, the question of whether a HT-WGS reactor, LT-WGS reactor and Prox reactor is required in this system still remains and that will be answered by the results that will be obtained from the membrane reactor.

Table 4. 3: Illustration of the products in the Prox reactor.

Component	**LT-WGS-out (kmol/hr)**	**PROX-out (kmol/hr)**	**Conversion (Fraction)**
C_3H_8	0.915	0.915	0
H_2O	16.9	16.9	0
CO	5.32	$1.35x10^{-9}$	1
CO_2	5.54	10.86	-0.490
H_2	30.9	30.9	0

4.9 Membrane Results

The results from the SR operated at temperature and pressure of 550 ^oC and 5 atm respectively at a steam to carbon ratio 3:1 were used as a feedstock to the Pd-based membrane reactor to evaluate the performance of a Pd-based membrane in relation to maximizing the yield of hydrogen from the feedstock as well as minimizing the CO content of the reformate.

Figure 4.11 illustrates the hydrogen transport, a single gas permeation in a membrane reactor operated at a temperature and pressure of 500 ^oC and 20 bar respectively The results obtained indicate that the H_2 transport obeys the law indicated by equation 25 and the value of n ranges from 0.5 – 1. The flux increases with in change in pressure.

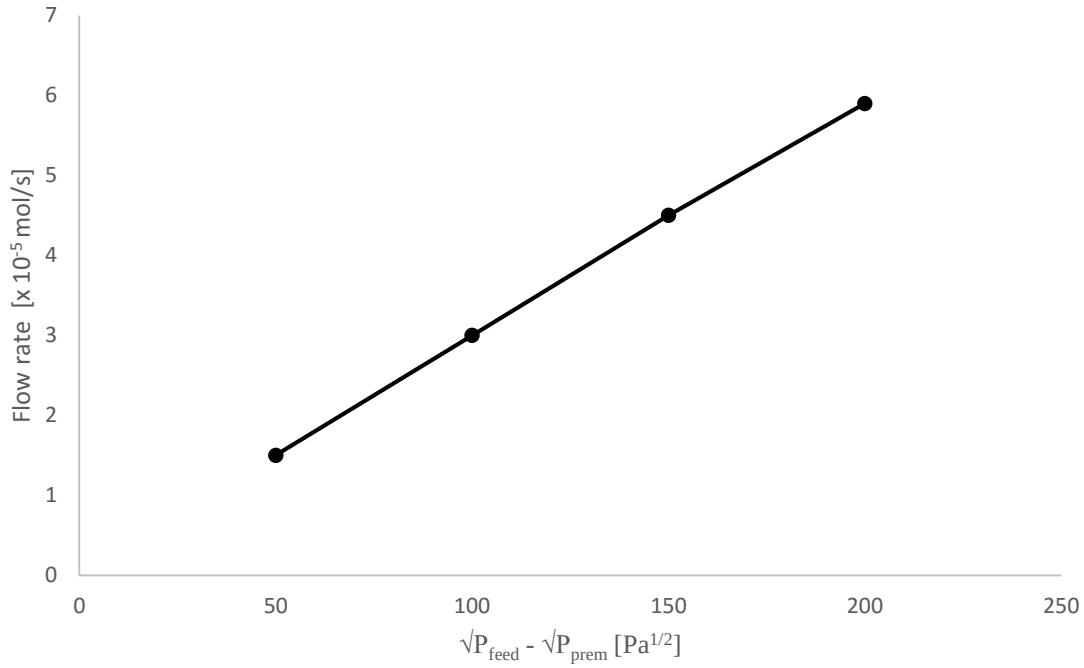

Figure 4. 11: Flux of hydrogen as a function of $(P^F)^n$ - $(P^P)^n$ at T = 500°C and P= 20 bar.

Figure 4.12 indicates the effect of the feed pressure on the membrane reactor conversion with the optimum SR reformate utilised as feedstock in the palladium-based membrane reactor. In the figure 4.13 below it is evident that increasing the pressure has impact on the conversion particularly at lower W_c/n^F_{co0}. It was observed that at 20 bar at a catalyst weight of 4 g-cat.h/mol-CO the CO conversion is at its maximum.

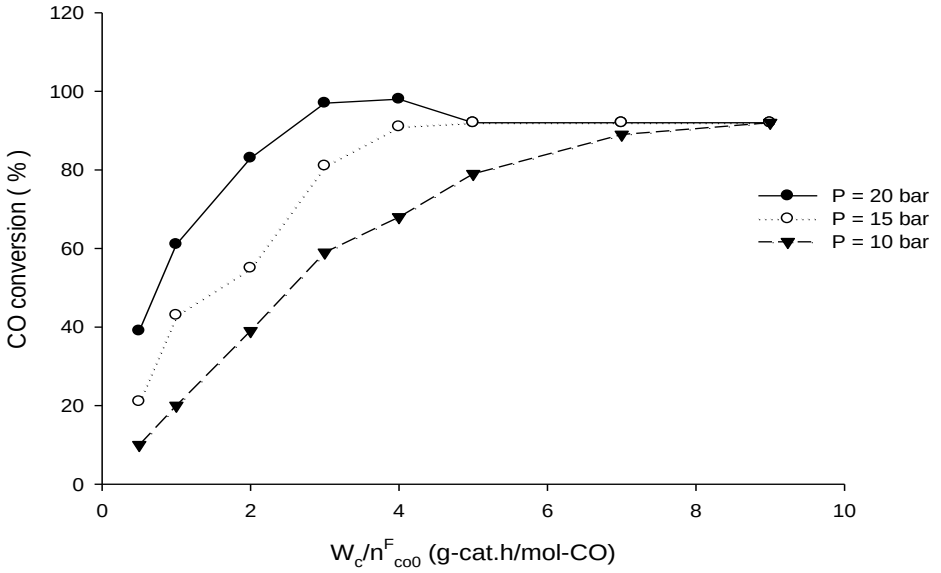

Figure 4. 12: Effect of pressure on CO conversion, T = 500°C and SR = 3.

Figure 4.13 represents the effect of pressure on hydrogen recovery with the optimum SR reformate utilised as feedstock in the palladium-based membrane reactor. It was observed that increasing the pressure has a positive effect on the H_2 recovery as an increase in pressure results in a direct increase in H_2 recovery. This was particularly noted at high pressure where maximum hydrogen recovery was obtained at 20bar at a catalyst weight of 4 g-cat.h/mol-CO while at the lowest it was obtained at 10bar at a catalyst weight of 7 g-cat.h/mol-CO.

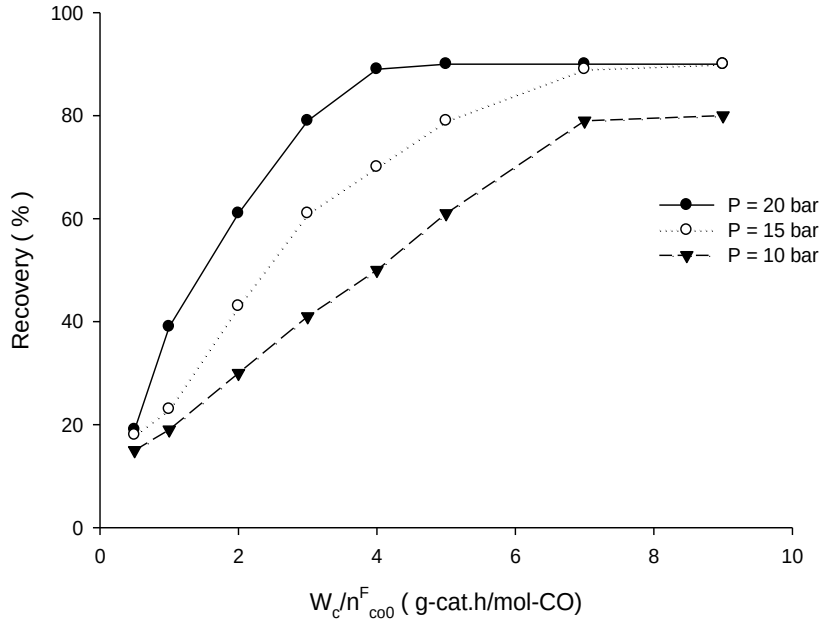

Figure 4. 13: Effect of pressure on H_2 recovery, T = 500°C and SR = 3.

The performance of a membrane reactor is determined by verifying the H_2 purity. In figure 4.14 it is shown that increasing the pressure results in a decrease in hydrogen purity and this is due to the fact that an increase in pressure results with CO having less contact time with other species to react therefore exiting the hydrogen in the permeate side.
The hydrogen purity at 500°C s and high W_c/n^F_{co0} = 0.1 was found to be 99.99%.

The results obtained from the pre-reformer and membrane reactor clearly indicate that is it is feasible to employ a palladium-based membrane reactor for the production of ultra-pure hydrogen from the products of a liquefied petroleum gas (LPG) pre-reformer and that prox reactor is not required in this process.

Chapter 5: Conclusion and Recommendation

The reforming of LPG simulations and optimisations were performed using Aspen plus version 7.1 and the performance of a Pd-based membrane in relation to maximizing the yield of hydrogen from the feedstock as well as minimizing the CO content of the reformate was evaluated using Engineering Equation Solver (EES).

5.1.1 Conclusion

From this work, it can be concluded that it is possible to produce high concentrations of hydrogen from LPG reforming. The gradual increase of temperature and the use of high water concentrations decrease the production of coke and increase the formation of H_2.

The following conclusions can the made regarding the SR and the Pd-based membrane reactor:

- The optimum S/C, temperature and pressure resulting in optimum yield is to have the SR operating at S/C = 3, T(^oC) = 500 at the pressure of 5atm.
- The ideal pre-reformer mixture to be fed into the palladium membrane reactor at optimal conditions are H_2 = 38.3 kmol/hr, H_2O = 13.7 kmol/hr, CO = 6.08 kmol/hr and C_3H_8 = 0.027 kmol/hr.
- The evaluation of the performance of a Pd-based membrane in relation to maximizing the yield of hydrogen from the feedstock as well as minimizing the CO content of the reformate clearly indicate that it is feasible to employ a palladium-based membrane reactor for the production of ultra-pure hydrogen from the products of a liquefied petroleum gas (LPG) pre-reformer. Based on the results that have been obtained from the membrane permeate it can be concluded that the optimal reformer conditions results in the optimal hydrogen recovery and CO conversion in the membrane reactor at a pressure of 20bar and temperature of 500^oC therefore, translating to a development of purification system.

5.1.2 Recommendation

After the steam reforming process for the production of ultra-pure hydrogen it is recommended that a palladium-based reactor be utilised for the production and separation of ultra-pure hydrogen therefore, removing WSG reactor and the Prox reactor after the steam reformer process. The cost analysis of the system can assist to improve the system.

Reference

Abatzoglou, N., & Fauteux-Lefebvre, C. (2015). Review of catalytic syngas production through steam or dry reforming and partial oxidation of studied liquid compounds. *Wiley Interdisciplinary Reviews: Energy and Environment*.

Abbasi, M., Farniaei, M., Rahimpour, M. R., & Shariati, A. (2014). Methane dry reformer by application of chemical looping combustion via Mn-based oxygen carrier for heat supplying and carbon dioxide providing. *Chemical Engineering and Processing: Process Intensification, 79*(0), 69-79. doi:http://dx.doi.org/10.1016/j.cep.2014.03.004

Abdollahi, M., Yu, J., Liu, P. K., Ciora, R., Sahimi, M., & Tsotsis, T. T. (2012). Ultra-pure hydrogen production from reformate mixtures using a palladium membrane reactor system. *Journal of Membrane Science, 390*, 32-42.

Al-Mufachi, N., Rees, N., & Steinberger-Wilkens, R. (2015). Hydrogen selective membranes: a review of palladium-based dense metal membranes. *Renewable and Sustainable Energy Reviews, 47*, 540-551.

Alimov, V., Busnyuk, A., Notkin, M., & Livshits, A. (2014). Pd–V–Pd composite membranes: Hydrogen transport in a wide pressure range and mechanical stability. *Journal of Membrane Science, 457*, 103-112.

Almansoori, A., Liu, H., Elkamel, A., & Fowler, M. (2015). Analysis of Hydrogen Economy for Hydrogen Fuel Cell Vehicles in Ontario.

Anderson, D. M., Nasr, M. H., Yun, T. M., Kottke, P. A., & Fedorov, A. G. (2015). Sorption-Enhanced Variable-Volume Batch–Membrane Steam Methane Reforming at Low Temperature: Experimental Demonstration and Kinetic Modeling. *Industrial & Engineering Chemistry Research, 54*(34), 8422-8436.

Augustine, A. S., Ma, Y. H., & Kazantzis, N. K. (2011). High pressure palladium membrane reactor for the high temperature water–gas shift reaction. *International Journal of Hydrogen Energy, 36*(9), 5350-5360.

Barbieri, G., Brunetti, A., Caravella, A., & Drioli, E. (2011). Pd-based membrane reactors for one-stage process of water gas shift. *RSC Advances, 1*(4), 651-661.

Bartels, J. R., Pate, M. B., & Olson, N. K. (2010). An economic survey of hydrogen production from conventional and alternative energy sources. *International Journal of Hydrogen Energy, 35*(16), 8371-8384. doi:http://dx.doi.org/10.1016/j.ijhydene.2010.04.035

Basile, A., Gallucci, F., & Paturzo, L. (2005). A dense Pd/Ag membrane reactor for methanol steam reforming: experimental study. *Catalysis Today, 104*(2), 244-250.

Battersby, S., Duke, M. C., Liu, S., Rudolph, V., & Costa, J. C. D. d. (2008). Metal doped silica membrane reactor: Operational effects of reaction and permeation for the

water gas shift reaction. *Journal of Membrane Science, 316*(1–2), 46-52. doi:http://dx.doi.org/10.1016/j.memsci.2007.11.021

Bereketidou, O., & Goula, M. (2012). Biogas reforming for syngas production over nickel supported on ceria–alumina catalysts. *Catalysis Today, 195*(1), 93-100.

Bhargav, A. (2010). Model development and validation of palladium-based membranes for hydrogen separation in PEM fuel cell systems.

Bhargav, A., Lyubovsky, M., & Dixit, M. (2014). Managing fuel variability in LPG-based PEM fuel cell systems–I: Thermodynamic simulations. *International Journal of Hydrogen Energy, 39*(30), 17231-17239.

Bi, Y., Xu, H., Li, W., & Goldbach, A. (2009). Water–gas shift reaction in a Pd membrane reactor over Pt/Ce0.6Zr0.4O2 catalyst. *International Journal of Hydrogen Energy, 34*(7), 2965-2971. doi:http://dx.doi.org/10.1016/j.ijhydene.2009.01.046

Bosko, M. L., Miller, J. B., Lombardo, E. A., Gellman, A. J., & Cornaglia, L. M. (2011). Surface characterization of Pd–Ag composite membranes after annealing at various temperatures. *Journal of Membrane Science, 369*(1), 267-276.

Bredesen, R., Peters, T. A., Boeltken, T., & Dittmeyer, R. (2015). Pd-Based Membranes in Hydrogen Production for Fuel cells. *Process Intensification for Sustainable Energy Conversion*, 209.

Castillo, J. M. V., Sato, T., & Itoh, N. (2015). Effect of temperature and pressure on hydrogen production from steam reforming of biogas with Pd–Ag membrane reactor. *International Journal of Hydrogen Energy, 40*(8), 3582-3591.

Chen, W.-H., Hsieh, T.-C., & Jiang, T. L. (2008). An experimental study on carbon monoxide conversion and hydrogen generation from water gas shift reaction. *Energy Conversion and Management, 49*(10), 2801-2808.

Chen, Y., Mahecha-Botero, A. s., Lim, C. J., Grace, J. R., Zhang, J., Zhao, Y., & Zheng, C. (2014). Hydrogen Production in a Sorption-Enhanced Fluidized-Bed Membrane Reactor: Operating Parameter Investigation. *Industrial & Engineering Chemistry Research, 53*(14), 6230-6242.

Cheng, X., Shi, Z., Glass, N., Zhang, L., Zhang, J., Song, D., . . . Shen, J. (2007). A review of PEM hydrogen fuel cell contamination: Impacts, mechanisms, and mitigation. *Journal of Power Sources, 165*(2), 739-756.

Corbo, P., Migliardini, F., & Veneri, O. (2011). Fuel Cells for Automotive Applications *Hydrogen Fuel Cells for Road Vehicles* (pp. 71-102): Springer London.

Dadda, B., Abboudi, S., & Ghezal, A. (2013). Transient two-dimensional model of heat and mass transfer in a PEM fuel cell membrane. *International Journal of Hydrogen Energy, 38*(17), 7092-7101.

Dai, X., Liang, J., Ma, D., Zhang, X., Zhao, H., Zhao, B., . . . Qiao, S. (2014). Large-pore mesoporous RuNi-doped TiO< sub> 2</sub>-Al< sub> 2</sub> O< sub> 3</sub>

nanocomposites for highly efficient selective CO methanation in hydrogen-rich reformate gases. *Applied Catalysis B: Environmental*.

Deutschmann, O., Beller, M., Renken, A., & van Santen, R. (2012). High temperature catalysis: role of heterogeneous, homogeneous, and radical chemistry. *Catalysis; Beller, M.; Renken, A.; van Santen, RA, Eds*, 365-389.

El Hawa, H. W. A., Paglieri, S. N., Morris, C. C., Harale, A., & Way, J. D. (2015). Application of a Pd–Ru composite membrane to hydrogen production in a high temperature membrane reactor. *Separation and Purification Technology, 147*, 388-397.

Enger, B. C., Lødeng, R., & Holmen, A. (2008). A review of catalytic partial oxidation of methane to synthesis gas with emphasis on reaction mechanisms over transition metal catalysts. *Applied Catalysis A: General, 346*(1), 1-27.

Erickson, P. A., & Vernon, D. R. (2014). Reformation of Hydrocarbon Fuels. *Handbook of Hydrogen Energy*, 23.

Faria, W. L. S., Dieguez, L. C., & Schmal, M. (2008). Autothermal reforming of propane for hydrogen production over Pd/CeO2/Al2O3 catalysts. *Applied Catalysis B: Environmental, 85*(1–2), 77-85. doi:http://dx.doi.org/10.1016/j.apcatb.2008.06.031

Gade, S. K., Thoen, P. M., & Way, J. D. (2008). Unsupported palladium alloy foil membranes fabricated by electroless plating. *Journal of Membrane Science, 316*(1–2), 112-118. doi:http://dx.doi.org/10.1016/j.memsci.2007.08.022

Gallucci, F., Fernandez, E., Corengia, P., & van Sint Annaland, M. (2013). Recent advances on membranes and membrane reactors for hydrogen production. *Chemical Engineering Science, 92*, 40-66.

Getman, R. B., Bae, Y.-S., Wilmer, C. E., & Snurr, R. Q. (2011). Review and analysis of molecular simulations of methane, hydrogen, and acetylene storage in metal–organic frameworks. *Chemical reviews, 112*(2), 703-723.

Ghasemzadeh, K., Morrone, P., Babalou, A., & Basile, A. (2014). A simulation study on methanol steam reforming in the silica membrane reactor for hydrogen production. *International Journal of Hydrogen Energy*.

Gökaliler, F., Göçmen, B. A., & Aksoylu, A. E. (2008). The effect of Ni:Pt ratio on oxidative steam reforming performance of Pt–Ni/Al2O3 catalyst. *International Journal of Hydrogen Energy, 33*(16), 4358-4366. doi:http://dx.doi.org/10.1016/j.ijhydene.2008.05.068

Gökaliler, F., Önsan, Z. I., & Aksoylu, A. E. (2012). Power-law type rate equation for propane ATR over Pt–Ni/Al2O3 catalyst. *International Journal of Hydrogen Energy, 37*(13), 10425-10429. doi:http://dx.doi.org/10.1016/j.ijhydene.2012.01.114

Guerra, C., Lanzini, A., Leone, P., Santarelli, M., & Brandon, N. P. (2014). Optimization of dry reforming of methane over Ni/YSZ anodes for solid oxide fuel cells. *Journal of Power Sources, 245*, 154-163. doi:http://dx.doi.org/10.1016/j.jpowsour.2013.06.088

Gutierrez, A., Karinen, R., Airaksinen, S., Kaila, R., & Krause, A. (2011). Autothermal reforming of ethanol on noble metal catalysts. *International Journal of Hydrogen Energy, 36*(15), 8967-8977.

Hahn, R., Gabler, A., Thoma, A., Glaw, F., & Lang, K. D. (2015). Small fuel cell system with cartridges for controlled hydrogen generation. *International Journal of Hydrogen Energy, 40*(15), 5340-5345. doi:http://dx.doi.org/10.1016/j.ijhydene.2014.11.080

Hardiman, K. M., Ying, T. T., Adesina, A. A., Kennedy, E. M., & Dlugogorski, B. Z. (2004). Performance of a Co-Ni catalyst for propane reforming under low steam-to-carbon ratios. *Chemical Engineering Journal, 102*(2), 119-130.

Hernantes, J., Rich, E., Laugé, A., Labaka, L., & Sarriegi, J. M. (2013). Learning before the storm: Modeling multiple stakeholder activities in support of crisis management, a practical case. *Technological Forecasting and Social Change, 80*(9), 1742-1755. doi:http://dx.doi.org/10.1016/j.techfore.2013.01.002

Holladay, J. D., Hu, J., King, D. L., & Wang, Y. (2009). An overview of hydrogen production technologies. *Catalysis Today, 139*(4), 244-260. doi:http://dx.doi.org/10.1016/j.cattod.2008.08.039

Hou, T., Yu, B., Zhang, S., Zhang, J., Wang, D., Xu, T., . . . Cai, W. (2015). Hydrogen production from propane steam reforming over Ir/Ce0.75Zr0.25O2 catalyst. *Applied Catalysis B: Environmental, 168–169*, 524-530. doi:http://dx.doi.org/10.1016/j.apcatb.2015.01.023

Inglesi, R. (2010). Aggregate electricity demand in South Africa: Conditional forecasts to 2030. *Applied Energy, 87*(1), 197-204. doi:http://dx.doi.org/10.1016/j.apenergy.2009.08.017

Ioanooa, S., Laguna, O. H., & Centeno, M. A. (2013). Microprocess Technology for Hydrogen Purification. *Renewable Hydrogen Technologies: Production, Purification, Storage, Applications and Safety*, 225.

Iulianelli, A., Liguori, S., Wilcox, J., & Basile, A. (2016). Advances on methane steam reforming to produce hydrogen through membrane reactors technology: A review. *Catalysis Reviews*, 1-35.

Iulianelli, A., Ribeirinha, P., Mendes, A., & Basile, A. (2014). Methanol steam reforming for hydrogen generation via conventional and membrane reactors: A review. *Renewable and Sustainable Energy Reviews, 29*, 355-368.

Jeong, D.-W., Potdar, H. S., Shim, J.-O., Jang, W.-J., & Roh, H.-S. (2013). H2 production from a single stage water–gas shift reaction over Pt/CeO2, Pt/ZrO2, and

Pt/Ce(1−x)Zr(x)O2 catalysts. *International Journal of Hydrogen Energy, 38*(11), 4502-4507. doi:http://dx.doi.org/10.1016/j.ijhydene.2013.01.200

Jörissen, L. (2012). Prospects of Hydrogen as a Future Energy Carrier *Fuel Cells in the Waste-to-Energy Chain* (pp. 189-203): Springer London.

Koc, R., Kazantzis, N. K., & Ma, Y. H. (2011). Process safety aspects in water-gas-shift (WGS) membrane reactors used for pure hydrogen production. *Journal of Loss Prevention in the Process Industries, 24*(6), 852-869.

Kolb, G., Keller, S., Tiemann, D., Schelhaas, K.-P., Schürer, J., & Wiborg, O. (2012). Design and operation of a compact microchannel 5kWel, net methanol steam reformer with novel Pt/In2O3 catalyst for fuel cell applications. *Chemical Engineering Journal, 207*, 388.

Kumara, M. A., Venumadhava, C., Sagara, T., Surendara, M., Lingaiaha, N., Raob, G. N., & Prasada, P. S. (2014). Catalytic tri-reforming of glycerol for hydrogen generation. *Indian Journal of Chemistry, 53*, 530-534.

Lai, E. P. (2013). Recent Advances of Liquefied Petroleum Gas Sensors–From Environmental to Biotechnology Applications. *J Pet Environ Biotechnol, 4*, e117.

Laosiripojana, N., Sutthisripok, W., Charojrochkul, S., & Assabumrungrat, S. (2011). Steam reforming of LPG over Ni and Rh supported on Gd-CeO_2 and Al_2O_3: Effect of support and feed composition. *Fuel, 90*(1), 136-141.

LeValley, T. L., Richard, A. R., & Fan, M. (2014). The progress in water gas shift and steam reforming hydrogen production technologies – A review. *International Journal of Hydrogen Energy, 39*(30), 16983-17000. doi:http://dx.doi.org/10.1016/j.ijhydene.2014.08.041

Liu, C. j., Ye, J., Jiang, J., & Pan, Y. (2011). Progresses in the Preparation of Coke Resistant Ni-Based Catalyst for Steam and CO2 Reforming of Methane. *ChemCatChem, 3*(3), 529-541.

Liu, H., Pan, Y., Liu, B., Sun, C., Guo, P., Gao, X., . . . Chen, G. (2016). Tunable integration of absorption-membrane-adsorption for efficiently separating low boiling gas mixtures near normal temperature. *Scientific reports, 6*.

Lloyd, P. (2014). *The status of the LP gas industry in South Africa.* Paper presented at the Industrial and Commercial Use of Energy (ICUE), 2014 International Conference on the.

Lomello-Tafin, M., Chaou, A. A., Morfin, F., Caps, V., & Rousset, J.-L. (2005). Preferential oxidation of CO in H 2 over highly loaded Au/ZrO 2 catalysts obtained by direct oxidation of bulk alloy. *Chemical communications*(3), 388-390.

Lukyanov, B., Andreev, D., & Parmon, V. (2009). Catalytic reactors with hydrogen membrane separation. *Chemical Engineering Journal, 154*(1), 258-266.

Maximini, M., Engelhardt, P., Brenner, M., Beckmann, F., & Moritz, O. (2014). Fast start-up of a diesel fuel processor for PEM fuel cells. *International Journal of Hydrogen Energy*.

Morell, R. (2001). Corporal punishment in Southg African schools: a neglected explanation for its persistence. *South African Journal of Education, 21*(4), 292-299.

Mortola, V., Damyanova, S., Zanchet, D., & Bueno, J. (2011). Surface and structural features of Pt/CeO2-La2O3-Al2O3 catalysts for partial oxidation and steam reforming of methane. *Applied catalysis. B, Environmental, 107*(3-4), 221-236.

Navarro, R., Guil, R., & Fierro, J. (2015). Introduction to hydrogen production. *Compendium of Hydrogen Energy: Hydrogen Production and Purification*, 21.

Niaz, S., Manzoor, T., & Pandith, A. H. (2015). Hydrogen storage: Materials, methods and perspectives. *Renewable and Sustainable Energy Reviews, 50*, 457-469.

Noureldin, M. M., Elbashir, N. O., & El-Halwagi, M. M. (2013). Optimization and selection of reforming approaches for syngas generation from natural/shale gas. *Industrial & Engineering Chemistry Research, 53*(5), 1841-1855.

Ockwig, N. W., & Nenoff, T. M. (2007). Membranes for hydrogen separation. *Chemical reviews, 107*(10), 4078-4110.

Okazaki, J., Ikeda, T., Tanaka, D. A. P., Sato, K., Suzuki, T. M., & Mizukami, F. (2011). An investigation of thermal stability of thin palladium–silver alloy membranes for high temperature hydrogen separation. *Journal of Membrane Science, 366*(1), 212-219.

Pastor-Pérez, L., Buitrago-Sierra, R., & Sepúlveda-Escribano, A. (2014). CeO2-promoted Ni/activated carbon catalysts for the water–gas shift (WGS) reaction. *International Journal of Hydrogen Energy, 39*(31), 17589-17599. doi:http://dx.doi.org/10.1016/j.ijhydene.2014.08.089

Patrascu, M., & Sheintuch, M. (2015). On-site pure hydrogen production by methane steam reforming in high flux membrane reactor: Experimental validation, model predictions and membrane inhibition. *Chemical Engineering Journal, 262*, 862-874.

Pegels, A. (2010). Renewable energy in South Africa: Potentials, barriers and options for support. *Energy policy, 38*(9), 4945-4954.

Pudukudy, M., Yaakob, Z., Mohammad, M., Narayanan, B., & Sopian, K. (2014). Renewable hydrogen economy in Asia – Opportunities and challenges: An overview. *Renewable and Sustainable Energy Reviews, 30*, 743-757. doi:http://dx.doi.org/10.1016/j.rser.2013.11.015

Rajasekar, N., Jacob, B., Balasubramanian, K., Sangeetha, K., & Sudhakar Babu, T. (2015). Comparative study of PEM fuel cell parameter extraction using Genetic Algorithm. *Ain Shams Engineering Journal*. doi:http://dx.doi.org/10.1016/j.asej.2015.05.007

Ratnasamy, C., & Wagner, J. P. (2009). Water gas shift catalysis. *Catalysis Reviews, 51*(3), 325-440.

Saadatinasab, M., Gharibi, H., & Zolfaghari, A. (2014). Determination of thermodynamic parameters of hydrogen permeation of palladium membrane for considering the effect of stainless steel support. *Iranian Journal of Hydrogen & Fuel Cell, 1*, 1-10.

Schädel, B. T., Duisberg, M., & Deutschmann, O. (2009). Steam reforming of methane, ethane, propane, butane, and natural gas over a rhodium-based catalyst. *Catalysis Today, 142*(1), 42-51.

Schneider, A., Mantzaras, J., & Jansohn, P. (2006). Experimental and numerical investigation of the catalytic partial oxidation of CH4/O2 mixtures diluted with H2O and CO2 in a short contact time reactor. *Chemical Engineering Science, 61*(14), 4634-4649.

Senanayake, S. D., Stacchiola, D., & Rodriguez, J. A. (2013). Unique Properties of Ceria Nanoparticles Supported on Metals: Novel Inverse Ceria/Copper Catalysts for CO Oxidation and the Water-Gas Shift Reaction. *Accounts of Chemical Research, 46*(8), 1702-1711. doi:10.1021/ar300231p

Sharaf, O. Z., & Orhan, M. F. (2014). An overview of fuel cell technology: Fundamentals and applications. *Renewable and Sustainable Energy Reviews, 32*, 810-853. doi:http://dx.doi.org/10.1016/j.rser.2014.01.012

Sharma, S., & Ghoshal, S. K. (2015). Hydrogen the future transportation fuel: From production to applications. *Renewable and Sustainable Energy Reviews, 43*, 1151-1158. doi:http://dx.doi.org/10.1016/j.rser.2014.11.093

Shelepova, E., Vedyagin, A., & Noskov, A. (2011). Effect of catalytic combustion of hydrogen on the dehydrogenation processes in a membrane reactor. I. Mathematical model of the process. *Combustion, Explosion, and Shock Waves, 47*(5), 499-507.

Siahvashi, A., Chesterfield, D., & Adesina, A. A. (2013). Propane CO2 (dry) reforming over bimetallic Mo–Ni/Al2O3 catalyst. *Chemical Engineering Science, 93*, 313-325. doi:http://dx.doi.org/10.1016/j.ces.2013.02.003

Solymosi, F., Tolmacsov, P., & Zakar, T. S. (2005). Dry reforming of propane over supported Re catalyst. *Journal of Catalysis, 233*(1), 51-59. doi:http://dx.doi.org/10.1016/j.jcat.2005.04.013

South Africa. Department of Minerals and Energy. 2003. White Paper on Renewable Energy.

Taner, T. (2015). Alternative Energy of the Future: A Technical Note of PEM Fuel Cell Water Management. *J Fundam Renewable Energy Appl, 5*(163), 2.

Velasco, J. A., Lopez, L., Cabrera, S., Boutonnet, M., & Järås, S. (2014). Synthesis gas production for GTL applications: Thermodynamic equilibrium approach and potential for carbon formation in a catalytic partial oxidation pre-reformer. *Journal of Natural Gas Science and Engineering, 20*, 175-183.

Watkins, P., & McKendry, P. (2015). Sustainable Energy Technologies and Assessments.

Wetwatana, U., Kim-Lohsoontorn, P., Assabumrungrat, S., & Laosiripojana, N. (2010). Catalytic Steam and Autothermal Reforming of Used Lubricating Oil (ULO) over Rh-and Ni-Based Catalysts. *Industrial & Engineering Chemistry Research, 49*(21), 10981-10985.

Weyten, H., Luyten, J., Keizer, K., Willems, L., & Leysen, R. (2000). Membrane performance: the key issues for dehydrogenation reactions in a catalytic membrane reactor. *Catalysis Today, 56*(1–3), 3-11. doi:http://dx.doi.org/10.1016/S0920-5861(99)00257-6

Winter, C.-J. (2009). Hydrogen energy — Abundant, efficient, clean: A debate over the energy-system-of-change. *International Journal of Hydrogen Energy, 34*(14, Supplement 1), S1-S52. doi:http://dx.doi.org/10.1016/j.ijhydene.2009.05.063

Xie, D., Zhang, E., Li, R., & Zhang, Y. (2014). Syngas CO cleaning for fuel cell applications by preferential oxidation: catalyst development and reactor design. *International Journal of Low-Carbon Technologies, 9*(1), 63-70.

Zeng, G., Tian, Y., & Li, Y. (2010). Thermodynamic analysis of hydrogen production for fuel cell via oxidative steam reforming of propane. *International Journal of Hydrogen Energy, 35*(13), 6726-6737. doi:http://dx.doi.org/10.1016/j.ijhydene.2010.03.099

Zhang, L., Wang, X., Tan, B., & Ozkan, U. S. (2009). Effect of preparation method on structural characteristics and propane steam reforming performance of Ni–Al< sub> 2</sub> O< sub> 3</sub> catalysts. *Journal of Molecular Catalysis A: Chemical, 297*(1), 26-34.

Zornoza, B., Casado, C., & Navajas, A. (2013). *Advances in hydrogen separation and purification with membrane technology*: Elsevier: Amsterdam, The Netherlands.

Appendix

Table 7. 1: Molar concentrations at varies steam carbon ratio's in the SR outlet stream at 550 °C and 1 atm.

S/C	PROPANE	WATER	CO	HYDROGEN	CO_2
1	1.64348829	2.08811085	8.3385259	20.5816442	0.33752513
1.5	1.21179628	6.16064904	9.45037261	23.7867175	0.52075443
2	1.02687031	11.0488028	9.8972387	25.1891112	0.62866625
2.5	0.9451619	16.2989328	10.0867756	25.8166583	0.6842546
2.6	0.93594849	17.3748299	10.1077845	25.8877835	0.6908859
2.7	0.92850181	18.4572167	10.1077845	25.9453522	0.69632776
2.8	0.92284268	19.5460527	10.1373048	25.9893214	0.70068306
2.9	0.91833974	20.6393515	10.1474525	26.024203	0.70404413
3	0.91508833	21.7373034	10.1547441	26.0494255	0.70650677

Table 7. 2: Molar concentrations at varies lengths in the SR outlet stream at 550 °C and 1 atm.

VARY 1	FC_3H_8	H_2O	FCO	FH_2	FCO_2
SR-REAC					
PARAM					
LENGTH					
METER	KMOL/HR	KMOL/HR	KMOL/HR	KMOL/HR	KMOL/HR
0.5	1.64994944	24.3130028	8.32127689	20.5342816	0.33539067
0.55	1.54299387	23.9539159	8.60392347	21.3211908	0.37361082
0.6	1.44623473	23.625664	8.85622635	22.0364793	0.41158534
0.65	1.35864778	23.3251284	9.08121248	22.6873626	0.44936006
0.7	1.27863413	23.0475517	9.28371759	23.284994	0.4868959
0.75	1.20532581	22.790351	9.46636685	23.835428	0.52417161
0.8	1.13791331	22.5511042	9.63159503	24.3443248	0.56118092
0.85	1.07566732	22.3276155	9.78158232	24.8167975	0.59793162
0.9	1.01814631	22.1185832	9.9176761	25.2559137	0.63440084
0.95	0.96478856	21.9223077	10.041547	25.6656203	0.67060315
1	0.91508833	21.7373034	10.1547441	26.0494255	0.70650677

Table 7. 3: Molar concentrations at diameter in the SR outlet stream at 500 °C and 1 atm.

VARY 1	FC_3H_8	H_2O	FCO	FH_2	FCO_2
SMR-REAC					
PARAM					
DIAM					

METER	**KMOL/HR**	**KMOL/HR**	**KMOL/HR**	**KMOL/HR**	**KMOL/HR**
0.5	3.24016402	29.37296	3.83994664	9.11346613	0.04607718
0.55	3.06737007	28.8395264	4.34327677	10.3380755	0.06112891
0.6	2.8994498	28.3183783	4.82965023	11.5309047	0.07851624
0.65	2.73767671	27.813359	5.29526947	12.6830164	0.0982163
0.7	2.5812879	27.3223631	5.74260645	13.7995675	0.12004574
0.75	2.43159817	26.8493311	6.1677128	14.8713584	0.14400857
0.8	2.28854578	26.3941842	6.57088032	15.8987149	0.16999824
0.85	2.15225664	25.9573715	6.95180242	16.8806841	0.19794353
0.9	2.02315943	25.540204	7.30921816	17.8142405	0.22781943
0.95	1.90003088	25.139209	7.64699443	18.7077497	0.25942881
1	1.783292	24.7556639	7.96388261	19.5582504	0.29275727
1.05	1.67274135	24.3890434	8.26056604	20.3670735	0.32772581
1.1	1.56811413	24.0386022	8.53788818	21.1360235	0.36428532
1.15	1.46896755	23.7031345	8.79729997	21.8680775	0.40231327
1.2	1.37553986	23.3833421	9.03807363	22.5615807	0.44182268
1.25	1.28717736	23.0773393	9.26224585	23.2210335	0.48273795
1.3	1.20376646	22.7848476	9.47021956	23.8471688	0.52499695
1.35	1.12507734	22.5052266	9.66273332	24.4415462	0.56855055
1.4	1.05084712	22.2377234	9.84061146	25.0059703	0.61336308
1.45	0.98097215	21.9820926	10.0042305	25.541101	0.65936898
1.5	0.91508833	21.7373034	10.1547441	26.0494255	0.70650677

Table 7. 4: Molar concentrations at varies pressures in the SR outlet stream at 550 ^{o}C and 1 atm.

VARY 1	**FC_3H_8**	**H_2O**	**FCO**	**FH_2**	**FCO_2**
SMR-REAC					
PARAM					
PRES					
ATM	**KMOL/HR**	**KMOL/HR**	**KMOL/HR**	**KMOL/HR**	**KMOL/HR**
0.49346163	4.38254561	32.8456667	0.45836382	1.07123303	0.00051523
0.98692327	3.97244414	31.6082022	1.68150813	3.94910345	0.00767534
1.4803849	3.45795866	30.0417383	3.20195706	7.57350928	0.03068284
1.97384653	2.9425226	28.4523291	4.70516418	11.2246627	0.07378389
2.46730817	2.47370957	26.9825571	6.04827044	14.5696868	0.13711674
2.9607698	2.06173357	25.6651557	7.20272509	17.5349922	0.2185901
3.45423143	1.70799289	24.5063417	8.1663551	20.108769	0.31618212
3.94769307	1.40743498	23.4929166	8.95627746	22.3244257	0.42793348
4.4411547	1.15369228	22.6073551	9.59317211	24.224958	0.55226694
4.93461633	0.94062907	21.8326288	10.0968251	25.8519372	0.68780361
5	0.91508833	21.7373034	10.1547441	26.0494255	0.70650677

Table 7. 5: Molar concentrations at varies lengths in the HT-WGS outlet stream at 500 ^{o}C and 1 atm.

VARY 1	**H_2**	**C_3H_8**	**H_2O**	**CO**	**CO_2**
HT-WGS					
PARAM					

LENGTH					
METER	**KMOL/HR**	**KMOL/HR**	**KMOL/HR**	**KMOL/HR**	**KMOL/HR**
0.1	26.28671	0.915088	21.50002	9.917462	0.943789
0.2	26.52399	0.915088	21.26274	9.680181	1.18107
0.3	26.76127	0.915088	21.02546	9.442899	1.418352
0.4	26.99855	0.915088	20.78818	9.205617	1.655634
0.5	27.23583	0.915088	20.55089	8.968335	1.892916
0.6	27.47312	0.915088	20.31361	8.731053	2.130198
0.7	27.7104	0.915088	20.07633	8.493771	2.367479
0.8	27.94768	0.915088	19.83905	8.25649	2.604761
0.9	28.18496	0.915088	19.60177	8.019208	2.842043
1	28.42224	0.915088	19.36449	7.781926	3.079325
1.1	28.65953	0.915088	19.1272	7.544644	3.316607
1.2	28.89681	0.915088	18.88992	7.307362	3.553888
1.3	29.13409	0.915088	18.65264	7.070081	3.79117
1.4	29.37137	0.915088	18.41536	6.832799	4.028452
1.5	29.60865	0.915088	18.17808	6.595517	4.265734
1.6	29.84593	0.915088	17.94079	6.358235	4.503016